CZECH TECHNICAL UNIVERSITY IN PRAGUE

FACULTY OF MECHANICAL ENGINEERING

Department of Instrumentation and Control Engineering

Master's Thesis

2023 Mohamad Ghaith Almasri

CZECH TECHNICAL UNIVERSITY IN PRAGUE

FACULTY OF MECHANICAL ENGINEERING
Department of Instrumentation and Control Engineering

3D Printing of Electrical Machines

Master's Thesis

Study Program:	Automation and Instrumentation Engineering
Study Branch:	Automation and Industrial Informatics
Division:	Electrotechnics
Supervisor:	Ing. Martin Novak, Ph.D.

Bc. Mohamad Ghaith Almasri

Prague, Feb 2023

Master’s Thesis Assignment

Declaration

I hereby declare that I have completed this thesis having the topic 3D Printing of Electrical Machines independently and I have included a full list of used references.

I do not have a compelling reason against the use of this thesis within the meaning of Section 60 of the Act No 121/2000 Sb., on copyright and rights related to copyright and on amendment to some other acts (The Copyright Act), as amended.

In Prague ……..... ……..……

Student´s signature

ACKNOWLEDGEMENTS

Foremost, I would like to express my sincere gratitude to my thesis advisor**,** Ing. Martin Novak, Ph.D. for the continuous support of my master's study and research, for his patience, motivation, enthusiasm, and immense knowledge.

Finally, I would like to thank my family and friends, especially, my dear friend Bc. Karim Taha for his unwavering support throughout this project.

Master's Thesis Title:

3D Printing of Electrical Machines

Abstract:

Key Words:

Název Diplomové Práce:

Abstrakt:

Klíčová Slova:

Table of Contents

List of Symbols and Abbreviations

3DP	Three-Dimensional Printing
AM	Additive Manufacturing
AMT	Additive Manufacturing Technology
EM	Electrical Machine
CAD	Computer Aided Manufacturing
SLM	Selective Laser Melting
FDM	Fused Deposition Modeling

1 Literature Review and Background Research

1.1 Introduction

Additive Manufacturing Technology (AMT) has been operating since 1991. It creates three-dimensional devices, equipment, and physical models using raw materials such as plastic, ceramics, or metal in powder, pastes, sheets, or filaments [1]. This manufacturing process is called "additive," which utilizes a layering technique to build the final product as instructed by a machine. The process of adding successive layers results in a three-dimensional object. AMT allows for mass customization, offers more design freedom, and eliminates the need for assembly. In addition, AMT can be used for low-volume production and small end-to-end supply chains [2]. Additive Manufacturing Technologies have gained increasing attention in recent years for their potential to revolutionize the manufacturing of electrical machines such as transformers and electromechanical power conversion devices [3]. Historically, electrical machine designs have been primarily planar, which can be accurately modeled in 2D. Nevertheless, with the new additive manufacturing technologies, designs can be more complex and inspired by different powder metallurgy EM cores, such as claw poles, pancake, and transverse flux machines, which can be realized with more refined internal structures. Besides, these designs can benefit from the optimization capabilities of modern computational systems, achieving machine weight and inertia reduction with enhanced topologies. However, there are still challenges to overcome in the AM space, such as slow production speed, internal design defects, limitations in printing with multiple materials, the need for post-processing, and its impact on the properties of the fabricated machine [4]. Furthermore, the feasibility of using AM for electrical machines depends on the specific machine design, the development of new materials and printing processes, and the improvement of quality control and testing methods [5, 6]. Nevertheless, compared to traditional manufacturing techniques, AM offers the ability to create 3D designs and maximize the efficiency of materials usage. These AM technologies are allowing the growth in the fabrication of small devices to sizeable complex equipment and sub-assembling parts in electronics and electrical engineering. Currently, research is focused on using AM to create

individual parts for various types of electrical machines, such as mechanical and thermal control units, coils/windings, permanent magnets, stator/rotor units, and transformers [8]. The continuous maturation of AM technologies' performance allows 3DP for EMs to continue improving [9].

1.2 EMs Working Principle and Assemblies

The basic principles of electromechanical devices and transformers are based on the conversion or transportation of energy between input and output [26]. The working principles of these devices are illustrated in Fig.1. (a), Fig.2. (a), and Fig.3. (a). The energy conversion can be seen in motors, where the input voltage creates mechanical energy that is delivered to the load. The rotor part of a motor is an essential component that produces the rotation of a shaft to supply mechanical power. It contains conductor windings that work with the magnetic field created by the stator using supply voltage. This magnetic field force causes the rotor and shaft to rotate in tandem [10]. Generators are similar in that they convert mechanical energy input into electrical output. This device comprises a stationary section (the stator) with windings wound around an iron core and a moving rotor, which can feature magnets, exciters, or conductors that initiate magnetic fields around the stator [10]. This induces voltage differences in the stator windings, ultimately producing an electric current from the output.

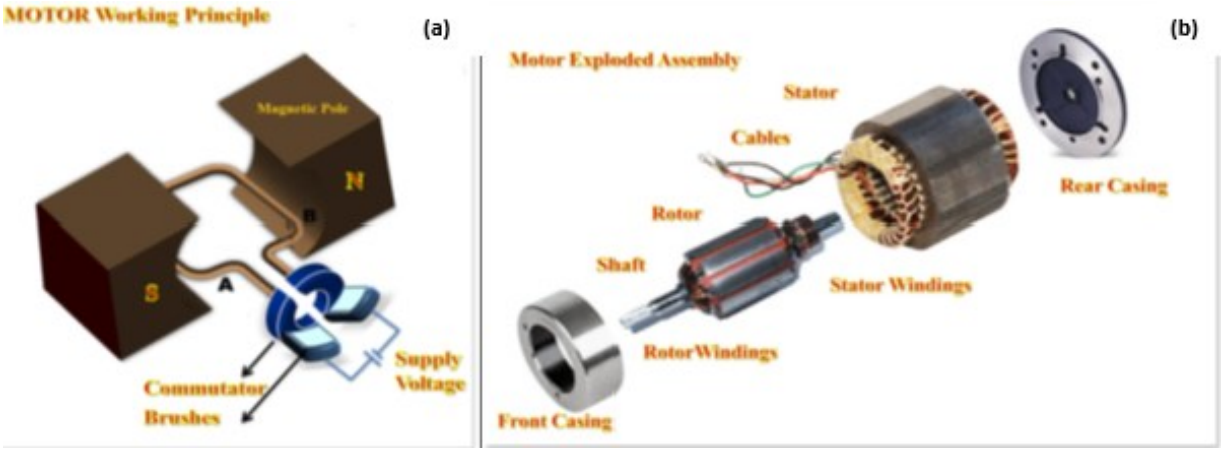

Fig. 1 a) Electric Motor Working Principle [10], b) Electric Motor and Its Assembly [10]

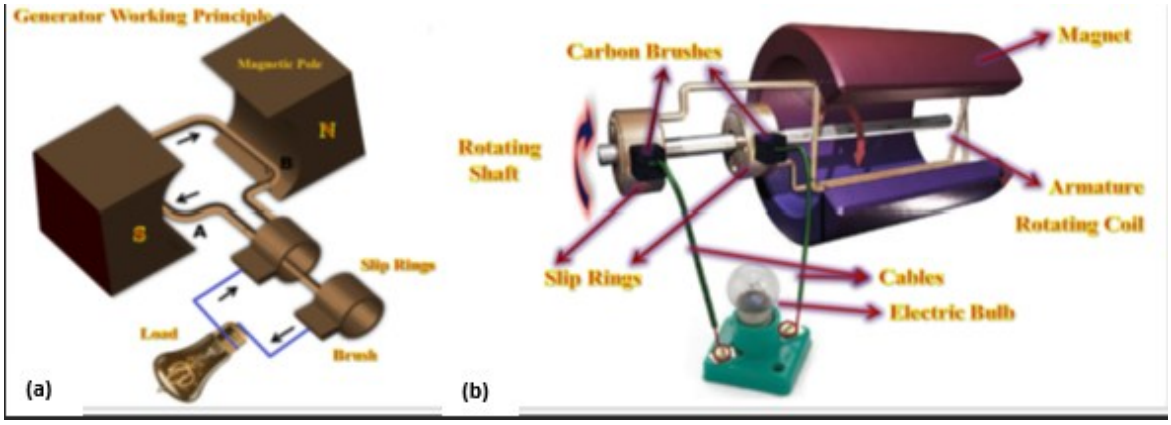

Fig. 2. a) Electric Generator Working Principle [10], b) Electric Generator and Its Assembly [10]

Transformers can be used to change the voltage levels in power systems. For instance, generators typically produce power at a relatively low voltage, which is more cost-effective, but by using transformers, this low voltage can be increased to a higher level. A transformer consists of two parts: a primary and secondary winding, as seen in Fig.3. (b). The primary winding is connected to a power source, which creates an alternating flux in the iron core [10]. The strength of this flux depends on the voltage and frequency of the power source, as well as the number of primary windings. This flux then induces a voltage in the secondary winding, which is determined by the number of secondary windings [10].

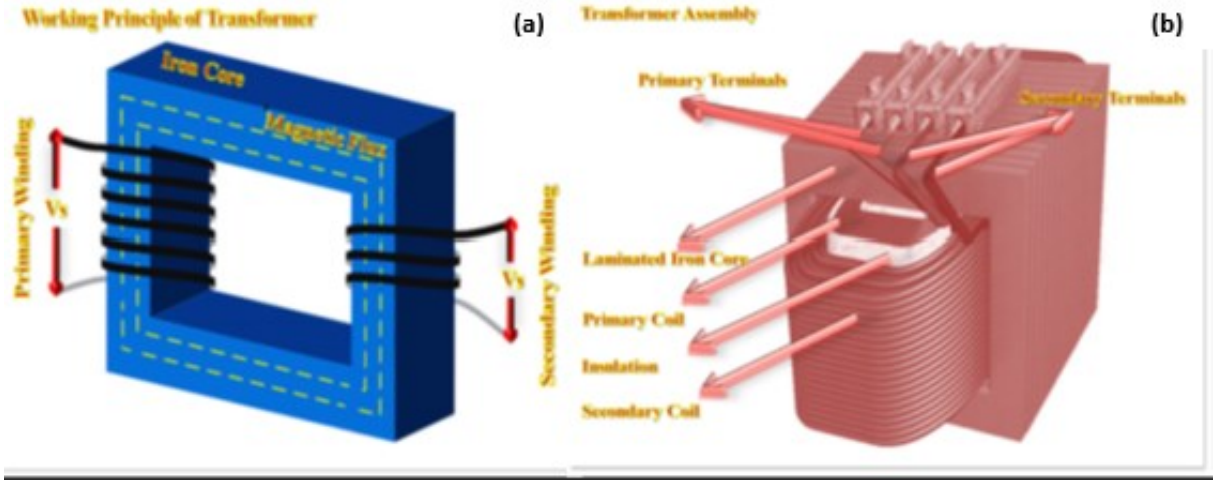

Fig. 3. a) Transformer Working Principle [10], b) Conventional Transformer [10]

1.3 Additive Manufacturing Working Principle

A 3D-printed component or an object or subassembly parts are made by collecting objects models/drawings data, photographs, scaling, and de-scaling structural information. This information cluster probably provides a clear-cut 3D digital model with integrated three-dimensional features [11], known as a virtual model. 3D printing uses 3D modeling application software to create three-dimensional objects. The main complications emerge during 3D-model creation due to the absence of specific object information, such as the object's geometrical dimensions and compact and complex solid surface textures. Contact and non-contact approaches (3D-scanning) are utilized for 3D-digital copying of an existing object, which was developed to reduce the complexity of the other digital data-collecting techniques. Subsequently, virtual replicas of the scanned object are used to design additional features using computer-aided design (CAD) software with the required resolution and accuracy. The final 3D virtual model is ready for physical 3D printing at this stage. The thin sequential parallel layers are constructed using slicing software commonly integrated within a 3D modeling application. The slicing software takes a 3D drawing, usually in stereolithography and fused deposition modeling (.STL) format, and sets execution printing instructions for each layer within the model. It calculates the amount of material needed for a 2D thin slicing layer. These horizontal layers are also called lattice model/lattice layers. When the 3D model is sliced into layers, the slicing software generates machine code (G-Code) that can be fed into a 3D printer via a USB or wireless fidelity (Wi-Fi) interface. After uploading the file into a 3D printer, the object is ready to be created layer-by-layer by controlling printing parameters like nozzle temperature, print speed, and material flow, either through a touch screen control or a USB interface with a computer (for example, Pronterface) or using both simultaneously. Lastly, the 3D printer reads every slice (2D image), which allows the 3D axis to move sequentially to create the three-dimensional physical object [12, 13].

1.4 Current State-of-the-Art AMTs for EMs

The advancements in 3D printing technology have enabled it to create three-dimensional topology-optimized electrical machine designs at a low cost [14]. With the availability of

extensive portfolios of additive manufacturing systems, researchers now have access to a wide range of design options and the ability to prototype and test their designs quickly. There are many 3D machine processing technologies, each with different processing conditions and fabrication requirements. Standard techniques include 3D printing (3DP), fused deposition modeling (FDM) [2], laminated object manufacturing (LOM) [2], selective laser melting (SLM), laminated engineered net shaping (LENS) [15], electron beam melting or laser beam melting (EBM/LBM) [8], contour crafting (paste-based extrusion), and pro-metal 3D printing. Another technique, called stereolithography (SLA), uses photoresistive materials and ultraviolet (UV) light as a power source to produce one layer of material at a time [1, 14]. The additive manufacturing group (ASTM F42) has established seven standard processing techniques for 3D printing, which include vat-photopolymerization, material jetting, binder jetting, material extrusion, powder bed fusion (PBF), sheet lamination, and directed energy deposition (DED) [3]. These advancements in AMT allow for modifications according to fabrication requirements and reduce waste resulting in cost savings. 3D printing of electrical machines is a technically challenging process as it requires tight tolerances for moving parts and the usage of multiple dissimilar materials, which is only achievable in some 3DP processes.

1.5 Glimpse into AM Capabilities for EMs

Advanced Manufacturing Techniques (AMTs) have allowed for the advancement of research in the field of electrical machines and electronics. One example of this, is the use of 3D printing in the fabrication of a magneto-mechanical generator, which was found to have a low resonance frequency, making it a suitable option for eliminating ambient oscillations [16]. In addition, the utilization of AMT has made it possible to produce a wideband electromagnetic vibration generator that can generate steady electric power at a predetermined frequency through the relative motion of magnets and coils over the cantilever through electromagnetic induction [16]. The use of 3D printing also enabled a lightweight stator with complex geometry to be created, making it a suitable option for wind power generation applications [17]. The use of AMT in producing electromagnets and other intricate parts is a novel idea, with companies like GE using the technology to create precise and complex components for their motors and engines [18]. Additionally, AMT provides freedom in the design process, allowing

for creating the best-performance geometries, even for metal structures on a microscale [19]. The use of rare earth magnets, such as Nd2Fe14B, can lead to innovative and efficient performances of synchronous machines, with efficiencies reaching up to 96% for industrial applications [20]. Using ferrite magnets or AlNiCo ferrites for EMs cores can also result in reduced size and heat reduction [20]. AMT can manufacture these magnets in several forms, including sintered and bonded, polymer bussed magnets raising their importance in applications from hard disk to electric motors where shape design flexibility and highly efficient magnets are extremely desirable [21]. In result, the utilization of AMT provides functional benefits with reduced complexity during printing and leads to improved performance in electric machines with magnetic materials and this was shown in one study through the use of laser beam melting and extrusion-based additive manufacturing technique [20, 21]. In an additional study, a novel class of electric motors with a hybrid topology was introduced, thanks to the 3D magnetic flux paths enabled by the advanced anisotropic properties of soft magnetic material winding cores produced through AMT [22]. These motors were found to provide significantly higher power output (up to 40%) and improved efficiency (with up to 15% lower losses) compared to electric motors produced through conventional manufacturing methods [22, 23].

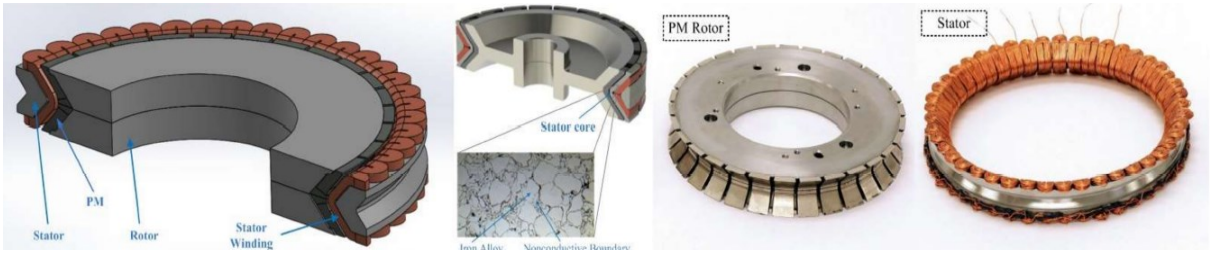

Fig. 4. Additively Manufactured 3D-Flux PM Brushless Machine with Spray-Formed Soft Magnetic Material Core [22]

One research study reported high-performance synchronous reluctance motors with different silicon steel grades and production methods. The study results showed that the choice of silicon steel significantly influences the losses of the motor and improves its efficiency by selecting the appropriate grade. The design also enabled reduced weight and material savings while preserving performance [24]. Such prototypes can be created through 3D printing methods, resulting in lightweight and stiff structures and producing machines in a single build.

However, different materials and 3D printing technologies can have varying effects on performance characteristics, making it a crucial factor in fabricating electromechanical devices [25]. Besides, It is also desired to reduce the stator length and size, which leads to reduced resistive losses and increased efficiency and power density of the induction motor. This can be achieved through advanced AMT by fabricating highly conductive copper windings and insulating layers selectively, leading to more compact designs for industrial applications [26].

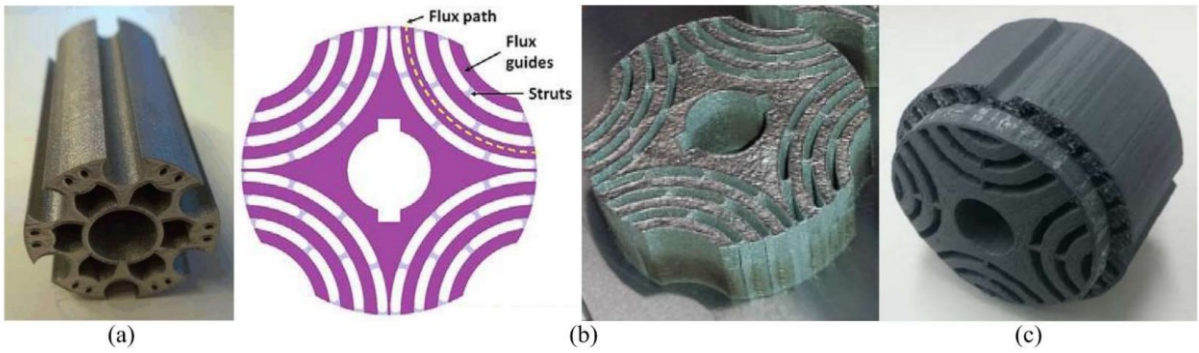

Fig. 5. Additively Manufactured Cores for Electrical Machines: (a) Rotor Prototype for an SRM with High-Saturation Flux Density [80], (b) SLM-Built Rotor with Non-Magnetic Bridges [81], (c) Rotor and Stator Core Packs for a Line-Start Synchronous Reluctance Mach [28]

Additional research presented a new design for reluctance motors that reduces torque ripple and losses, resulting in high efficiency. This design features an asymmetric skew rotor and honeycomb structure fabricated by 3D printing techniques, with the pole pieces, slots, and skew rotor contributing to reduced torque ripple and losses [27].

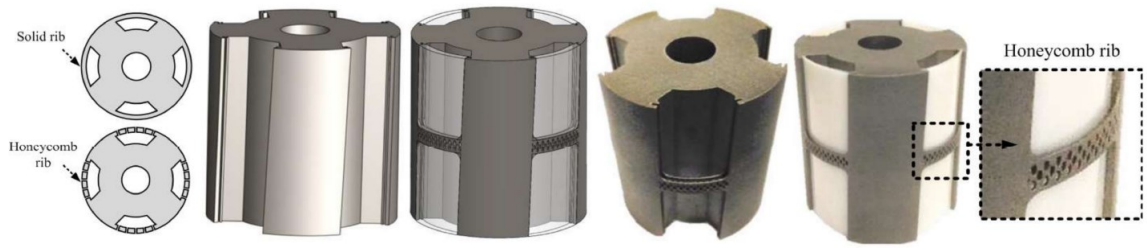

Fig. 6. 3D Printed Skewed Rotor with Honeycomb Structure Cores for Reduced Torque Ripples [27]

One study proposed that AM methods that incorporate coils and cooling systems are necessary because conventional approaches, such as solid cores or wires, experience skin effects and high resistance, leading to heat losses. Various coil geometries were used to force

the current throughout the cross-section, which helped address these resistance issues in electromechanical devices. The conventional approach has been replaced by layer-by-layer additive manufacturing technology, which enhances cooling efficiency with a fractal approach [28].

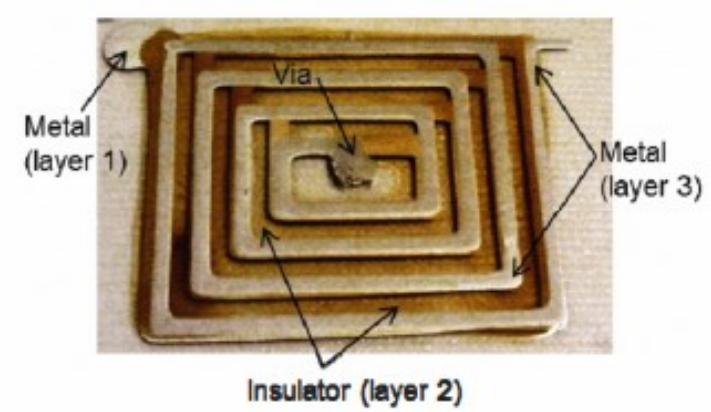

Fig. 7. Three-Layer Coil Structure Manufactured Using Syringe Derived Materials. The Coil is 5.5 x 3.5 cm [28]

In another research, a group of researchers fabricated coils and electrical contacts using a multi-functional additive manufacturing technique [29]. These improvements in the structure are likely beneficial for electromechanical devices such as, linear variable differential transformers (LVDT), rheostats, and membrane switches. Moreover, the ability to print tight, curved, and straight paths with a polymer while automatically starting and stopping the printed fiber results in the creation of efficient conductive junctions, which are crucial for the proper functioning of electromechanical components [29]. According to one study, the metal AMT technique was able to produce helical winding with optimized parameters, resulting in a reduction of AC winding loss at 400 Hz and 200A_{RMS}. This decrease in winding losses was achieved through the use of shaped windings. The electrical conductivity of additively fabricated metal winding was found to be 51% lower than aluminum windings. However, it was later improved to over 85%. This shows that the AM process enhances functional characteristics, including electrical conductivity, making it a potential design variable for adjusting resistivity properties for specific winding applications. The results also indicate that the AM process offers dimensional accuracy, making multilayer windings suitable for electromechanical energy conversion devices and transformers [30].

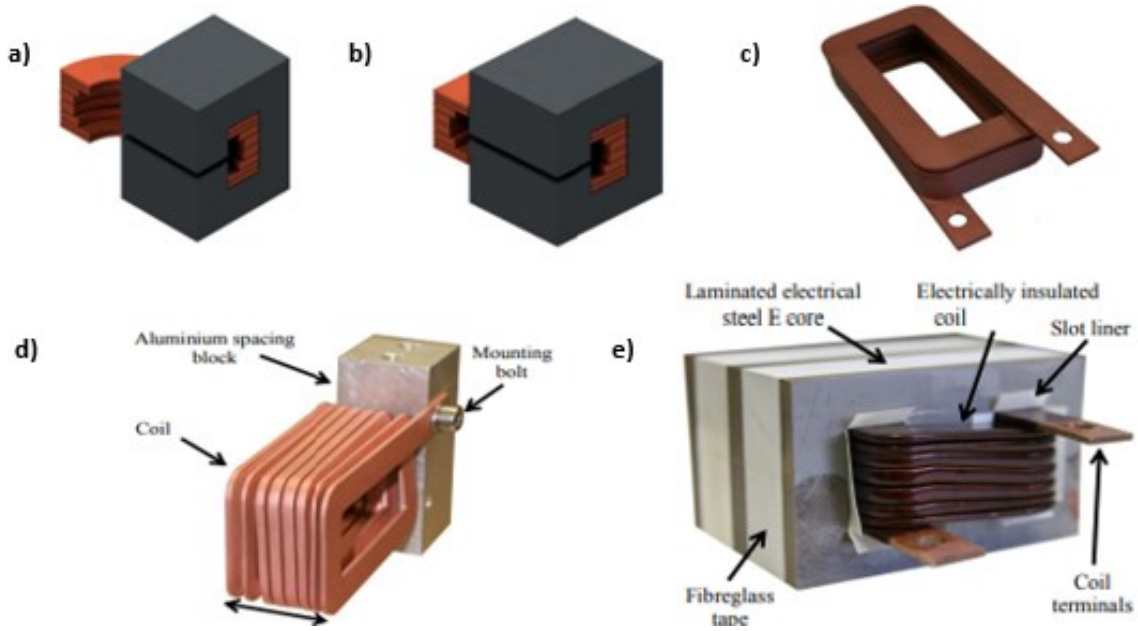

Fig. 8. Shaped Profile Windings for Minimal AC Losses in Gapped Inductors: (a) Semi-Circular End-Windings [30], (b) Semi-Square End-Windings [30], (c) Copper Coil with Non-Uniform Conductor Profiles Produced Using an AM Process [30], (d) Coil Mounted to an Aluminum Spacing Block Prior Insulation Process [30], (e) AM Copper Winding Mounted on the Electrical Steel Core [30]

1.6 Significance of Research in 3DP of EMs

It has been reported that a significant portion of energy consumption in the USA is attributed to using motors in various applications. The National Electrical Manufacturing Association (NEMA) states that electric motor systems consume 70% of the total generated electric power. These findings highlight the growing need for electromechanical energy conversion devices and the drive for energy conservation and efficiency-enhancing technologies [31, 32]. It is essential to consider the efficiency and lifespan of the machine being used during the energy consumption process when creating an economical product design. The majority of energy consumption comes from power-generating stations and application-driven stations, making the motors and generators crucial components [33]. Therefore, the design and production of these electrical machine components are vital in power generation plants and energy conservation devices. The demand for these economical product designs enables the creation of new prototypes and technologies. Prototyping is a crucial phase in developing new products and often involves modifying the original design to improve efficiency and

compatibility. These changes are not necessarily due to mistakes but relatively to discover new capabilities that can now be achieved and tested without limitations and the possibility of combining multiple functions within existing EM designs. There are various traditional and advanced methods for prototyping. However, the focus here is on additive manufacturing technology, or 3D printing, as it is the leading prototyping technology for creating cost-effective and efficient models with a shorter supply chain, reduced waste, and quicker production time [34, 35]. Additionally, the United Technologies Research Center is working on developing high-performance electric machines for use in electric traction and renewable energy applications [36]. Therefore, AMT offers a solution to overcome the complex problems that traditional fabrication methods face, for instance, magnetic anisotropy, which is a widespread issue in electromechanical conversion devices and results in magnetic losses and eddy current losses [37]. Besides, the presence of harmonics in the air gap caused by the eccentricity and double periodicity of magnetic anisotropy can lead to torque and radial forces on the stator in industrial machines. This is considered an abnormal operating condition [38]. Although there are methods available to measure this anisotropy, it can be challenging to control it through traditional techniques. However, the implementation of programmable electromagnets in a 3D printing arrangement has the potential to solve this issue. Garrett Clay and his team have developed a 3D inkjet-printed magnetic material with low hysteresis loss anisotropy due to its thin-layered architecture and control under a programmable electromagnetic force field [39]. In addition, a new 3D screen printing technique was introduced by Fraunhofer IFAM Dresden, allowing the production of intricate machine parts with precision ranging from micrometers to centimeters and the capability of using various materials such as metals, ceramics, and composites. With the integration of this additive manufacturing technology and the compatibility of the materials under optimized sintering temperatures, the resulting machine parts are cost-effective, highly efficient, and have a high torque and power density. [40, 41]. Furthermore, the efficiency of a motor largely relies on its torque density. In conventional manufacturing, the internal windings are fully covered with insulation, and a liquid coating is applied to prevent short circuits. Unfortunately, this liquid coating directly correlates with temperature, negatively affecting the torque density and thus reduces the machine's overall efficiency [41].

One research group has proposed an innovative solution for the problem of reduced overall efficiency in motor applications through the use of advanced 3D screen printing techniques. This process involves integrating ceramic materials into the machine's design. By incorporating ceramic layers as insulation material, the problem of reduced torque density can be controlled, resulting in the prevention of reduced output efficiency. The use of ceramics as an advanced temperature-controlled material significantly increases the machine's efficiency [41, 42]. Additionally, the 3D screen printing technology provides more efficient products than traditional methods, resulting in machines with improved conductive structures. This enhances the filling factor and leads to higher current density and high torque density, ultimately resulting in a higher efficiency level with well-designed structural parameters [41].

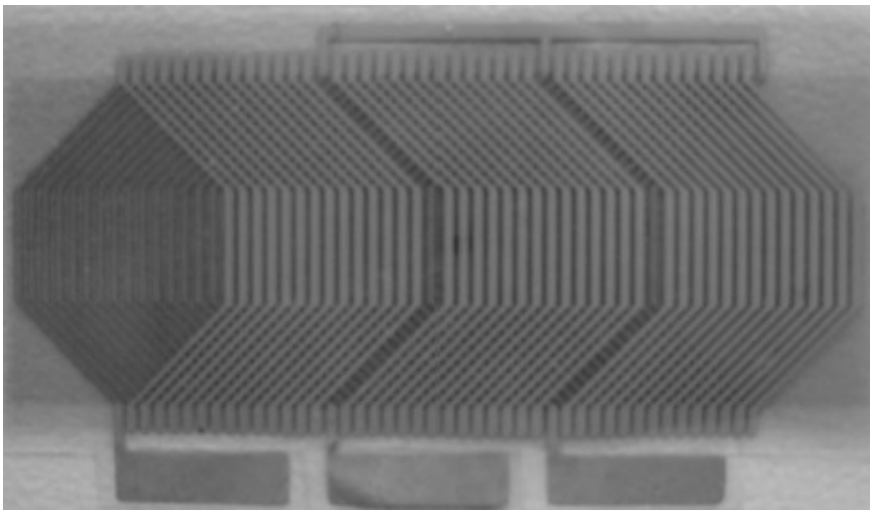

Fig. 9. Sample of a Screen-Printed Air-Gap Winding of Three Phase Synchronous Small-Power Electrical Machine [41]

Moreover, the use of permanent magnets (PMs) has been widely popular in high-rated machines due to their high intrinsic torque density. However, these materials are unsuitable for synchronous reluctance machines due to their internal torque characteristics, which lead to high ripple currents. Nevertheless, with the help of AM technologies, it is possible to address these issues while still enjoying design freedom, design durability, and controlled magnetic properties in an economically efficient manner of machine fabrication [35].

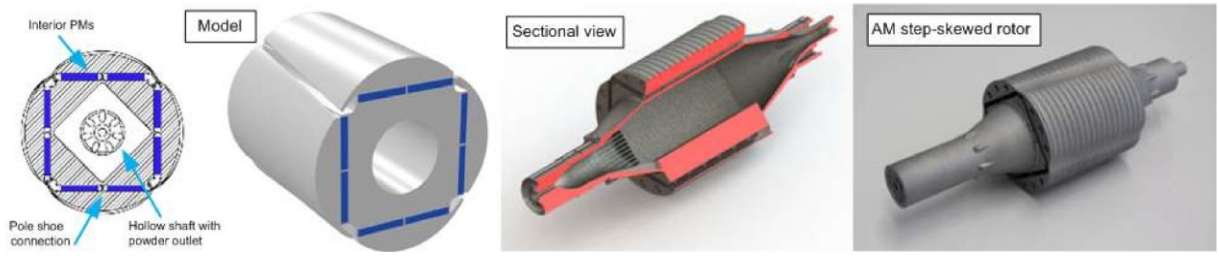

Fig. 10. Additive Manufacturing Interior Magnet-Skewed Rotor for PM Synchronous Machine with Hollow Shaft and Lightweight Construction [82]

The efficiency of a machine is also affected by the intrinsic stresses and heat losses that are induced by the materials used, as well as the impact on heat dissipation and maintenance control [43, 44]. The energy consumption in motors is a critical issue due to factors such as heat generated from the motor and friction; for instance, every 10-degree Celsius increase in temperature results in a 50% reduction in insulation life. The heat generated during the operation of the bearing system also causes the grease to have a shorter lifespan, increasing the risk of bearing failure. This could be due to improper greasing or the use of incompatible grease systems. However, these problems can be effectively addressed by using the additive manufacturing/3D printing technique, which provides a uniform insulation thickness. Besides, the advanced integrated instrumentation in AMT allows for proper grease levels to be maintained. Energy-efficient motors have better efficiency compared to standard motors, showing an improvement of two to eight percent. This enhancement in performance is attributed to advancements in technology, including the utilization of additive manufacturing and improved design and manufacturing processes through CAD and model analysis [45]. The use of high-performance materials and optimized structural designs reduce energy loss, through the implementation of lower electrical loss steels and thinner stator laminations [46, 47], as well as longer cores and more efficient cooling fans which can further reduce waste and improve energy efficiency [45]. The utilization of state-of-the-art 3D printing technology with integrated instrumentation can attain these crucial requirements at a reduced economic cost. According to one study, a thermal and mechanical stress analysis was conducted on an induction motor made with additive manufacturing and a high copper fill factor. The results revealed that the high copper fill factor in the stator core enhances internal thermal conduction and energy density but also can create a challenge for thermal management. The

traditional manufacturing methods may result in limitations to manage these challenges. In contrast, the additive manufacturing approach can quickly produce machines with desired designs and desired performance and overcome those challenges at the minimum cost through simulation techniques [48]. In research by Malinowski et al., the purchase price of a motor only accounts for 2% of its total cost over a 20-year lifespan, while the electricity to run the motor continuously is 11 times the purchase price. By looking beyond the initial cost, manufacturers can save thousands of dollars in energy costs. Implementing additive manufacturing technology in the future could be a leading fabrication method for industrial and commercial applications [49]. Research on AMTs for 3D printing electrical machines can potentially improve their performance, reduce their cost significantly, and reduce the environmental impact of manufacturing by decreasing the amount of material and the number of manufacturing steps required [50].

1.7 Technology Review about Suitable AMTs for EMs

1.7.1. Selective Laser Melting (SLM)

1.7.1.1. SLM Working Principle, and its Strengths and Weaknesses

SLM, short for Selective Laser Melting, is an additive manufacturing method categorized as a powder bed fusion process. It involves a high-intensity laser for melting and fusing metal powders to create 3D parts based on computer-aided design data [52]. The SLM process begins with the preparation of CAD data and continues through the removal of fabricated components from the building platform. Before uploading the CAD files to the SLM machine, they must be processed by software such as Magics to provide support structures for overhanging features and generate slice data for laser scanning of individual layers [52]. After melting each cross-sectional layer, the build platform is lowered, and a new layer of powder is deposited while the first layer cools and solidifies. The process is sequentially repeated until the 3D part is constructed [51]. The working principle is illustrated in Fig. 7.

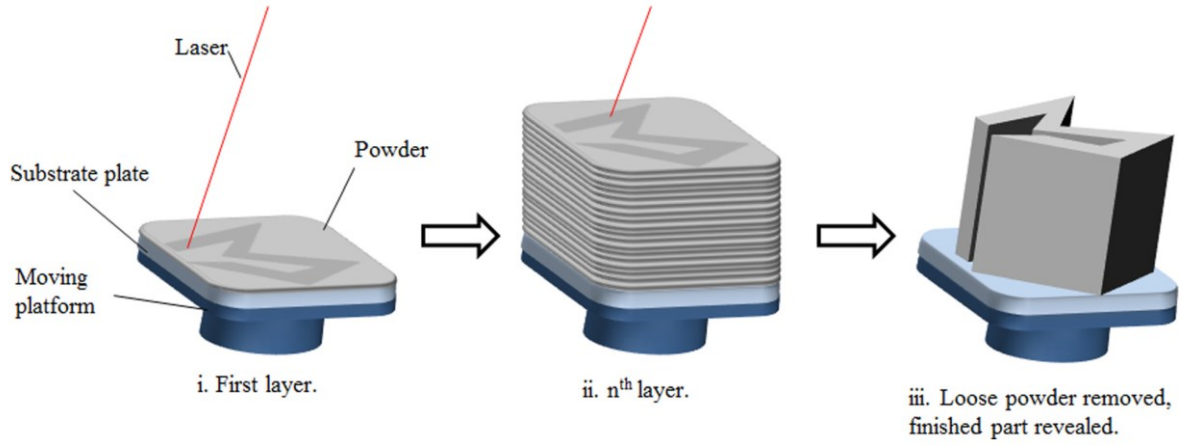

Fig. 11. Concept of SLM Process. (i) High-Power Laser Melts Selective Areas of the Powder Bed. (ii) Process Repeats for Successive Layers. (iii) Loose Powder Removed and Finished Part Revealed [52]

Laser power, scanning speed, hatch spacing, and layer thickness are modified to construct a single melt vector that merges completely with neighboring melt vectors and the preceding layer. The loose powders are removed from the building chamber, and the component can be manually separated from the substrate plate or by electrical discharge machining once the laser scanning process is finalized [52]. In the SLM process, to shield the heated metal components against oxidation, the building chamber is usually filled with nitrogen or argon gas to provide an inert atmosphere. Also, some SLM machines can pre-heat the substrate plate or the whole building chamber. The thickness of the layer often goes from 20 to 100 µm [29]. The thickness selection is essential to balance achieving satisfactory resolution and allowing for fine powder flowability [53]. In SLM, the main reason for poor resolution and specific build tolerance is the powders with larger particulate sizes. In contrast, smaller powders tend to agglomerate because of Van der Waals forces, resulting in poor powder flowability and deposition [52]. SLM can produce dense and near-net-shape components without the need for post-processing other than removing parts and supports from the substrate plate. This makes SLM a superior way to manufacture parts. The main strengths of SLM technology are that it improves product quality, processing time, and manufacturing reliability compared to other laser-based AM techniques. Many physical phenomena that are essential to the SLM process in general and also to the field of electrical machine 3D construction are the absorptivity of the powder material to laser irradiation, the balling phenomena that disrupt the construction of steady melts, and the thermal instability

undergone by the material during the melting procedure lead to crack formation and part failure [52].

1.7.1.2. Materials Portfolio of SLM for EMs Application

Electrical machines are mainly constructed of conductive, non-conductive (insulation), and ferromagnetic materials (EMs cores), as in electrical transformers. For the SLM process, the primary materials studied and researched are metals like steel, titanium, and nickel, which can be sorted under the ferromagnetic class and used for forming EMs cores. However, on the other hand, new research interest is emerging for materials such as aluminum, copper, magnesium, cobalt-chrome, tungsten, and gold [52], which are essential for developing electrically conductive applications. Optimization studies of the SLM operation showed that the SLM components' quality for EMs applications depends on the materials' properties, specifically the powder morphology and content and the processing or printing parameters [54]. Below, in Table 1 are examples of different studied AM Soft Magnetic materials used in SLM AM technique.

Ta ble 1. Magnetic Properties of Different AM Soft Magnetic Materials Using SLM

Material Composition	*μ_{max} & Saturation Flux Density (Ms)*	*Hysteresis Losses*	*Heat Treatment*	*References*
50Fe-49.9Co-0.1Si	μ_{max} = 2600 Ms = 2.35 T	Comparable to VACOFLUX 50	1100 °C for 4 h	[92]
Fe-6.9%wt.Si	μ_{max} = 24,000	4 W/kg at 1T, 50 Hz	1150 °C for 1 h	[93]
Fe-80%Ni	Ms = 550 Am^2/kg	BH loop is available. Losses are not calculated.	Non	[94]
Ni-Fe14-Cu5-Mo4	Ms = 0.33 T	BH loop is available. Losses are not calculated.	Non	[95]

For conductive materials, pure copper would be the preferred selection for the 3d-printing of electrically conductive materials. However, the 3d-printing of highly pure copper is exceptionally challenging because of its thermal problems driven by copper's high conductivity [55]. Using SLM for printing copper is also challenging due to the nature of copper's high reactivity to atmospheric oxygen, even when low concentrations are in play [52].

The pure copper printed parts using SLM have a good physical performance, an electrical conductivity of 88% IACS [55], a high relative density of 99.6% [55], a thermal conductivity of 336 W/mK [55], and a tensile strength of 149 MPa [55], as presented in Table 1 below:

Table 2. Property Comparison of Copper Parts Manufactured Conventionally vs. SLM [55]

Manufacturing Method	*Relative Density (%)*	*Electrical Conductivity (%IACS)*	*Tensile Strength (MPa)*	*Thermal Conductivity (W/mK)*
Pure Copper (Conventional Mfg. method)	100	100	200	400
SLM	99.6	88	149	336

Some of the materials portfolio that is suited for the use of insulation in electrical machines and electronics is Ceramics. In SLM, Ceramic materials are well-studied, and the primary employed types in bed-fusion AMT include Li2O-AI2O3-SiO2 (LAS) glass [52], alumina (Al2O3) [52], silica (SiO2) [52], yttria-stabilized zirconia (YSZ) [52], tri-calcium-phosphate (TCP) [52], alumina-silica mixture [52], silicon carbide [52], and silicon monoxide [52]. Of the ceramics mentioned, Alumina (Al2O3) and Silica (SiO2) are most commonly used for electrical insulation in electronics and electrical machines due to their high dielectric strength and thermal stability. Alumina has excellent electrical insulation properties and is commonly used as an insulating material in high-temperature applications. Silica is known for its high mechanical strength and low thermal expansion coefficient. Yttria-Stabilized Zirconia (YSZ) is also used for high-temperature applications due to its high thermal stability and dielectric strength, but it is less commonly used for electrical insulation.

1.7.1.3. Applications and Opportunities

SLM is state-of-the-art AM Technology that produces electrical machine elements such as conductive components and soft magnetic cores. Those components comprise air gaps partitioning for splitting individual turns in coils, which lowers the effect of the induced eddy currents in soft magnetic cores [56]. Due to the absence of multi-material abilities of SLM manufacturing systems, air gaps are produced, which in EMs are needed to realize coil inter-turn insulation and raised intra-core resistance [56]. More increased resistance in the core

restricts the induction of classical eddy currents, lowering the joule heating and losses of the magnetic part. In cases—such as magnetic gears, couplers, or rotors of synchronous machines—laminating or segregating the core structure would not be necessary when the printed parts are coupled through a quasi-static magnetic field [51]. In the case of quasi-static fields, with the flux nearly constant and steady, all core loss components are minimal. To reach the highest core and machine air gap magnetic saturation, these components should be printed fully densely, without air gaps. This indicates that despite limited multi-material printing abilities, SLM systems are ably fitted for printing parts for stationary magnetic applications.

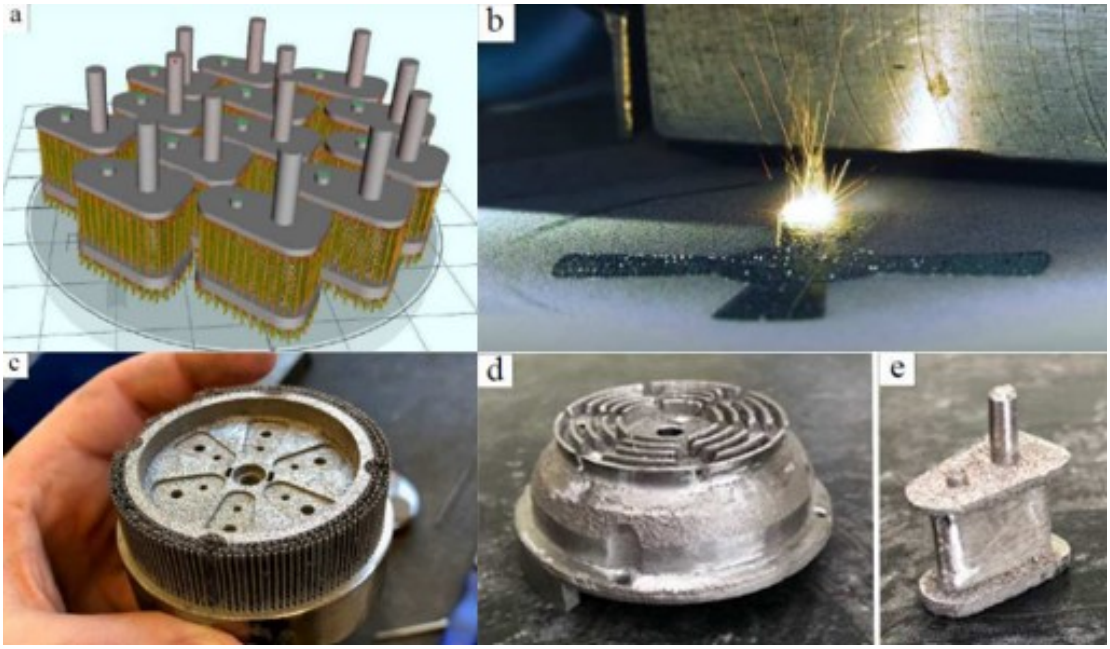

Fig. 12. (a) Layout of the Printed Stator Teeth Arranged on the Build Plate in Printing Pre-Processing [51], (b) SLM Printing Process of the Machine Rotor [51], (c) Stator Half of the Machine on Build Platform Just After Printing [51], (d) Post-Processed Stator Half with the Support Structure Removed [51], (e) Post-Processed Stator Tooth [51]

Additionally, the SLM technique makes it possible to create novel designs for heat sinks and heat transfer devices used in heat transfer applications, especially in energy applications [57]. Induction heat coils have various custom designs that are tailored to different applications, with complex structures including curved paths or helical shapes, and sometimes with hollow spaces for water cooling. Due to the customization and manual fabrication, the production process of these coils is often time-consuming. However, 3D printing offers the advantage of

efficiently producing complex and customized parts with a shorter lead time. The material used in induction coils must be highly conductive, which is why they are typically made of highly pure copper. Martin et al. suggested that using direct SLM technique can lead to more precise fabrication of induction coils compared to traditional hand-made methods [58].

Fig. 13. AM Shaped-Profile Coils with Low AC Loss for High-Speed Electrical Machines [83, 84]

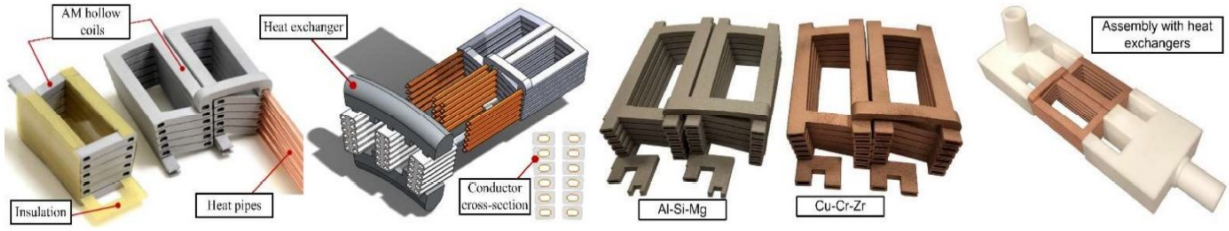

Fig. 14. AM Coils of Hollow Conductors integrated with Cooling Channels for Direct Heat Ex-Change [85]

1.7.2. Fused Deposition Modeling (FDM)

1.7.2.1. FDM Working Principle, and its Strengths and Weaknesses

The FDM method, invented by Scott Crump of Stratasys in 1989, is the most widely used material extrusion-based additive manufacturing process [59]. The FDM setup includes a roller storing filaments and an extrusion head that is connected to the filaments and moves in the X and Y directions while the build platform moves in the Z direction. The movement of the extrusion head is controlled by an electric motor, and the filaments used are typically between 1.75 to 3.0 mm in diameter. FDM's production process comprises three stages: pre-processing, production, and post-processing. In the pre-processing stage, the product design

is created using CAD software and saved in STL format. Before slicing the file, essential parameters such as slicing parameters, building orientation, and machine temperature must be taken into consideration, as these factors significantly affect the final product's mechanical properties [60]. The fabrication process of FDM involves three stages: pre-processing, production, and post-processing. In the pre-processing stage, the product's design is created using CAD software and saved in STL format. The essential parameters for the printing process, such as slicing parameters, building orientation, and temperature conditions, are then considered before slicing the file. The slicing process is carried out using software, resulting in a G-code, a computer numerical controller code that controls the extrusion process. The feedstock material connected to the extrusion head is then regulated by temperature and heated to a semi-liquid stage to form 2D layers on the build platform, which are then stacked on top of each other to create 3D objects [61].

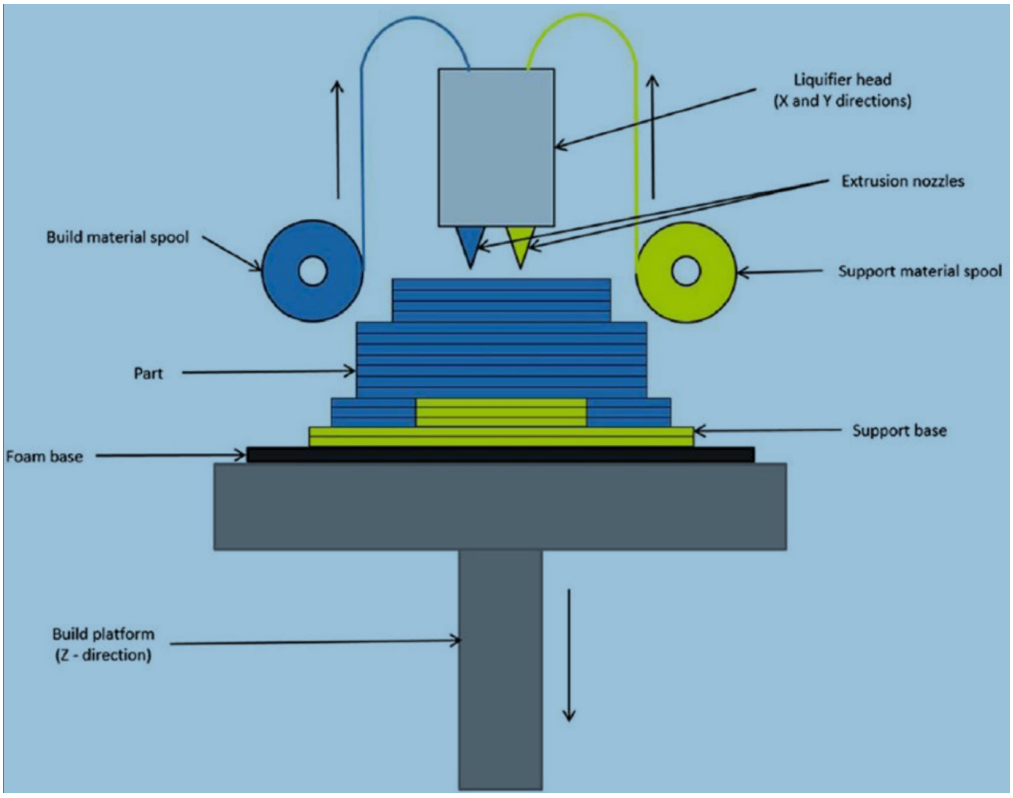

Fig. 15 FDM Process and its Working Layout [79]

The filament is heated between 150 to 300℃ and printed onto the plate with a dimensional accuracy of 100 µm [62]. The support base is first printed, followed by the required object,

with the building platform moving downwards after every layer is printed. The finalization of the product is done through post-processing. This step is crucial in FDM as the printed parts are not immediately ready for use. After the printing is complete, the product is taken off the build platform, and the supporting structures are removed. This process primarily aims to enhance the product's surface quality [63, 64]. According to Kumbhar and Mulay [65], post-processing is used to improve the surface finish of the printed parts. Post-processing can be divided into mechanical and chemical methods. The chemical method involves painting, coating, heating, and vapor deposition [66], while the mechanical method encompasses machining, sanding, abrasive techniques, vibratory finishing, and barrel finishing to enhance the surface quality and mechanical properties of the parts [67, 68]. Different mechanisms in FDM methods have been reported by Daminabo et al. [69] and Bryll et al. [70], and they are classified based on the heads and feed mechanism used. The single-head FDM process utilizes only one filament for production, making it a traditional method. This technique employs composite materials, including polymers mixed with fiber, wood, and metals. However, the limitation of this method is that it cannot produce products using more than one type of material. On the other hand, the dual-head method uses two different filaments, enabling the creation of components using two distinct materials. This method is faster than single-head and creates skeletal structures like honeycombs and square cells. The in-nozzle impregnation process is a unique method where the polymer filament and add-on materials, such as carbon fiber and glass fiber, are fed directly into the nozzle and mixed before printing. This FDM method offers several advantages, including ease of access, low cost of machinery, and the ability to print multicolor products. Despite this, the main drawbacks of the in-nozzle impregnation method are poor surface quality and the need for support structures.

1.7.2.2. Materials Portfolio of FDM for EMs Application

FDM is a material extrusion process using thermoplastic polymers. Acrylonitrile butadiene styrene (ABS), polylactic acid (PLA), and polycarbonate (PC) are the base material of this FDM process [59]. The choice of materials for FDM is generally limited to polymer-based materials with varying physical, mechanical, and thermal characteristics. The selection of the polymer material is dependent on the specific application and requirements. However, currently, the

available types of polymers are limited, restricting the advancement of FDM technology. Also, materials with high melting points cannot be used in this process since commercially available FDM machines have a melting capacity of around 300°C. As a result, thermoplastic polymers and various materials with low melting temperatures are suitable for FDM. In order to enhance the quality and properties of polymers, various efforts have been made to incorporate fillers such as ceramics, nanoparticles, metals, and wood fibers. The materials used in FDM printing for electrical applications include iron, nickel, and cobalt-based alloys, polycarbonate, acrylonitrile butadiene styrene, polyethylene terephthalate, and nylon-based filaments, and carbon-filled filaments and copper and silver-based filaments. It is important to note that these materials' actual properties and suitability depend on the specific application and the quality of the FDM printing process. For polymer ceramic composites, the standard ceramic composites used are alumina, silica, zirconia, calcium phosphate, and bioactive glass–ceramics [71], which can be used for electrical and thermal insulation applications in electrical machines. The use of metal powder in the fabrication of polymer-metal composites has limitations, including the impact of viscosity. However, the addition of plasticizers and surfactants can improve this issue [72]. The most commonly used metal fillers in PMCs are aluminum and iron powder. Fafenrot et al. compared the mechanical properties of magnetic iron and bronze fill powder reinforced with PLA [73]. The results showed that the composite's strength was lower than the original material [73], but further research could refine this method and give more understanding of its magnetic performance for Electrical machines applications. Various materials have been utilized in the development of electrically conductive nanocomposites, such as metallic nanowires and nanoparticles, carbon nanotubes, carbon nanofibers, and graphene, due to their exceptional conductivity. These advanced composites have various practical applications, including sensors and electromagnetic shielding in aerospace and household industries [74].

1.7.2.3. Applications and Opportunities

A research study delved into the possibility of creating a transformer core using fused deposition modeling techniques. The use of additive manufacturing methods through FDM can result in the production of an optimized transformer core geometry, leading to increased

efficiency. The study tested the construction and efficiency of magnetic transformers fabricated using a magnetic thermoplastic polymer composite material [86]. The study successfully demonstrated the 3D printing of a toroidal core geometry and compared its performance with identically-shaped standard cores [86]. The results showed that the fill pattern of the printed cores does not have a significant impact on performance, but the largest fill factors provide the best results. However, the printed core's inability to saturate as easily as a standard ferrite is a challenge that needs to be overcome for the technology to be successful. To enhance performance, higher Fe content and magnetically responsive particulate with low coercivity and susceptibility are required [86]. The study also showed that the transformer geometry and turn ratio could be adjusted to optimize performance. The results of the study provide insight into the structural and magnetic properties of the composite filament material and pave the way for further improvements in the performance of printed cores through FDM [86].

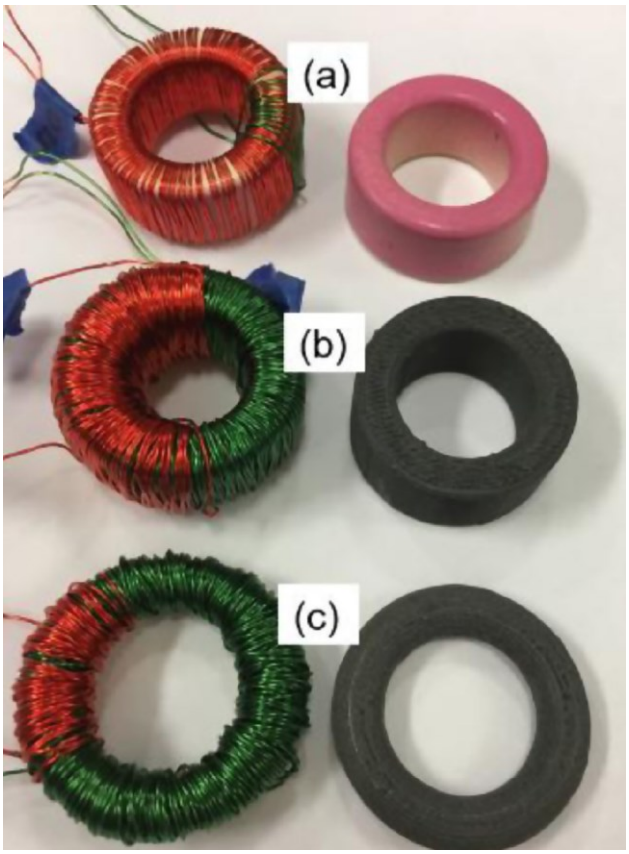

Fig. 16. Transformer Cores Used for Testing: (a) Commercial Core, (b) 3D Printed Transformer Core (Same Shape as the Commercial Core, (c) Toroidal Shaped Transformer Core [86]

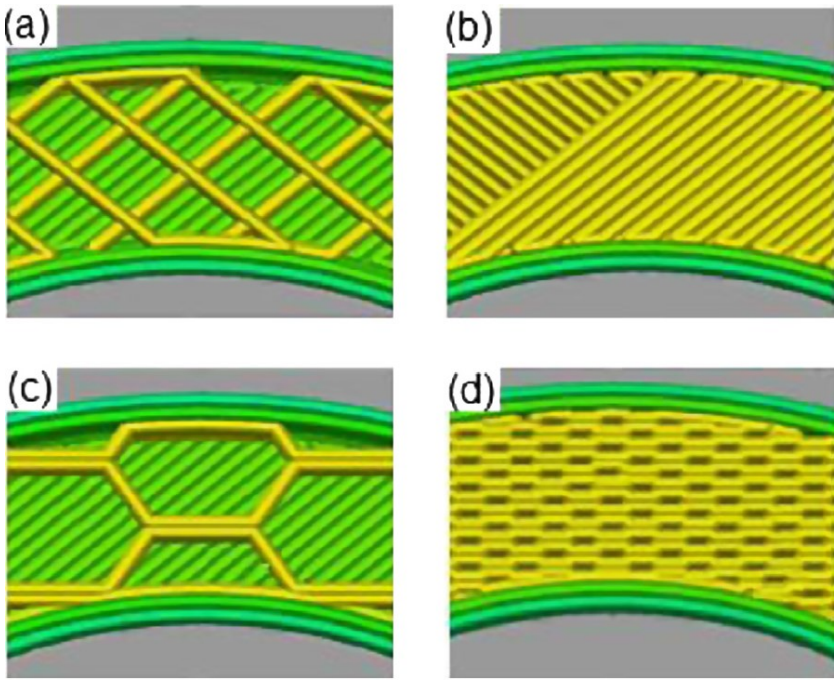

Fig. 17. Horizontal Cross-Section of Transformer Cores Modeled on FDM Printer with Different Fill Pattern and Fill Percent. (a) Rectangular Fill Pattern with20%, (b) Rectangular Fill Pattern 100% Fill, (c) Honeycomb Fill Pattern with 20% Fill, (d) Honeycomb Fill Pattern with 100% Fill [86]

The 3D-printed polymer composites can be utilized in various forms in combination with electrical materials as electronic instruments. By using FDM, the carbon-black/PCL composites can be integrated into electronic sensors to convert piezoresistive to capacitive. These capacitive sensors can be either printed as part of a custom interface system or embedded in smart vessels [75]. One research group studied the use of FDM-printed PLA/graphene electrodes for electrochemical sensing and found that a basic activation process involving the partial dissolution of polylactic acid-insulating polymer through DMF contributed to the rise in electroactivity [76]. These electrodes were also established for the electroanalysis of picric and ascorbic acids with successful sensing efficiency. Electrodes made of carbon nanotube (CNT)/zinc oxide (ZnO) and CNT/copper (Cu) blended with PLA were used for electronic tongue research as cyclic voltammetric sensors [77]. Dawoud et al. developed a carbon black-filled acrylonitrile butadiene styrene (ABS) composite strain sensor using FDM, which was capable of analyzing internal stresses [78].

1.7.3. Multi-Material Extrusion (Paste-Based 3D Printing)

1.7.3.1. MME Working Principle, and its Strengths and Weaknesses

The 3D Multi-Material Printing process involves using pastes from various target materials, depositing them additively layer by layer in the same manner as in FDM printers. Paste extrusion-based 3d printers are mainly add-on hardware to modify or build on existing FDM printers. The single, dual, or multiple extrusion heads move in the X and Y directions while the build platform moves in the Z direction. This can be achieved through multiple motion mechanisms to control the movement of the paste extruder and build objects. The Cartesian mechanism is the most common and uses three linear axes (X, Y, and Z) to move the extruder. The Delta mechanism uses three arms that move circularly to control the extruder's movement, while the CoreXY mechanism uses two perpendicular drives to control the movement of the extruder. Upon examining the current devices available, two main types of design for paste and clay extrusion equipment have been identified. The first design resembles a syringe and is either electrically or pneumatically actuated [87]. For those with an electric motor, the rotational motion is converted into linear translation with a drive-screw and nut mechanism or a pinion-rack mechanism [87]. There are open-source devices made using 3D printed parts to modify existing FDM printers with add-on hardware to produce 3D objects using paste-like materials [87]. One example is the Universal Paste Extruder created by RichRap, which operates using a drive belt mechanism to power the piston that pushes the feedstock through the nozzle [88]. However, there are limitations to this design. The extruder tube can only hold a limited amount of feedstock, and it is unable to feed more material during the fabrication process, resulting in limited productivity for small-volume objects. The use of linear motion to drive the piston may lead to the usage of linear guides, which can increase the weight and center of gravity and affect the dynamic performance of the 3D printer [87]. Additionally, the feedstock retraction function, which is specific to the material extrusion process, cannot be utilized during fabrication with the use of pneumatically actuated pistons or other mechanisms, such as the belt drive used in the Universal Paste Extruder. The feedstock retraction function enhances the quality of 3D printed objects by letting the

extruder retract a small volume of feedstock before repositioning the extruder head, guaranteeing no material leaks onto the part during the printing process [87]. An alternative design to the piston-type extruder is the electrically actuated auger screw design [89]. This design uses a separate container to store pressurized feedstock, which is then fed to the extruder. This design enables the continuous feeding of material during the fabrication process, allowing for the creation of larger objects.

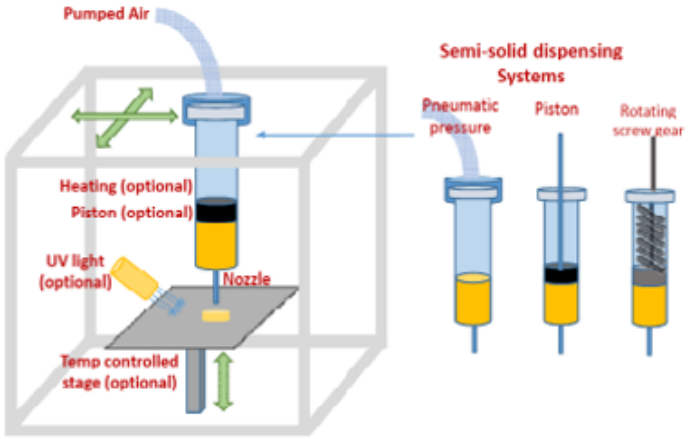

Fig. 18. Schematic Illustration of the 3D Extrusion-Based Printing Technologies [90]

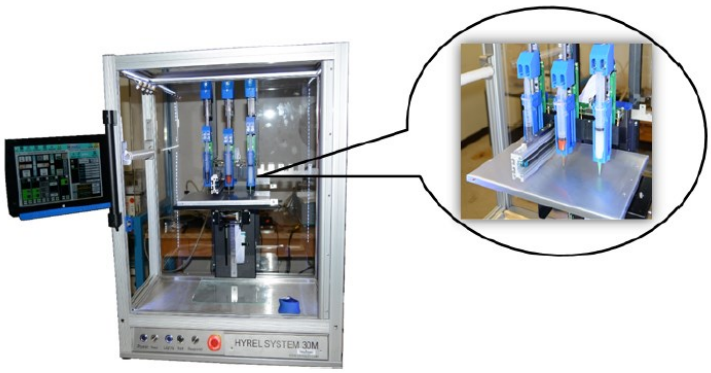

Fig. 19. The Multi-Extruder Paste-Extrusion 3D Printer [91]

However, this feature also comes with an increased complexity of the AM machine, requiring additional electric motors, pressure sensors, compressors, pneumatic valves, etc [87]. This additional complexity can make it difficult for the paste extruder to be integrated as a simple replacement for the typical thermoplastic extruder used in material extrusion applications. Another issue noted is the need for or the complicated process in implementing fine-tuning

options for extrusion parameters. For example, the speed of extrusion and control of the amount of material deposited can be critical for some materials, such as air-drying clays, where the drying process must happen at a specific rate. Conventional syringe-based paste extruders often rely on large nozzle diameters and layer heights for object creation, resulting in a lack of detail and surface finish [87].

Table 3. Comparison Between Existing Syringe-Based Paste Extruders [87]

Model	*Add-On*	*Retraction*	*Heated Build Material*	*Print Speed [mm/s]*	*Build Material Vol. [mL]*	*Min. Layer Height [µm]*	*Nozzle Size [mm]*
Fab@Home Model4	No	Yes	Yes	10	10	100	0.1-1.54
"Universal Paste Extrude" By RipRap	Yes	No	No	20	10	200	0.2-1.54
Discov3ry by Structure 3D Printing	Yes	Yes	No	20	60	200	0.25
Paste & Food Extruder by Printrbot	Yes	Yes	No	15	60	300	1.54

1.7.3.2. Materials Portfolio of MME for EMs Application

Significant advancements have been made in the 3D printing of materials that were previously limited to traditional manufacturing methods, such as scaffolds for tissue engineering, cell cultures, live tissue, food, medical implants, ceramics, types of cement, metals, and composites [87]. Implementing those materials in an AM process has been made possible by using specially designed paste extruders [87]. It is crucial that AM technology stays up-to-date with the latest material advancements. This involves exploring new materials that can be used in the AM process and improving technology to utilize existing paste-like materials. Conductive pastes used in paste extrusion additive manufacturing are crucial materials for building electrical components in electrical machines. Some common examples include silver

nanoparticle paste, silver-filled epoxy, copper nanoparticle paste, carbon-filled epoxy, nickel nanoparticle paste, graphite-filled silicone, aluminum nanoparticle paste, conductive polymers such as PEDOT: PSS, and conductive adhesives such as conductive silver glue. The electrical conductivity, resistivity, and density of these printed materials play a significant role in determining their performance, with higher conductivity and lower resistivity materials generally preferred. Generally, the density of the printed material is positively correlated with its electrical conductivity, meaning that higher-density materials tend to have better conductivity. The viscosity and density of the pastes also affect their printability, with lower viscosity and density pastes being easier to extrude and resulting in smoother prints. In comparison, higher viscosity and density pastes can be more challenging to extrude and result in more irregular prints. To achieve optimal results, selecting a conductive paste with an appropriate viscosity and density is essential, as adjusting the viscosity as needed before printing. These materials offer several advantages in additive manufacturing, including the ability to create complex and intricate electrical components with high precision, flexibility in design and material choice, and the ability to produce components rapidly and cost-effectively. However, there are also some disadvantages to consider, such as the potential for reduced electrical conductivity compared to traditional manufacturing methods, difficulties in achieving consistent and uniform material properties, and limitations in material strength and durability. Ferrite pastes are magnetic materials that can be used in paste-based extrusion 3D printers for building magnetic components in electrical machines. Some typical materials used for ferrite pastes include barium ferrite, strontium ferrite, and nickel-zinc ferrite. These materials exhibit magnetic properties such as high magnetic permeability and low magnetic loss, making them well-suited for applications such as electromagnetic shielding, inductors, and transformers. The magnetic properties of the printed component will depend on several factors, including the composition and size of the ferrite particles, the composition of the binder, and the processing conditions used during the printing process. In general, ferrite pastes offer high magnetic performance and good stability, making them a popular choice for building magnetic components in electrical machines. One example of a magnetic paste used in one study is Poly-Mag paste. It is made of a soft magnetic powder and a thermoset polymer called benzocyclobutene (BCB), which acts as a binder [91]. BCB is known for its low dielectric constant, good thermal stability, and ease of processing. The Poly-Mag paste is formulated

using Permalloy powder with an average particle size of 12 µm and additional organic components to ensure good particle dispersion, flowability, and a viscosity [91]. To create the windings of their magnetic component, they used a nanosilver paste created for chip bonding [91]. This paste must be sintered after printing at temperatures below 250°C to achieve excellent electrical and thermal properties.

Table 4. Electrical Resistivity of Low-Temperature Sintered 3D-Printed Winding and that of Bulk Silver [91]

Material	*Electrical Resistivity* $[10^{-8}\Omega\,.\,m]$
3D Printed Silver Winding	4.8
Pure Silver Wire	1.6

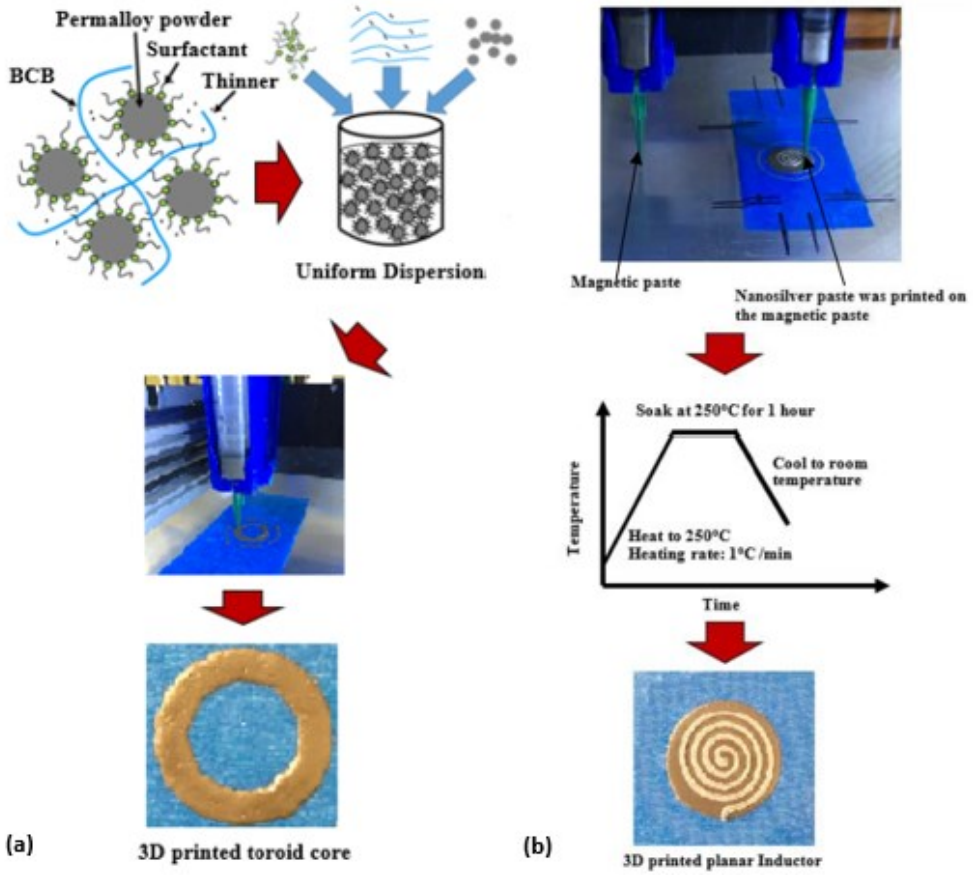

Fig. 20. (a) Low-Temperature Curable Poly-Mag Paste [91], (b) Full Process of Multi-Material Paste Extrusion [91]

Some typical materials used for non-conductive pastes include ceramic materials, such as bismuth silicate [96] and barium titanium [97], and polymer materials, such as epoxy and

silicone. These materials exhibit excellent electrical and thermal insulation properties, making them ideal for applications such as insulation layers, dielectric materials, and heat sinks. Also, these ceramic pastes are used to prevent electromigration and electromagnetic interference in electromechanical devices, thereby improving system performance. Not to mention, ceramic pastes are used for printing passive components such as resistors, conductors, and dielectrics. The printed component's electrical and thermal insulation properties will depend on several factors, including the composition and size of the ceramic or polymer particles, the composition of the binder, and the processing conditions used during the printing process. In general, non-conductive pastes offer high electrical and thermal insulation performance, making them a popular choice for building insulation components in electrical machines. Some of the material development advantages and disadvantages of the paste-based 3d printing process are being managed. The problems of electromigration, such as the high current density in copper conductors in electromechanical devices, are being addressed through the advancement of nanoparticle-based dielectric and conductive inks/pastes. Researchers have developed UV-curable inks/pastes containing oligomers, monomers, photo-initiators, colorants, and additives that effectively minimize electromigration.

1.7.3.3. Applications and Opportunities

One research study showed the potential of high-performing additive manufacturing technology components through the use of magnetic paste-based 3D printing. Two magnetic pastes, one a low-temperature curable iron paste (over 250°C) and the other a high-temperature steerable ferrite paste (over 900°C) were utilized to produce a constant flux inductor and a planar inductor. The study results indicate that the 3D-printed inductors have an inductance and DC resistance that aligns well with the finite element analysis (FEA) simulated models. This proves the opportunities for an AM process to produce low-cost, functional electrical components for EMs. Furthermore, Ding and colleagues have utilized a high-temperature steerable NiZn ferrite paste to create a transformer through layer-by-layer 3D printing. The performance of the fabricated transformer was compared to commercially available components, and the results showed the potential for producing high-performance magnetic components using 3D printing, allowing for the exploration of unique shapes,

materials, and dimensions to enhance component efficiency and energy density. Although the utilization of paste-based extrusion has been seen primarily in lower-end applications such as PCB transformers, low-power transformers, and microchannel heatsinks in microelectronics , it has now expanded to higher-end applications like current transformer parts for technical education and kilovolt pulse transformers for radar transmitters. This growth has the potential to advance the integration of this AM process and lead to the manufacture of high-voltage power transformers for practical power system applications in the future. One study highlighted the design of high-performance tooth coils for high-speed switched reluctance machines (SRM) aimed for automotive usage. The primary focus was calculating the conductor losses by considering the eddy current effects caused by pulse-shaped phase currents. The study presented a novel approach for producing ceramic-insulated copper coils using a paste-based multi-material additive manufacturing technique. The comparison between conventional resin-insulated coils and ceramic-insulated windings was evaluated based on the SRM characteristics at a specific operating point and considering the thermal behavior of the winding structures. The results indicated a considerable increase in the current loading capability of the proposed winding structure and higher operating temperatures for the machine. Paste-based multi-material additive manufacturing technique offers the ability to create electrical machine windings with intricate shapes. This is achieved by integrating electrical insulation directly onto the conductors, which is essential for low-voltage applications. One study highlighted the design of windings for electrical machines using multi-material AM, showcasing the design versatility and possible performance improvements. The study used a Permanent Magnet generator as a demonstration. The benefits of incorporating shaped profile copper conductors with ceramic insulation in the windings were analyzed in terms of thermal behavior and power losses, revealing the substantial potential for this manufacturing method in such applications. Furthermore, in a recent study, a flexible coreless transformer was printed using paste-based extrusion AMT. This type of transformer can be used in various applications for RF band, such as voltage conversion and impedance matching for maximizing power transfer.

2 Design and Implementation of a Dual Paste Extruder for an Existing 3DP

2.1 Design Considerations

There are several important factors to consider when designing a device that can replace the thermoplastic material extruder on a typical desktop extrusion 3D printer. The first of these involves the electromechanical components of the thermoplastic filament extruder. Many desktop material extrusion printers utilize stepper motors for feeding the material into a heated nozzle that is controlled using a temperature sensor, which is vital for this study's design considerations. The printer also requires electronics for controlling components such as the stepper motor drivers, mechanical end-stops, ADCs for temperature control, voltage regulators, and relays for heating element switching. Another factor is the size of the 3D printer and the constraints placed on the dimensions of the extruder carriage and the mass allowed on the axis holding the extruder. Additionally, major 3D printer manufacturers develop proprietary Software that cannot be used for setting up different extruder types, so the only option is to use open-source firmware and software.

2.2 VoxeLab Aquila 1st Edition Assembly

This Cartesian-style FDM 3D printer equipped with a single extruder is used to implement the paste extruder in this study. The printer has a maximum build volume (mm) of 200mm ×200mm ×200mm and includes dual T8 (8 mm) lead screws for improved spatial control of the Z-axis. Also, the printer has four stepper motors, one for each axis (X, Y, and Z) and one for the filament extruder. Also, it has the necessary electronics, including low-current stepper motor drivers and Analog-to-Digital Converters for temperature control through thermistors. This 3D printer operates on open-source VoxeLab firmware. In order to meet the demands of specific paste-like material applications for building electrical machines, the paste extruder design will employ disposable 60 mL syringes as the feedstock holder, which can be efficiently adjusted to different tube sizes and can be refilled smoothly when required.

Note: Before modifying the VoxeLab Aquila with the new paste dual extruders, multiple design iterations of the extruder were conducted on the CTU FME Lab 3d printer. The goal is to check the feasibility of the needed dual extruders by experimenting with all needed design requirements, Hardware add-ons, connectivity between Hardware and Software, and printing parameters of the selected printing materials. The only difference between the two printers is the motion mechanism, where the CTU FME Lab Printer is an XYCore, and the VoxeLab Aquila is a Cartesian-style printer. This difference can be handled in the firmware configuration.

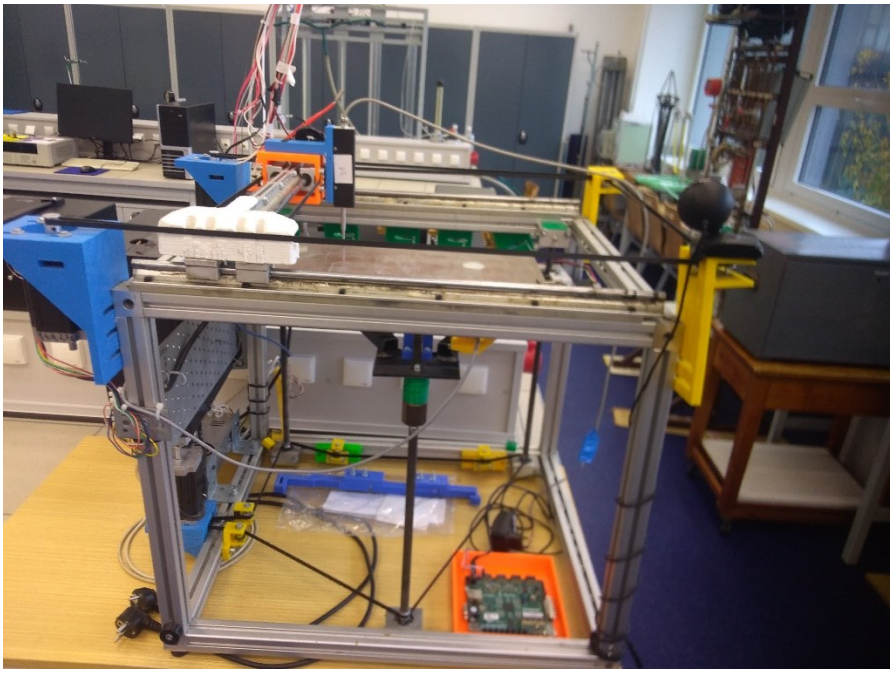

Fig. 21. CTU FME Lab 3D Printer

2.3 Multi-Material Paste Extruder Design

The universal paste extruder design was modified based on the original extruder design of Ofer Levinger. This design is open-source and shared on https://www.thingiverse.com. Below in Fig.21 is the complete assembly of Levinger's design, which later was modified to suit the modified printer and extrusion application needs for this study.

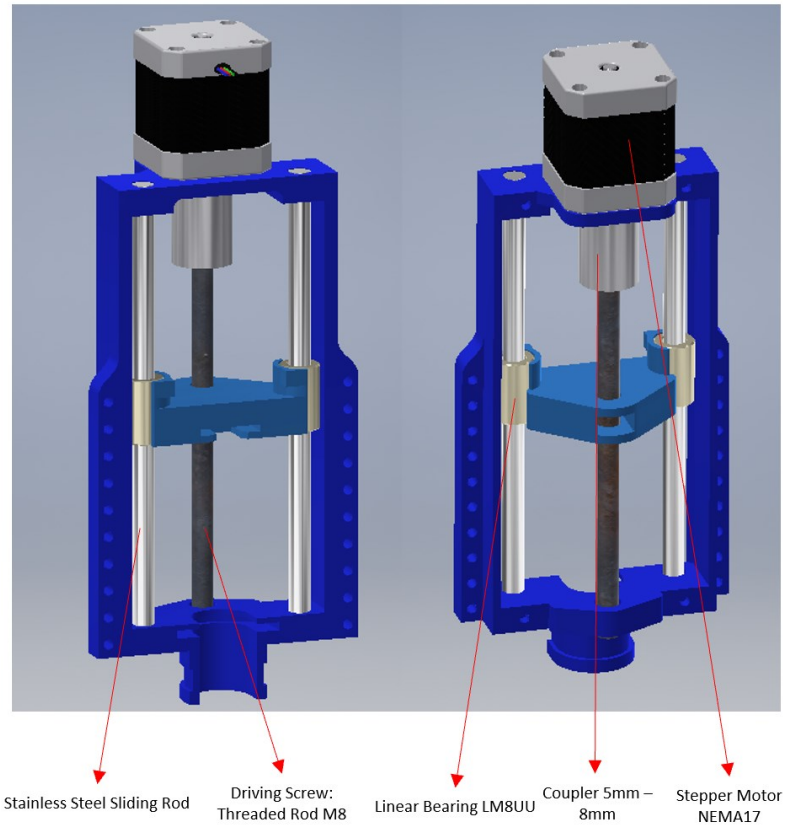

Fig. 22. Levinger's Universal Paste Extruder Full Assembly []

In Levinger's design, the paste extruder uses one of the stepper motors that initially came with the thermoplastic material extruder, which can lower the need for extra modifications on the 3d printer. The stepper motor is a NEMA17-sized motor typically used in desktop 3D printer extruders. The stepper motor is used in 200 micro steps per turn setting. The stepper motor is directly mounted on the extruder's holder, which can decrease the complication of the build. The motor's shaft is connected to the drive screw through a 5-8 mm coupler.

To drive the feedstock through the nozzle, a lead screw and nut control the syringe plunger via a designed component (Plunging Driver) that can allow the extrusion and retraction of the paste material based on the rotation control of the stepper motor. In the first iteration of the extruder design (Levinger's original design), the plunging driver used two linear guides and bearings while the nut was pre-tensioned against the lead screw. This allowed to stop the lead screw from rotating with no effect. The spacing between the threads on the lead screw is 1.25mm.

2.3.1. 1st Design Iteration

The original universal paste extruder shown in Fig.22 was modified to be mounted firmly on the printer shown in Fig.21. Additional mounting piece was designed and added to the full assembly of the extruder, as shown below in Fig.23. The design was tested, and it was found that some modifications are needed. The feedstock syringe is placed tightly between the mounting piece and the extruder, which will obstruct the refilling of the printing material. Besides, the high-viscous printing material caused permanent deformation on the extruder, as shown below in Fig.23. As a result, a higher torque stepper motor is considered to overcome the extrusion of the high-viscosity paste.

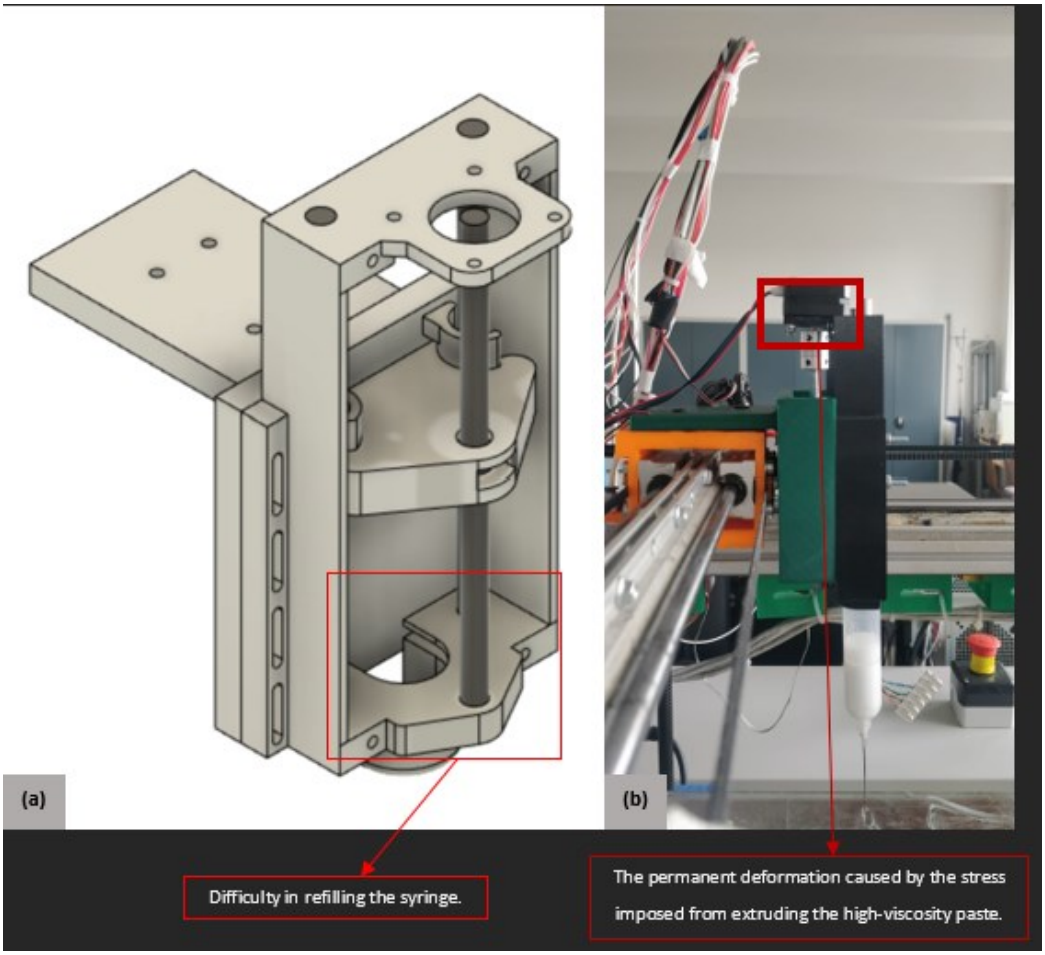

Fig. 23. 1st Design Iteration: (a). The Full Assembly of the Extruder on Fusion360, (b) Testing the Extruder on CTU FME Lab 3D Printer

2.3.2. 2nd Design Iteration

In this design, a bigger motor mounting space was considered for the higher torque motor, and the material feedstock syringe cavity was flipped for ease of refilling, as shown below in Fig.24. Additional support for the motor was added to absorb the emerging stresses that can arise from extruding high-viscous pastes. The design was tested, and it was seen that there was a slight misalignment between the screw drive and the motor shaft due to the not-so-accurate coupling during assembly and the way the linear guide bearings were attached to the plunging driver. Therefore, when the pressure increased in the extrusion process, the plunging driver tilted due to this misalignment. As a result, an additional bearing at the bottom end of the drive screw was considered, plus a new design for fitting the bearings directly in the plunging driver was reviewed.

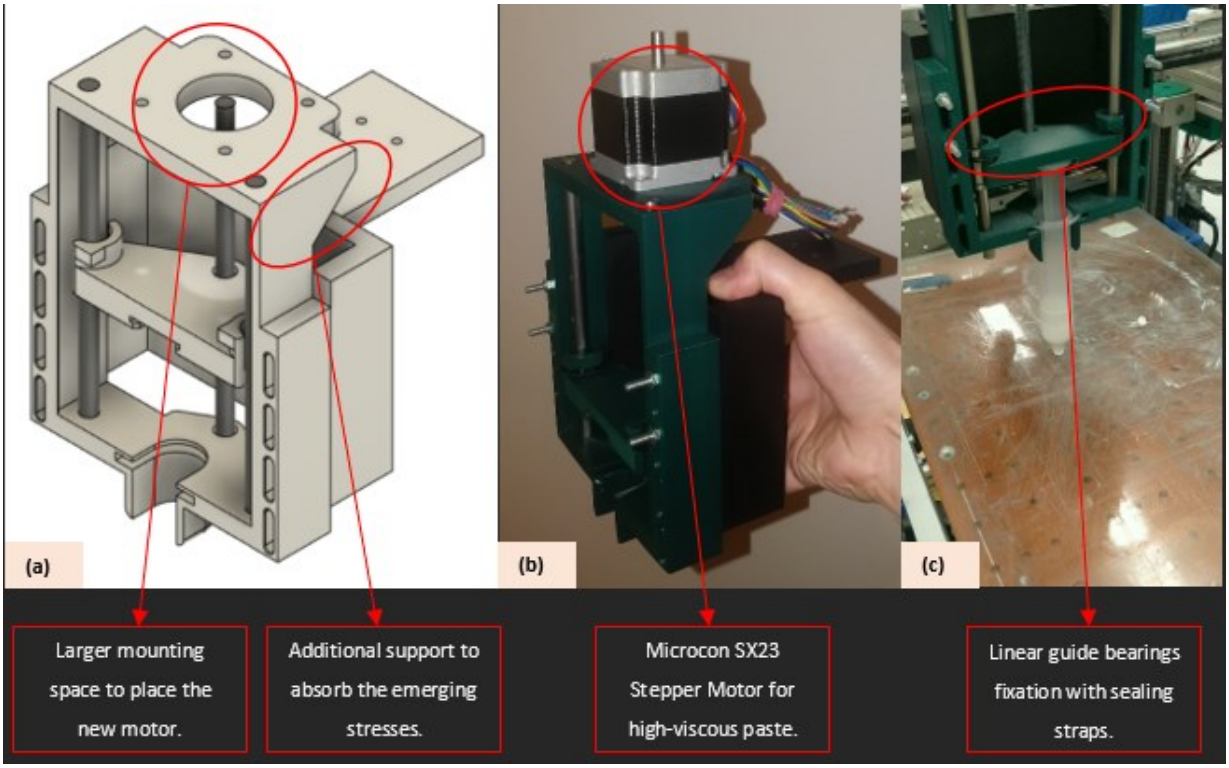

Fig. 24. 2nd Design Iteration: (a) The Full Assembly of the Extruder on Fusion360, (b) Full Assembly with Microcon SX23, (c) Linear Guide Bearings Fixation to the Plunging Driver

2.3.3. 3rd Design Iteration

The considered corrections from the previous iteration test were implemented for this design iteration. New fit holes for the linear guide bearings and a T-nut were added to the plunging driver to increase stability when the pressure starts to accumulate from the highly viscous printed material. A space for an additional bearing at the bottom of the lead screw was added to eliminate the misalignment of the motor shaft and the lead screw during assembly. Lastly, an additional extruder was added for printing different materials simultaneously. For holding the dual extruders, a U-bracket was designed to sit on the linear guides of the X-Y axes. The dual extruders were tested and showed acceptable strength and stability during the extrusion of the printing material.

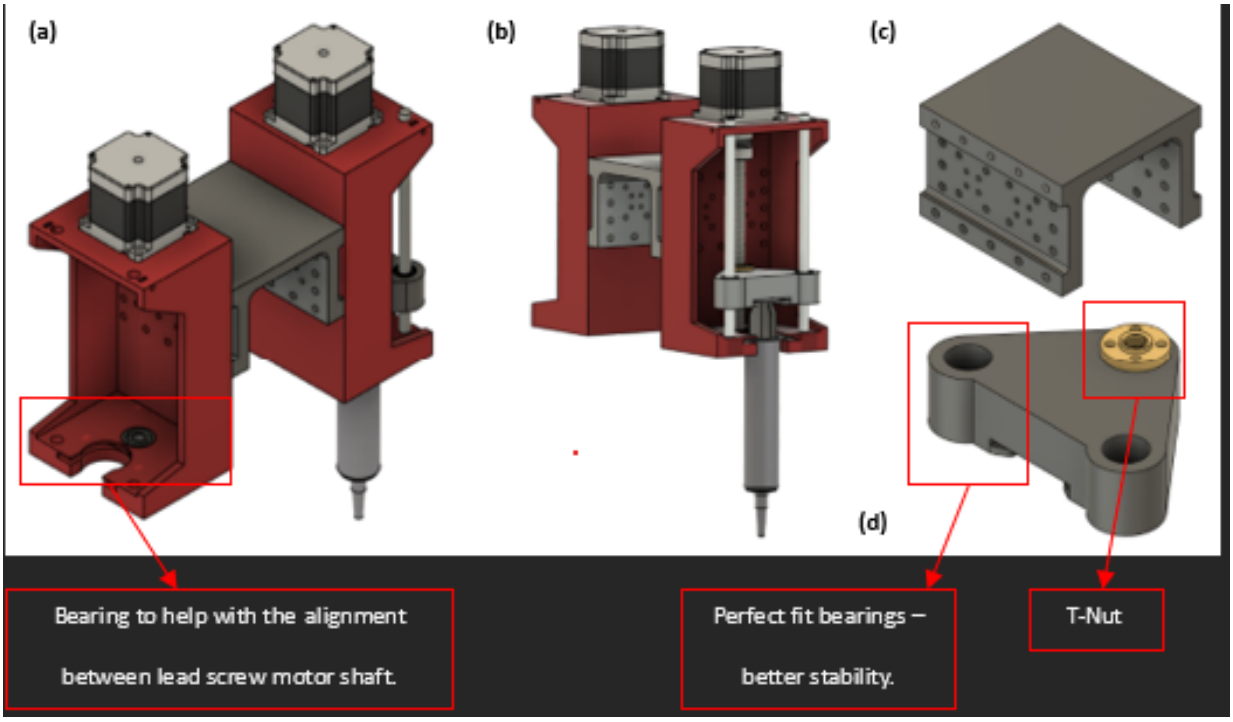

Fig. 25. 3rd Design Iteration: (a) Front Side - Full Assembly of the Extruder on Fusion360, (b) Back Side - Full Assembly of the Extruder on Fusion360, (c) U-Bracket, (d) Plunging Driver

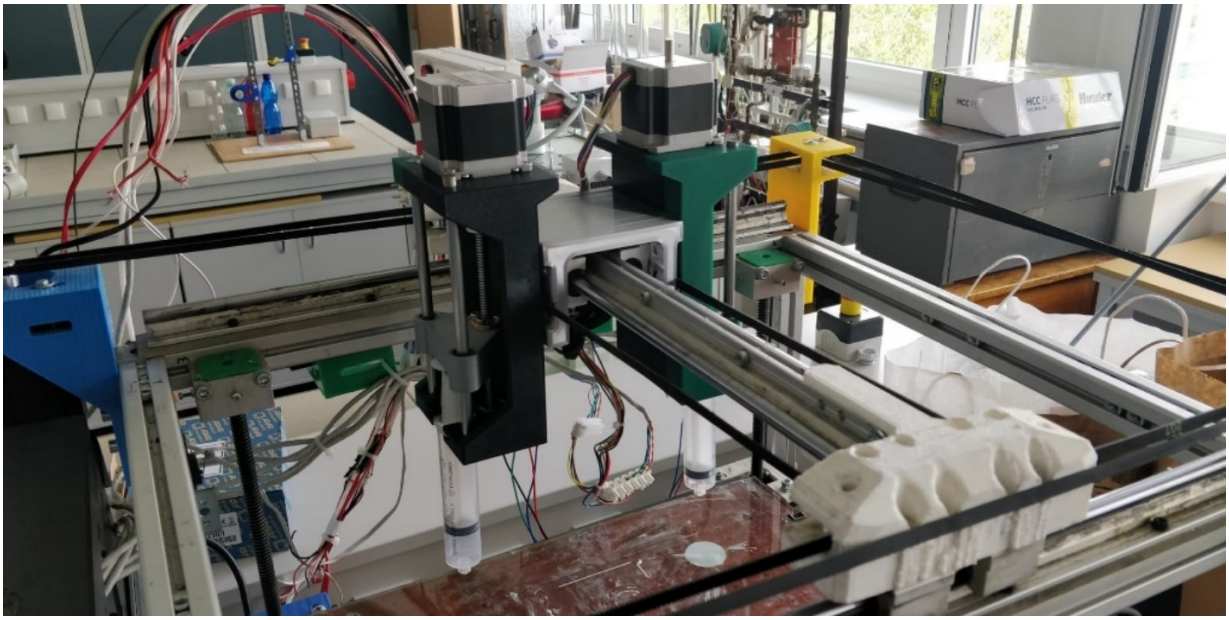

Fig. 26. 3rd Design Iteration: Testing on CTU FME Lab 3D Printer

2.3.4. 4th Design Iteration

This design was made based on the understanding gained through testing on the CTU FME Lab printer to create the best extruder to fit the VoxeLab Aquila printer. The main change in this design was removing the linear guides driving the plunging driver and replacing them with a direct plunging method to reduce the overall size of the extruders to create enough printing space on the printer bed. This design's total printing space is 80mm x 80mm x 80mm. Besides, removing those guides reduced the overall weight because the two extruders are placed next to each other for this build. A small fin on the direct plunger was added to eliminate rotating the plunger housing when extrusion pressure is high. A special mounting piece was designed to hold the two extruders on the X-axis linear guide, where the original Aquila printer's filament extruder was placed. The design of this multi-material extruder showed adequate performance when tested.

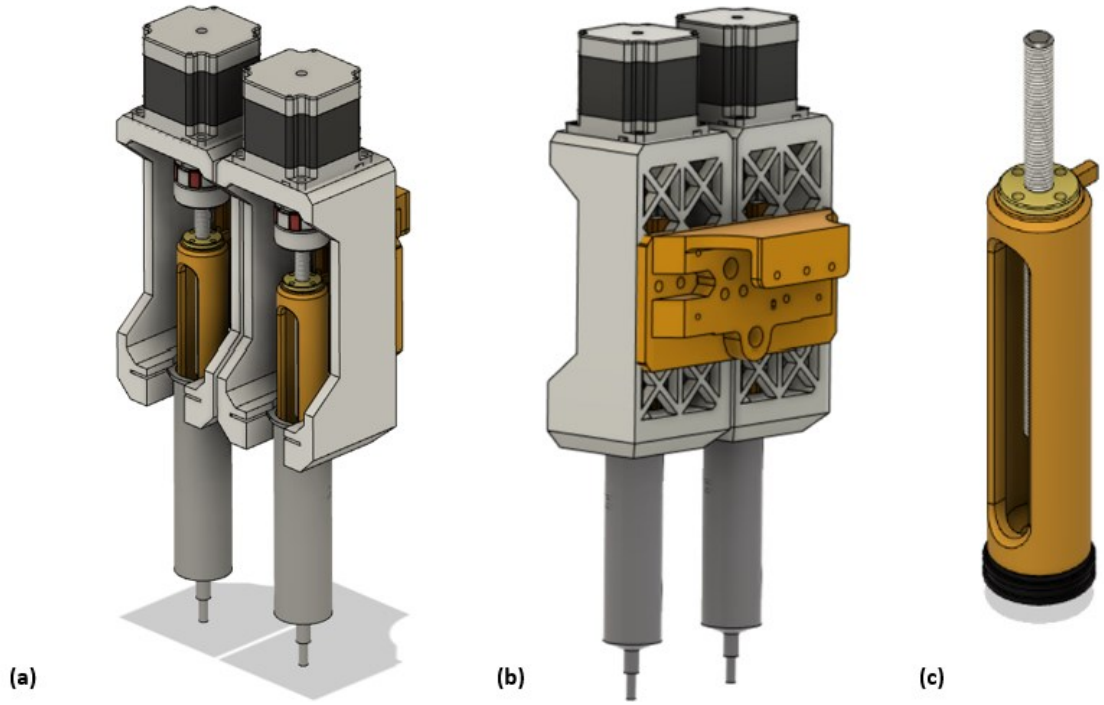

Fig. 27. 4th Design Iteration - Aquila Printer Multi-Material Extruder: (a) Front Side - Full Assembly of the Extruder on Fusion360, (b) Mounting Piece, (c) Direct Plunging Method

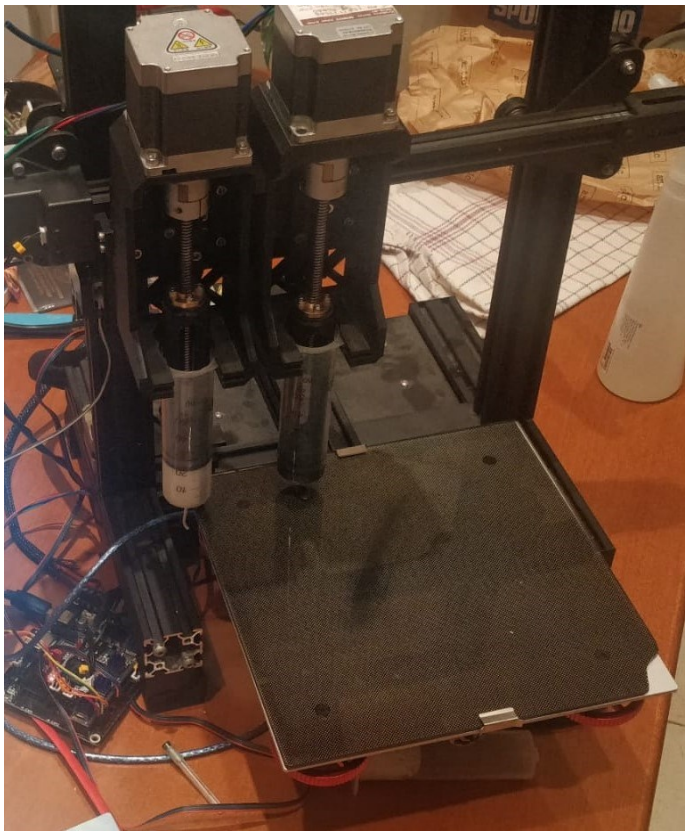

Fig. 28. 4th Design Iteration Testing and Implementation

2.4 Hardware Description

The basis for the multi-material extrusion setup is a fully assembled (RepRap) VoxeLab Aquila 1st Edition. The conversion towards a paste printer consists of firmware (Marlin) modifications (following chapter) and the replacement of the plastic extruder with the newly designed dual paste extruder (following chapter). The paste printing concept is based on a drive screw controlled by a stepper motor driving the plunging part for paste deposition. Due to the open and modular nature of the extrusion parts, modifications to the "syringe holder" (see Fig. 3.1, part (2)) allow an adjustment regarding different syringe diameters and volumes. Subsequently, it allows gaining control of the amount of hydrogel deposited, following the principle: small diameter syringe >> small amounts of paste deposition >> slow printing of geometries of refined elements. <Or> Large diameter syringe >> large amounts of paste deposition >> fast printing of geometries with bold elements.

In this study, the approach was optimized using syringes with a volume of 60 mL. Additionally, path planning software ("Prusa Slicer") was used. This software allows the arrangement of the 3d printing information of the 3d CAD model. It creates a path to deposit the paste with the preferred tracks to ensure the created 3d object preserves the designed details without any errors in its geometry.

The designed approach for paste extrusion in this study comes along with some strengths:

- The RepRap basis and GPL license allow personal modifications, and they are well-documented and driven by a large community.
- The open-source software ('Prusa Slicer') adds crucial parameters such as nozzle diameters, material and printer settings, and options to import customized and standard designs (e.g., transformers).
- The use of Marlin Firmware (an open-source firmware) is developed by a community of volunteers and is released under the GNU General Public License. It allows running the microcontroller board of the 3D printer, which is compatible with a wide range of 3D printer hardware and helps control various printer components, including the stepper motors, extruder, and temperature sensors.

- The extruder conversion is economically feasible, costing around 150€, and allows personal modifications/improvements thanks to the GPL license.

2.4.1. Build Design Files

Table 5. Build Design Files

	Design File Name	*Design File Type*	*Location of file*
1.	***Main Housing***	SETP & STL	Author (Index)
2.	***Adapter Bracket***	STEP & STL	Author (Index)
3.	***Plunger***	STEP & STL	https://www.thingiverse.com/thing:3487917
4.	***Plunger Guide***	STEP & STL	Author (Index)
5.	***Micron SX23-1414***	STEP	https://grabcad.com/library/microcon-sx23-1414-1
6.	***T8 Lead Screw***	STEP & STL	Author (Index)
7.	***Lead Screw Nut***	STEP	https://grabcad.com/library/tr8x8-4-8mm-4-start-lead-screw-nut-1
8.	***Coupler***	STEP	https://grabcad.com/library/flex-couplers-spring-and-rubber-insert-style-1
9.	***60mL Syringe***	STEP	https://grabcad.com/library/syringe-60ml-2
10.	***Y-Axis Limit Trigger***	STEP & STL	Author (Index)

- All open-source CAD models are open source for private use which includes educational purposes without requiring consent from the author of the model.

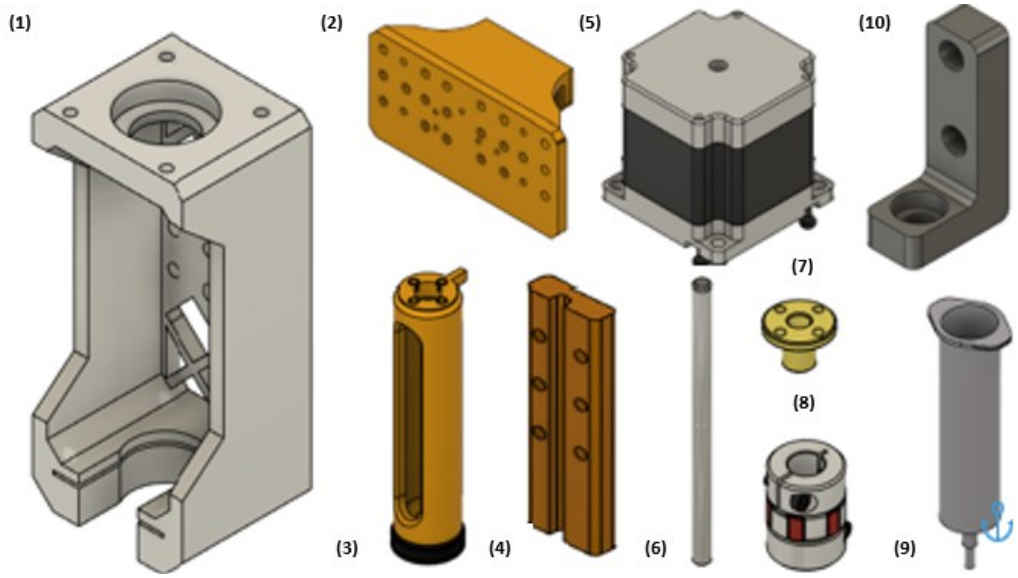

Fig. 29. The Extruder Modification Consists Of: (1) Main Housing, (2) Adapter Bracket, (3) Plunger, (4) Plunger Guide, (5) Microcon SX23, (6) T8 Lead Screw, (7) Lead Screw Nut, (8) Coupler, (9) 60 mL Syringe, (10) Y-Axis Limit Triger

2.4.2. Brief Description of Each Part

- **Main Housing**: Custom 3D printed (PLA plastic) bracket to house the main assembly of the extruder.
- **Adapter Bracket**: 3D printed (PLA plastic) bracket made of two parts. Firstly, an adapter that attaches the Main Housing assembly onto the existing printer's x-axis carriage. Secondly, a bracket to join the first adapter with the dual extruder Main Housing.
- **Plunger**: 3D printed (PLA plastic) plunger to extrude the paste out of the syringe.
- **Plunger Guide**: 3D Printed (PLA plastic) guide for the plunger to prevent it from rotating in the syringe.
- **Micron SX23-1414**: Nema-23 Motor to power as the extruder force.
- **T8 Lead Screw**: T8 lead screw is responsible for torque delivery from the Nema motor to the plunger.
- **Lead Screw Nut**: T8 Nut with a pitch of 2mm.
- C**oupler**: High torque coupler 8mm – 8mm.
- **60mL Syringe**: 60mL volume syringe where the paste is filled and extruded from the nozzle with no needle attachment.

- Y-Axis Limit Trigger: Custom 3D printed (PLA plastic) acting as the x-axis limit switch trigger.

2.4.3. Bill of Material (BOM)

Table 6. Dual Paste Extruder Bill of Material

Designator	*Component*	*Number of Units*	*Cost Per Unit [EUR]*	*Total Cost [EUR]*	*Source of Materials*	*Material Type*
M3 x 5,7mm Threaded Inserts	ISP-GWEM3	24	0.10	0.24	3DJake	Brass
M4 x 6,35mm Threaded Inserts	ISP-GWEM4	8	0.18	1.44	3DJake	Brass
Stepper 2-Phase Motor 1.3Nm	57CM13	2	34	68	CNC Shop CZ	-
Flexible Coupling 6Nm	LK20-C25	2	14.52	29.04	CNC Shop CZ	-
Lead Screw						
T8x2mm Lead Screw Nut	B07QWCRCQZ	2	4.80	9.60	Amazon	Brass
60mL Syringe	N/A	2	0.75	1.5	Local Pharmasist	Plastic
M3 Bolts	B08GCKPWRC	10	0.02	0.2	Amazon	304 Stainless Steel
M4 Bolts	B08GCKPWRC	24	0.02	0.48	Amazon	304 Stainless Steel
BigTree SKR 2 V1.1 Control Board	N/A	1	75	75	3DJake	-
VoxeLab Aquila V1 3D Printer	N/A	1	175	175	VoxeLab	-
TMC 2209 V1.3 Stepper Motor Drivers	BIQU-ZZB000316	5	7.16	35.8	3DJake	-
PolyLite PLA Filament Roll	PM-PA02015	1	30.6	30.6	3DJake	PLA Plastic

2.4.4. Build Instructions

The majority of the Dual Paste Extruder is 3D printed from PLA filament. All STL files have been prepared and saved in their intended printing orientation. During the printing process, supports for specific components is required. All parts are recommended to be printed with 60% infill and three perimeters with a layer height of 0.25 mm. Some print settings may vary depending on the printer used.

1) Adapter Bracket

- Melt 4xM3 threaded inserts using a soldering iron into their designated holes from the front side of the Adapter Bracket (A), as shown with the blue arrow in Fig.30 (a).
- Melt 2xM4 threaded inserts into their designated holes, as shown with the red arrow in Fig.30 (a).
- Melt 3xM4 threaded inserts into the back of the Adapter Bracket (A), as shown with the orange arrow in Fig.30 (b).
- Melt 24xM4 threaded inserts on the front side of the Adapter Bracket (B), as shown with a yellow arrow in Fig.30.

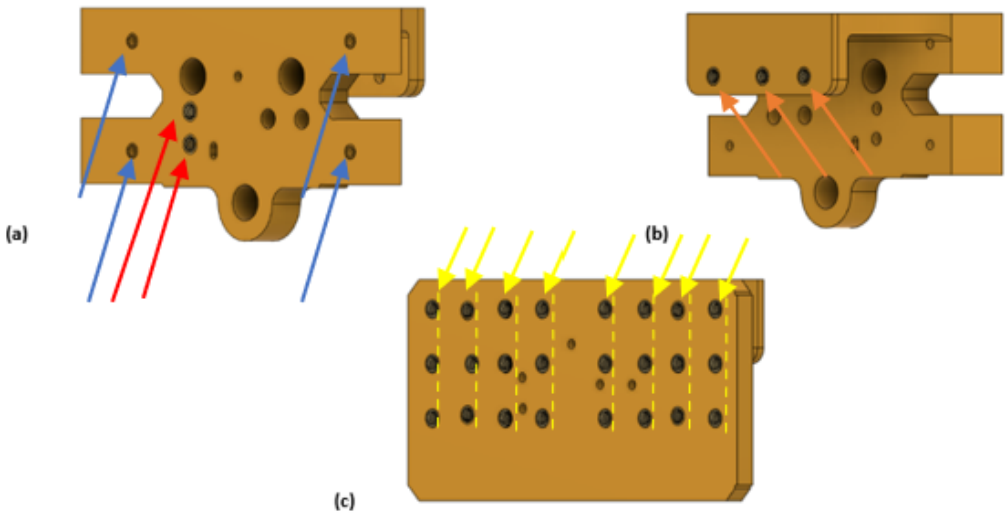

Fig. 30. Adapter Bracket: (a) Adapter Bracket (A) - Front Side, (b) Adapter Bracket (A) - Back Side, (C) Adapter Bracket (B)

2) Main Housing

- Melt 8xM3 threaded inserts using a soldering iron into their designated holes on the Main Housing Assembly, as shown with the blue arrow in Fig.31(a) for the appearing bolts in the figure. The Nema 23 motors will later be bolted down into those holes.
- Bolt down the Main Housing assembly (two parts) onto Adapter Bracket (B) using the threaded inserts placed in previous steps, as shown with the red arrow in Fig.31(b).
- Bolt down both Nema 23 Motors onto the Main Housing assembly, as shown with the blue arrow in Fig.31(b) for the bolts appearing in the figure.

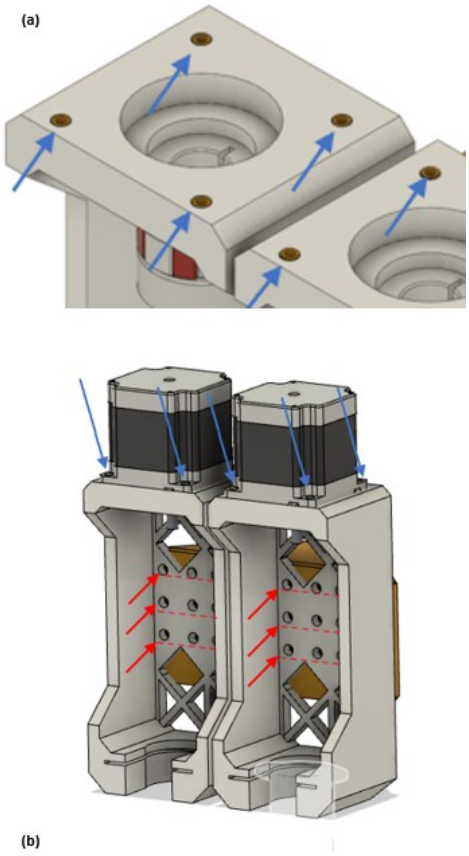

Fig. 31. Main Housing: (a) Motor Mounting Area, (b) Bracket Connection to the Adapter Bracket

3) Plunger Guide

- Bolt down the plunger guide onto the main housing using the threaded inserts placed in the previous steps, as shown with the red arrow in Fig.32.

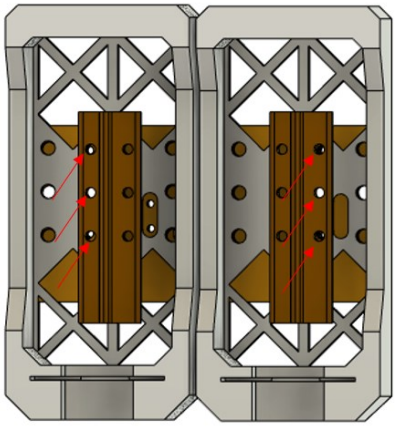

Fig. 32. Plunger Guide Mounted to the Main Housing

4) Plunger

- Melt 4xM3 threaded inserts into each of the two plungers, as shown with the red arrow in Fig.33(a).
- Bolt down the T8 Lead Screw nuts onto both plungers, as shown with the blue arrow in Fig.33(b).
- Bolt down the Lead Screw onto both the T8 nuts, as shown with the red arrow in Fig.33(b).
- Attach the seal to the bottom of the plunger, as shown with the yellow arrow in Fig.33(b).
- Place the Ceramic and Conductive pastes in their respective syringes.
- Place the plunger into Syringe, as shown with the orange arrow in Fig.33(c).

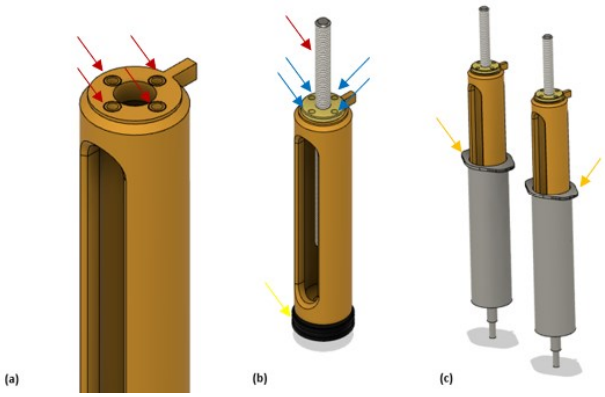

Fig. 33. Plunger: (a) Plunger, (b) Bolting T-Nut and Lead Screw into the Plunger, (c) Inserting Plunger to the Syringe

5) Extruder Full-Assembly

- Place the Lead Screw into the flex coupler and tighten the coupler's bolts, as shown with the red arrow in Fig.34.
- Extrude until the paste has a continuous smooth flow to remove any air gaps in the syringe.

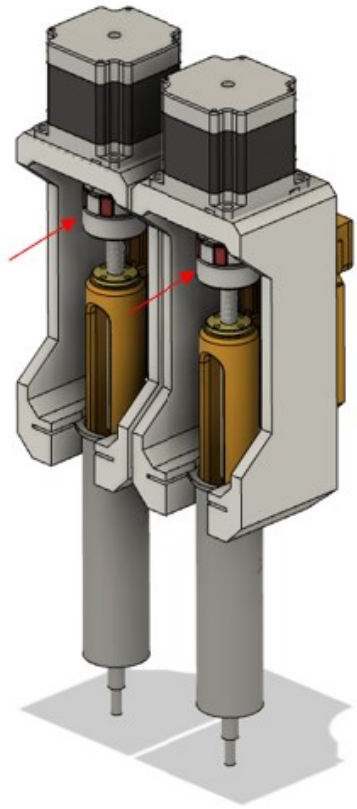

Fig. 34. Extruder Full-Assembly

3 Dual-Extruder Build Verification

3.1 Materials Suitable for 3DP of EMs Using Paste-Extrusion

For 3DP of EMs and particularly printing of coreless transformers, as this is the target in this research, materials such as conductive and non-conductive pastes are the main elements used in the fabrication process. Therefore, a review of available -off the shelf- (ready-to-buy) conductive and non-conductive materials is essential to select the suitable material in terms of viscosity, resistivity, operating temperature, and curing temperature compatibility between the two types of materials. Since the conductive and non-conductive pastes will be cured together after printing, mainly with heating (sintering), it is crucial to have the two materials' curing temperatures ranges in the vicinity of one another. For conductive pastes, the researched materials are mainly silver-based pastes. They are the standard option for screen printing of PCBs and electronics. Silver pastes can be used for the extrusion method designed and shown in the previous chapters. In this material review, considering different materials, such as copper, were evaluated. Unfortunately, with the needed material properties, Silver is the ubiquitous choice. Below, in Table.7, the required information for material suitability for 3DP of conductive elements in EMs, material post-processing, and material characteristics when operating after fabrication are presented. As for non-conductive pastes, there are different types of materials available in the market that can serve as insulators in EMs. Some of the mentioned in the review are ceramics, polymers, and resin-based materials. The primary factors for these materials to function in EMs applications, such as curing and operating temperatures, are discussed and presented in Table.8. Assessing the options selected in the material review will be based on the material's viscosity. Paste viscosity we are looking for 80 to 110 [Pa. s]. This viscosity range will allow printing not to agitate the material to disperse and allow for shape and bulk formation. ***Note:*** Higher paste viscosities can still be used, but higher ranges will affect the fluidity of the paste, which can directly affect the printing speed, thus, fill density too. To have good quality print, printing conditions must be optimized.

3.1.1. Conductive Pastes Review

Table 7. Conductive Pastes Review: Ready-to-Buy Materials

Conductive Pastes; Their Types and Specifications

Company	Description	Viscosity	Conductivity (Resistivity)	Curing Temperature	Operating Temperature	Shelf Life
Polychem UV/EB International Corp.	Thermo-Setting Conductive Silver Adhesive: This silver conductive adhesive is a two-component system with 100% solid content. It has low shrinkage, high electric conductivity, and heat resistance.	Component A: silver paste; Viscosity: @ 30°C, 10 [rpm] Brookfield #52 Spindle: 20,000 [cPs] = 20 [Pa. s]. Component B (hardener): dark brown liquid; Viscosity: @ 30°C, 10 [rpm] Brookfield #52 Spindle: 500 [cPs] = 0.5 [Pa. s]. (*1)	Bulk Resistivity: 0.000015- 0.000060 [Ω.cm]. (*2)	Temperature 115°C x 60 [seconds]. Temperature 130°C x 30 [seconds]. Temperature 140°C x 30 [seconds]. (*3)	High temperature resistance.	12 months from the date of delivery. (*4)
NANOSHEL	Silver Palladium Conductive Paste Molecular Formula: AgPd Stock No: NS6130-12-001045, CAS: N/A	200-500 [Pa. s]	**Needs to be Requested	Dry conditions: Ventilating Baking, Drying Box, 120°C – 150 °C. Sintering: 780 - 880°C (10 Minutes at Peak)	**Needs to be Requested	12 months within its production. Stored at temperature 5-10°C
DZP Technologies	This aqueous silver conductive paste is explicitly created for printing and coating on flexible and stretchable substrates. It can be utilized in a broad range of applications and can be applied using various methods, including manual and semi-automatic screen printers, bar coating, rod coating, and more.	**Needs to be Requested	9[m Ω /sq] @ 25µm thickness when cured at 200 °C	Low-temperature cure at any temperature between 50°C and 200°C.	Thermally stable up to 220°C once cured.	Stored at room temperature with shelf life usually exceeding 12 months.

Conductive Pastes; Their Types and Specifications

Company	Description	Viscosity	Conductivity (Resistivity)	Curing Temperature	Operating Temperature	Shelf Life
Dycotec Materials	Dycotec DM-SIP_3100S: a thermoplastic nanosilver-based paste system. This paste has high coverage, low-temperature sintering temperature, excellent adhesion, and excellent electrical conductivity.	Viscosity after mixing 2-4 [Pa. s] (Cone and plate 50 s^{-1}, 20°C)	Volume Resistivity: <20 [μΩ.cm] at 140°C _ <12.5 [μΩ.cm] at 200°C	Typical drying parameters used are 130-140°C for 20 mins. (*4)	**Needs to be Requested	Containers should be stored in a cool location at a storage temperature between 10-25˚C with lids tightly sealed. The paste shelf-life for an unopened container is 6 months from date of shipment.
TED PELLA, INC	EPO-TEK H2OE is a two-component, 100% solid silver-filled epoxy system. Conductive epoxy consists of a silver resin paste and a silver resin hardener (1:1). It is a smooth, thixotropic paste, 100 % solids system characterized by outstanding high-temperature properties and excellent solvent.	@ 23°C, 100 [rpm]: 2200 – 3200 [cPs] = 2.2 – 3.2 [Pa. s]	Volume Resistivity: @ 23°C: ≤ 0.0004 [Ω.cm]	175 °C: 45 [seconds] 150 °C: 5 [min] 120 °C: 15 [min] 100 °C	Will withstand 200 °C for 1,000 hours	One year at 23 °C
Sun Chemical	C2150107D1: Sliver Platinum Paste 80:20	18 – 25 [Pa. s]	**Needs to be Requested	Dry at 150°C for 10 minutes in a box oven.	800 – 850°C with a dwell time of 10 -30 minutes.	In a sealed container, stored correctly, the shelf life is minimum 6 months from despatch.
	C2060217P3: Silver Topcoat Paste	11 – 18 [Pa. s]	Volume Resistivity: 3.4 x 10^{-6} [Ω.cm]	Dry at 120-150°C for 10-15 minutes.	A peak temperature between 550 - 625°C	In a sealed container, stored correctly, the shelf life is minimum 6 months from despatch.
CREATIVE MATERIALS, INC	The 118-15A/B is a two-part, heat-curing, silver-filled epoxy adhesive that is incredibly easy to use due to its 1 to 1 mix ratio. The system is perfect for making electrical and mechanical attachments on electrical devices and components.	Paste **Needs to be Requested	Volume Resistivity: 0.0001 – 0.0004 [Ω.cm]	90 mins @ 80°C or 15 mins @ 120°C or 5 mins @ 150°C or 45 secs @ 175°C	Useful Temperature Range: -55 to 200	12 months at 25°C, in unopened, unmixed containers

Conductive Pastes; Their Types and Specifications

Company	Description	Viscosity	Conductivity (Resistivity)	Curing Temperature	Operating Temperature	Shelf Life
DUPONT	The ME902 adhesive system is designed to be electrically conductive, and it is well-suited for use in applications that involve stencil printing and syringe dispensing.	40 – 90 [Pa. s]	100 – 150 [mΩ/sq/mil]	Box oven: 120°C for 20 minutes in a well-ventilated oven.	**Needs to be Requested	Shelf life of material in unopened containers is six months from date of shipment.
AEZIS	The EXINNO Paste is a conductive paste that has been specifically formulated for use in screen printing. It is particularly well-suited for printed, electronic products used on film-based substrates and ideal for mass production through ROLL TO ROLL. The EXINNO Paste utilizes advanced technologies for powders, binders, and pastes, allowing it to meet customers' needs in various applications quickly.	EXINK-AS100P: 38000 ± 5000[cPs] = 38 ± 5 [Pa. s] EXINK-FP100P: 150000 ± 10000[cPs] = 150 ± 10 [Pa. s] (Brookfield DV2 + LV Spindle no.15, 20[rpm], 25°C)	EXINK-AS100P: 40 x 10^{-6} [Ω.cm] EXINK-FP100P: 80 x 10^{-6} [Ω.cm]	20 mins @ 120°C	**Needs to be Requested	**Needs to be Requested
Master Bond	Master Bond EP3HTSDA-2 is a single-part, silver-filled system that offers exceptional thermal and electrical conductivity and low thermal resistance with fast curing.	Paste consistency. **Needs to be Requested	<0.001 [Ω.cm]	It cures rapidly at 120-150°C.	The service temperature range extends from -80°F (-60°C) to +550°F (285°C).	The system is not pre-mixed or frozen and has an unlimited working life at room temperature. It can be stored simply in a refrigerator and dispenses smoothly and efficiently.
BIONEER	The AccuPaste™ Silver Conductive Paste is a substance that can be utilized on electrode material to maintain constant conduction properties without the film coating separating, even under high temperatures up to 350°C.	240000 [cPs] = 240 [Pa. s]	7.6 x 10^{-5} [Ω.cm]	30 minutes at 300°C	-20 ~ 300°C	Room temperature **Needs to be Requested

Conductive Pastes; Their Types and Specifications

Company	Description	Viscosity	Conductivity (Resistivity)	Curing Temperature	Operating Temperature	Shelf Life
AREMCO	The conductive adhesive, 556-HT-UHC, can be utilized in various industries to address various electrical, electronic, and thermal design problems.	40000 – 50000 [cPs] = 40 – 50 [Pa. s]	< 0.0003 [Ω.cm]	Recommended: 2 hours at 175°F (80°C). Alternate Cure: 30 mins at 250°F (120°C) or 15 mins at 300°F (150°C).	Continuous: 390°F (200°C) Intermittent: 480°F (250°C)	6 months

(*1) Pot life (after mixing component A and B): 10 min.

(*2) Those numbers are the typical values and are not specifications.

(*3) Depending on the thickness and thermal conductivity of the substrates, the curing conditions shall be adjusted. Since #051908-1R has very good high temperature resistance, prolonged cure time up to three hours will not degrade its properties.

(*4) The paste can be dried using either a convection oven or using IR heating. Drying times may be reduced to achieve the optimum resistivity depending on manufacturing process set-up.

(*4) Recommend Storage Conditions: Stored in a dark, dry, and cool place. Always keep caps closed. Note: Low temperature (-15 °C ~ -20 °C) storage will not affect any of its properties, but the bottle shall not be opened until it returns to room temperature to avoid water contamination to the silver adhesive

- **Conductive Paste Material Review Result**

Fig.35 below shows the materials that fall in the preferred viscosity range. Only four materials fall in this range or higher. Three of the four materials require thinner to reduce their viscosities and make them dispensable using an automated syringe extrusion method. Unfortunately, the cost of those materials to conduct the research experience is high and out of the study budget. Therefore, cheaper options, such as conductive adhesives for circuit tracks repairs, will be considered. However, those materials are hard to be printed using the designed process due to their short working life and limited ability to be applied automatically using the paste extrusion printer.

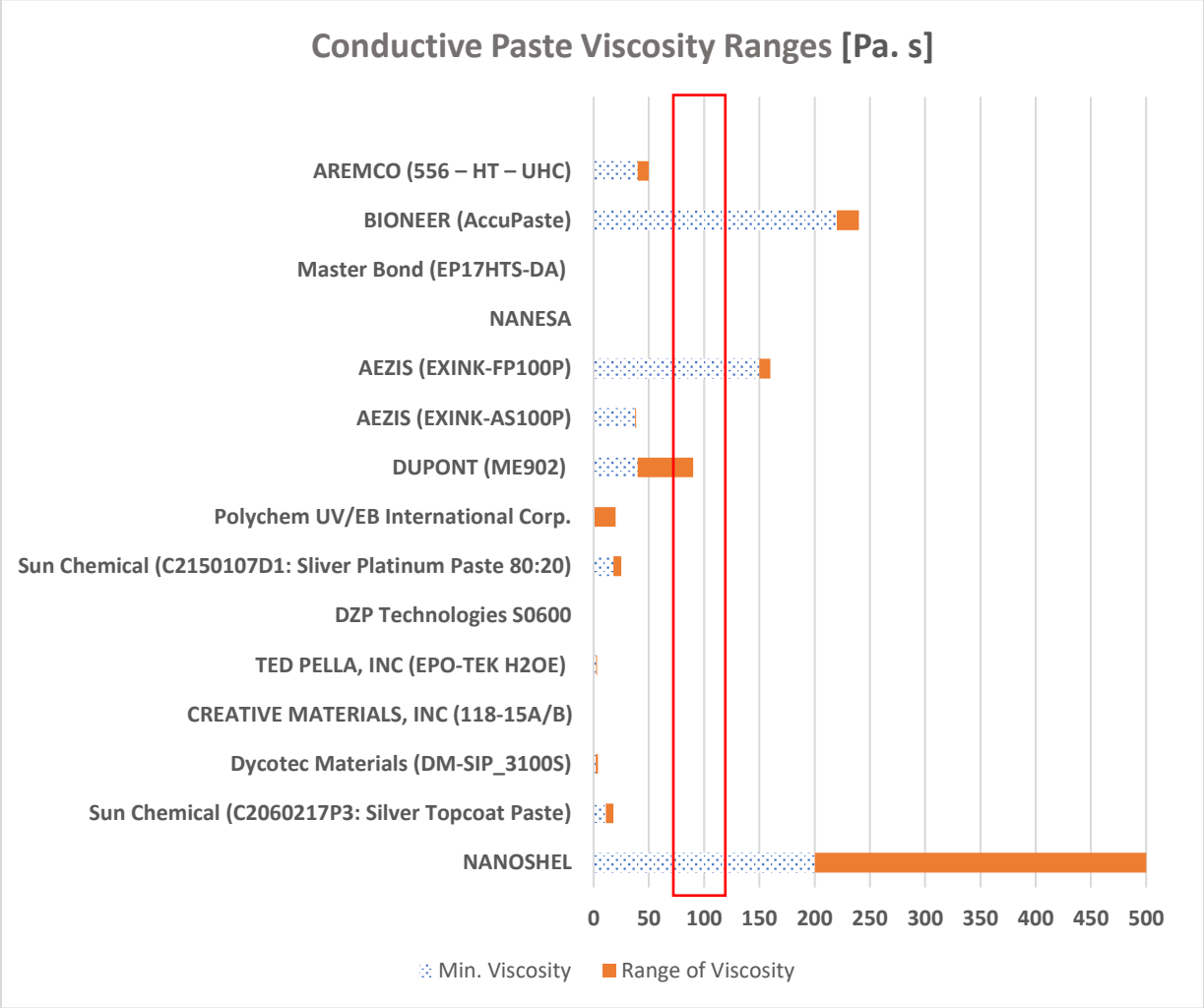

Fig. 35. Conductive Pastes with Acceptable Viscosity Ranges

3.1.2. Non-Conductive Pastes Review

Table 8. Non-Conductive Pastes Review: Ready-to-Buy Materials

Non-Conductive Pastes; Their Types and Specifications

Company	Description	Viscosity	//////////////	Curing Temperature	Operating Temperature	Shelf Life
CREATIVE MATERIALS, INC	The product labeled 122-01 is a solitary electrical insulator made from polyimide that can withstand solvents. It is both an adhesive and a coating and can be applied using a screen-printing method, dipping, or a syringe dispenser.	20000 [cPs] = 20 [Pa. s]	——	Optimal results are achieved by curing the product at 200°C for one hour or 30 minutes at 150°C followed by an additional 30 minutes at 250°C. The product can be utilized on various surfaces and yield good outcomes when cured at temperatures ranging from 150°C to 250°C. To ensure resistance to solvents, it is recommended to cure the product for a minimum of one hour at 180°C.	Useful Temperature Range -55 to +230°C Thermal Stability Good to +325°C	1 year when stored at 23°C or less.
TED PELLA, INC	PELCO® High-Performance Ceramic Adhesive is a dispersion of Aluminum Oxide in an inorganic silicate aqueous solution. It is specially formulated for bonding and sealing ceramics, metals, and quartz for applications demanding electrical and thermal insulation at high continuous service temperatures and low VOC's for ultra-high vacuum.	High viscosity paste – viscosity can be reduced by adding water. Density: 2.3 [g/cc] **Needs to be Requested	——	The product should be air-set for 1 to 4 hours, followed by a 2-hour heat cure at a temperature of 93°C (200 °F) to attain final electrical and mechanical properties. Blistering may occur if the glue line is too thick or heating occurs too rapidly. The temperature has an impact on the adhesive's strength, with higher temperatures leading to almost complete insolubility when exposed to temperatures above 260°C (500 °F). The adhesive must be properly cured before being used at elevated or cryogenic temperatures.	High service temperature. – Up to 1650°C (3000°F), strength improves with temperature.	6 months minimum after receipt of paste – can be increased by adding water and/or removing skin that can form on the top layer.
Selmag Enterprise Co., Ltd.	The Insulation Paste, IF-300TC, is an insulating adhesive that cures with heat and is comprised of a single liquid containing heat-curing acrylic resin.	10 – 15 [Pa. s]	Insulation resistance	Curing conditions: 120～150°C x 30 minutes.	65°C／95% RH ／1000 [hours]	6 months (stored at 25°C).

Non-Conductive Pastes; Their Types and Specifications

Company	Description	Viscosity	///////////	Curing Temperature	Operating Temperature	Shelf Life
	The Insulation Paste IF-300 G1 is a light green insulating paste that cures with heat and is also made up of a single liquid. However, its primary components are heat-curing polyester resin and three Polycyanamide resins.		value; ≧ 10^{11} [Ω.cm]	Curing conditions: 120°C x 30 minutes.	* The above values are the experimental values of the research, not the guaranteed data.	
	///	50 – 80 [Pa. s]		Curing conditions: 120〜150°C x 30 minutes.	**Needs to be Requested	
AREMCO	Aremco manufactures ceramic adhesives that are designed for high temperatures and are made using a variety of ceramics fillers and inorganic binders. They are excellent for bonding, potting, sealing ceramics, composites, graphite, refractory metals, quartz, and semiconductors.	20000 – 90000 [cPs] = 20 – 90 [Pa. s]	Application Temperature 50 - 90°F	Air Set 1-4 hours Heat Cure 200°F (90°C) for 2 hours	Temperature limit 3200°F (1760°C)	6 months
McMASTER-CARR	The ceramic adhesive paste can resist high temperatures and deliver superior electrical insulation. When used on vertical surfaces, these pastes do not sag or drip during the hardening process, while thick liquids can flow into smaller areas and are simple to spread.	190000 [cPs] = 190 [Pa. s] 130000 [cPs] = 130 [Pa. s] 90000 [cPs] = 90 [Pa. s]	___	Room-temperature begins to harden in 20 mins. Reaches full strength in 48 hours.	Maximum temperature 2300°F (1260°C)	6 months
Sun Chemical	This paste has excellent insulation and opacity properties.	10 – 14 [Pa. s]	___	Dry at 130°C for 10-15 minutes in a box oven or using a belt dryer.	**Needs to be Requested	In a sealed container, stored correctly, the shelf life minimum 12 months from dispatch.

Non-Conductive Pastes; Their Types and Specifications

Company	Description	Viscosity	///////////	Curing Temperature	Operating Temperature	Shelf Life
Hunan National Silver New Materials Co., Ltd.	The paste described is a high-temperature overglaze paste that is eco-friendly and suitable for use as an overlay or interbedded insulation. The paste is compatible with a range of ceramic substrates.	30 – 70 [Pa. s]	___	100~150 °C / (8-10 minutes).	850°C fired dielectric overglaze paste.	6 months from date of shipment.

- **Non-Conductive Paste Material Review Result**

Fig.36 below shows the insulation materials that fall in the preferred viscosity range. Three materials are in the range of the required viscosities and are possible to extrude using an automated syringe extrusion method without any additives. Besides, their curing temperatures can go well with the conductive pastes curing temperatures. However, similar to the conductive materials, the cost of those pastes to conduct the research experience is high and out of the study budget. Therefore, cheaper options, such as ceramic clay used for children modeling games, will be selected. This clay requires to be thinned by using any non-conductive thinner material. The best option will be pure water since it is an excellent insulator. The details of material preparation will be discussed in the following chapter.

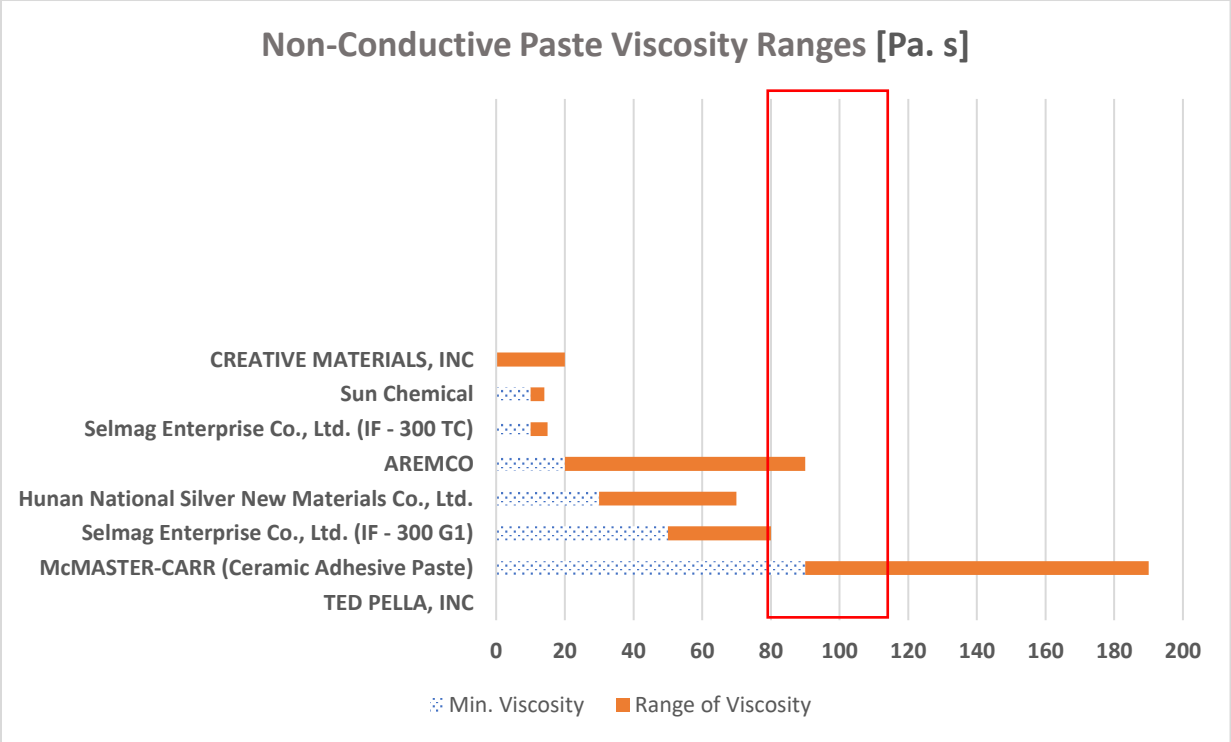

Fig. 36. Non-Conductive Pastes with Acceptable Viscosity Ranges

3.2 Firmware / Software Settings

Marlin Firmware is a GPLv3 open-source firmware for 3D printers that provides various advanced features and customization options. It is designed to run on a range of microcontrollers and is compatible with a wide range of 3D printer models. One of the many features of Marlin is the ability to modify a filament printer to work with a paste or clay extruder. This is achieved by modifying the firmware to adjust the extruder settings and enabling the use of new extruder motors capable of handling thicker, more viscous materials. Once all needed modifications are made, Marlin can control the modified 3D printer and create a wide range of 3D models using different materials beyond just filament. To modify the VoxeLab Aquila printer to be used in paste printing, the "Configuration.h" file in Marlin Firmware was edited. The file contains a range of settings and configuration options for the 3D printer. This file is used to customize various aspects of the printer's behavior, including its hardware settings, firmware features, and user interface options. For this study, in the "Configuration.h" file, the number of extruders, the type of motherboard in use, the type of motor drives, printer bed size, end-stops, and thermistors being used were all set and shown below in the figures. Additionally, various firmware features, such as automatic bed leveling, printing PID tuning, and EEPROM settings, were also modified and presented in this section. The "Configuration.h" file is typically included as part of the Marlin Firmware package and can be edited using a text editor. Changes made to the file will be compiled into the firmware when uploaded to the 3D printer.

- Identifing type of motherboard as BTT SKR V2 RevB.

```
86  // @section machine
87
88  // Choose the name from boards.h that matches your setup
89  #ifndef MOTHERBOARD
90    #define MOTHERBOARD BOARD_BTT_SKR_V2_0_REV_B // Changed baord to SKR 2 Rev B
91  #endif
```

Fig. 37. Type of Motherboard Identification

- Serial port set to -1 for communication via USB.

```
/**
 * Select the serial port on the board to use for communication with the host.
 * This allows the connection of wireless adapters (for instance) to non-default port pins.
 * Serial port -1 is the USB emulated serial port, if available.
 * Note: The first serial port (-1 or 0) will always be used by the Arduino bootloader.
 *
 * :[-1, 0, 1, 2, 3, 4, 5, 6, 7]
 */
#define SERIAL_PORT -1 // Changed from default 0 to -1 for USB serial port
```

Fig. 38. Serial Port Setting

- Changing stepper motor drivers to **TMC2209.**

```
 * Stepper Drivers
 *
 * These settings allow Marlin to tune stepper driver timing and enable advanced options for
 * stepper drivers that support them. You may also override timing options in Configuration_adv.h.
 *
 * Use TMC2208/TMC2208_STANDALONE for TMC2225 drivers and TMC2209/TMC2209_STANDALONE for TMC2226 drivers.
 *
 * Options: A4988, A5984, DRV8825, LV8729, TB6560, TB6600, TMC2100,
 *          TMC2130, TMC2130_STANDALONE, TMC2160, TMC2160_STANDALONE,
 *          TMC2208, TMC2208_STANDALONE, TMC2209, TMC2209_STANDALONE,
 *          TMC26X,  TMC26X_STANDALONE,  TMC2660, TMC2660_STANDALONE,
 *          TMC5130, TMC5130_STANDALONE, TMC5160, TMC5160_STANDALONE
 * :['A4988', 'A5984', 'DRV8825', 'LV8729', 'TB6560', 'TB6600', 'TMC2100', 'TMC2130', 'TMC2130_STANDALONE', 'TMC2160', 'TMC2160_STANDA
 */
#define X_DRIVER_TYPE  TMC2209 // Changed driver to TMC2209
#define Y_DRIVER_TYPE  TMC2209 // Changed driver to TMC2209
#define Z_DRIVER_TYPE  TMC2209 // Changed driver to TMC2209
//#define X2_DRIVER_TYPE A4988
//#define Y2_DRIVER_TYPE A4988
//#define Z2_DRIVER_TYPE A4988
//#define Z3_DRIVER_TYPE A4988
//#define Z4_DRIVER_TYPE A4988
//#define I_DRIVER_TYPE  A4988
//#define J_DRIVER_TYPE  A4988
//#define K_DRIVER_TYPE  A4988
//#define U_DRIVER_TYPE  A4988
//#define V_DRIVER_TYPE  A4988
//#define W_DRIVER_TYPE  A4988
#define E0_DRIVER_TYPE TMC2209 // Changed driver to TMC2209
#define E1_DRIVER_TYPE TMC2209 // Changed driver to TMC2209
//#define E2_DRIVER_TYPE A4988
//#define E3_DRIVER_TYPE A4988
//#define E4_DRIVER_TYPE A4988
//#define E5_DRIVER_TYPE A4988
//#define E6_DRIVER_TYPE A4988
//#define E7_DRIVER_TYPE A4988
```

Fig. 39. Changing Stepper Motor Driver

- Identifiing two extruders available.

```
// @section extruder

// This defines the number of extruders
// :[0, 1, 2, 3, 4, 5, 6, 7, 8]
#define EXTRUDERS 2 // Changed to 2 extruders
```

Fig. 40. Dual-Extruder Identification

- Setting dummy values for extruder 1 and 2 heating temperatures as 25°C.

```
529   *  Custom/Dummy/Other Thermal Sensors
530   *  ------
531   *     0 : not used
532   *  1000 : Custom - Specify parameters in Configuration_adv.h
533   *
534   *   !!! Use these for Testing or Development purposes. NEVER for production machine. !!!
535   *   998 : Dummy Table that ALWAYS reads 25°C or the temperature defined below.
536   *   999 : Dummy Table that ALWAYS reads 100°C or the temperature defined below.
537   *
538   */
539  #define TEMP_SENSOR_0 998 // Changed to dummy 25C for E1
540  #define TEMP_SENSOR_1 998 // Changed to dummy 25C for E2
541  #define TEMP_SENSOR_2 0
542  #define TEMP_SENSOR_3 0
543  #define TEMP_SENSOR_4 0
544  #define TEMP_SENSOR_5 0
545  #define TEMP_SENSOR_6 0
546  #define TEMP_SENSOR_7 0
547  #define TEMP_SENSOR_BED 1 // Changed to temp sensor 1 for bed.
548  #define TEMP_SENSOR_PROBE 0
549  #define TEMP_SENSOR_CHAMBER 0
550  #define TEMP_SENSOR_COOLER 0
551  #define TEMP_SENSOR_BOARD 0
552  #define TEMP_SENSOR_REDUNDANT 0
553
554  // Dummy thermistor constant temperature readings, for use with 998 and 999
555  #define DUMMY_THERMISTOR_998_VALUE  25
556  #define DUMMY_THERMISTOR_999_VALUE 100
```

Fig. 41. Extruders Temperatures Settings

- Enabling bed PID tuning for more accurate bed temperature readings.

```
723  /**
724   * PID Bed Heating
725   *
726   * If this option is enabled set PID constants below.
727   * If this option is disabled, bang-bang will be used and BED_LIMIT_SWITCHING will enable hysteresis.
728   *
729   * The PID frequency will be the same as the extruder PWM.
730   * If PID_dT is the default, and correct for the hardware/configuration, that means 7.689Hz,
731   * which is fine for driving a square wave into a resistive load and does not significantly
732   * impact FET heating. This also works fine on a Fotek SSR-10DA Solid State Relay into a 250W
733   * heater. If your configuration is significantly different than this and you don't understand
734   * the issues involved, don't use bed PID until someone else verifies that your hardware works.
735   * @section bed temp
736   */
737  #define PIDTEMPBED // enabled PID tuning for bed
```

Fig. 42. Printing BED PID Tunning

- Enabling long extrudes up to 400[mm].

```
817  // @section safety
818
819  /**
820   * Prevent extrusion if the temperature is below EXTRUDE_MINTEMP.
821   * Add M302 to set the minimum extrusion temperature and/or turn
822   * cold extrusion prevention on and off.
823   *
824   * *** IT IS HIGHLY RECOMMENDED TO LEAVE THIS OPTION ENABLED! ***
825   */
826  //#define PREVENT_COLD_EXTRUSION // Commented out prevent cold extrusion
827  //#define EXTRUDE_MINTEMP 170 // Commenred out to allow for cold extrusions
828
829  /**
830   * Prevent a single extrusion longer than EXTRUDE_MAXLENGTH.
831   * Note: For Bowden Extruders make this large enough to allow load/unload.
832   */
833  #define PREVENT_LENGTHY_EXTRUDE
834  #define EXTRUDE_MAXLENGTH 400  // CHANGED FROM 200 TO 400
```

Fig. 43. Editing Material Extrusion Length

- Enabling Classic Jerk.

```
/**
 * Default Jerk limits (mm/s)
 * Override with M205 X Y Z . . . E
 *
 * "Jerk" specifies the minimum speed change that requires acceleration.
 * When changing speed and direction, if the difference is less than the
 * value set here, it may happen instantaneously.
 */
#define CLASSIC_JERK // Enabled Classic Jerk
#if ENABLED(CLASSIC_JERK)
  #define DEFAULT_XJERK 10.0
  #define DEFAULT_YJERK 10.0
  #define DEFAULT_ZJERK  0.3
  //#define DEFAULT_IJERK  0.3
  //#define DEFAULT_JJERK  0.3
  //#define DEFAULT_KJERK  0.3
  //#define DEFAULT_UJERK  0.3
  //#define DEFAULT_VJERK  0.3
  //#define DEFAULT_WJERK  0.3

```

Fig. 44. Classic Jerk

- Manual Bed Leveling.

```
/**
 * The "Manual Probe" provides a means to do "Auto" Bed Leveling without a probe.
 * Use G29 repeatedly, adjusting the Z height at each point with movement commands
 * or (with LCD_BED_LEVELING) the LCD controller.
 */
#define PROBE_MANUALLY // Enabled Manual Bed Leveling

```

Fig. 45. Enabling Manual Bed Leveling

- Defining printer bed size and axes software limits.

```
// @section geometry

// The size of the printable area
#define X_BED_SIZE 170  // Changed X axis to 170mm
#define Y_BED_SIZE 150  // Changed Y axis to 150mm

// Travel limits (linear=mm, rotational=°) after homing, corresponding to endstop positions.
#define X_MIN_POS 0
#define Y_MIN_POS 0
#define Z_MIN_POS 0
#define X_MAX_POS X_BED_SIZE
#define Y_MAX_POS Y_BED_SIZE
#define Z_MAX_POS 100 // Changed Z-axis to 100mm
//#define I_MIN_POS 0
//#define I_MAX_POS 50
//#define J_MIN_POS 0
//#define J_MAX_POS 50
//#define K_MIN_POS 0
//#define K_MAX_POS 50
//#define U_MIN_POS 0
//#define U_MAX_POS 50
//#define V_MIN_POS 0
//#define V_MAX_POS 50
//#define W_MIN_POS 0
//#define W_MAX_POS 50
```

Fig. 46. Bed Size and Axes Software End-Stops

- Enabling mesh preview of bed level.

```
1875   */
1876  //#define AUTO_BED_LEVELING_3POINT
1877  //#define AUTO_BED_LEVELING_LINEAR
1878  //#define AUTO_BED_LEVELING_BILINEAR
1879  //#define AUTO_BED_LEVELING_UBL
1880  #define MESH_BED_LEVELING // Enabled Mesh Bed Leveling
```

Fig. 47. Mesh Preview for Manual Bed Leveling

- Enabling EEPROM settings to allow for firmware override.

```
2168  /**
2169   * EEPROM
2170   *
2171   * Persistent storage to preserve configurable settings across reboots.
2172   *
2173   *   M500 - Store settings to EEPROM.
2174   *   M501 - Read settings from EEPROM. (i.e., Throw away unsaved changes)
2175   *   M502 - Revert settings to "factory" defaults. (Follow with M500 to init the EEPROM.)
2176   */
2177  #define EEPROM_SETTINGS     // Persistent storage with M500 and M501 // Enabled EEPROM override
2178  //#define DISABLE_M503        // Saves ~2700 bytes of flash. Disable for release!
2179  #define EEPROM_CHITCHAT       // Give feedback on EEPROM commands. Disable to save PROGMEM.
2180  #define EEPROM_BOOT_SILENT    // Keep M503 quiet and only give errors during first load
2181  #if ENABLED(EEPROM_SETTINGS)
2182    //#define EEPROM_AUTO_INIT  // Init EEPROM automatically on any errors.
2183    //#define EEPROM_INIT_NOW   // Init EEPROM on first boot after a new build.
2184  #endif
```

Fig. 48. EEPRPM Settings

3.3 Printer Control and Slicing Software

Pronterface host interface software was used for controlling the printer X-, Y-, and Z-axis movements and the extruders motors. The software was downloaded from https://github.com/kliment/Printrun/releases/tag/printrun-20150310. Default Pronterface settings were used at 250 0 0 0 baud rate. Print configurations were made using Prusa Slicer Software. "STL" files designed for printing various constructs were established using Autodesk Fusion360 software. Preparing STL files for 3D printing (i.e., slicing) was achieved using Prusa Slicer software. The standard configurations made in Prusa Slicer are presented in Table 9.

Table 9. Prusa Slicer Configurations Used for Printing

Setting	Type	Value	Enabled/Disabled
Layer Height Settings	Layer Height	1.2 [mm]	//
	First Layer Height	1.2 [mm]	//
Quality Settings	Extra Perimeters if Needed	//	Enabled
	Detect Thin Walls	//	Enabled
	Thick Bridges	//	Enabled
	Detect Bridging Perimeters	//	Enabled
Skirt Settings	Loops (minimum)	1	//
	Distance from Brim/Object	6 [mm]	//
	Skirt Height	1 [layers]	//
	Draft Shield	//	Disabled
	Minimal Filament Extrusion Length	0[mm]	//
Printing & Travel Speeds	Perimeters	2.5 [mm/s]	//
	Small Perimeters	2.5 [mm/s]	//
	External Perimeters	2.5 [mm/s]	//
	Infill	2.5 [mm/s]	//
	Solid Infill	2.5 [mm/s]	//
	Top Solid Infill	2.5 [mm/s]	//
	Travel	50 [mm/s]	//
	Z-Travel	0 [mm/s]	//
	First Layer Speed	2.5 [mm/s]	//
	Max Print Speed	20 [mm/s]	//
	Max Volumetric Speed	0 [mm/s]	//
Printer Settings	Bed Shape	220*220*200 [mm]	//
	Max Print Height	200 [mm]	//
	Z-Offset	0 [mm]	//
	Extruders	2	//
	Single Extruder Multi-Material	//	Disabled
	Firmware	Marlin 2	//

	Format of G-code Thumbnails	PNG	//
	Use Relative E Distance	//	Disabled
	Use Firmware Retraction	//	Disabled
	Use Volumetric E	//	Disabled
	Enable Variable layer Height Feature	//	Enabled
Extruder (1) – Ceramic Paste Extruder Settings	Nozzle Diameter	2 [mm]	//
	Layer heights Min	0.1 [mm]	//
	Layer Height Max	0 [mm]	//
	Extruder offset	X: 0 [mm] , y: 0 [mm]	//
	Retraction Length	100 [mm]	//
	Retraction Speed	8 [mm]	//
	Minimum Travel After Retraction	2 [mm]	//
	Retract on Layer Change	//	Disabled
Extruder (2) – Conductive Paste Extruder Settings	Nozzle Diameter	2 [mm]	//
	Layer heights Min	0.1 [mm]	//
	Layer Height Max	0 [mm]	//
	Extruder offset	X: 78 [mm] , y: 0 [mm]	//
	Retraction Length	100 [mm]	//
	Retraction Speed	4 [mm]	//
	Minimum Travel After Retraction	2 [mm]	//
	Retract on Layer Change	//	Disabled

3.4 Microcontroller Circuit Design and Wiring

For control of the paste 3D printer, BTT SKR V2 RevB was interfaced with Marlin Firmware. TMC2209 drivers were utilized for operating the extra Nema-23 extruders' stepper motors. Furthermore, for defined mechanical control of the stepper motors, Mechanical End stop V1.2 was utilized. The microcontroller was powered using a 12V power supply.

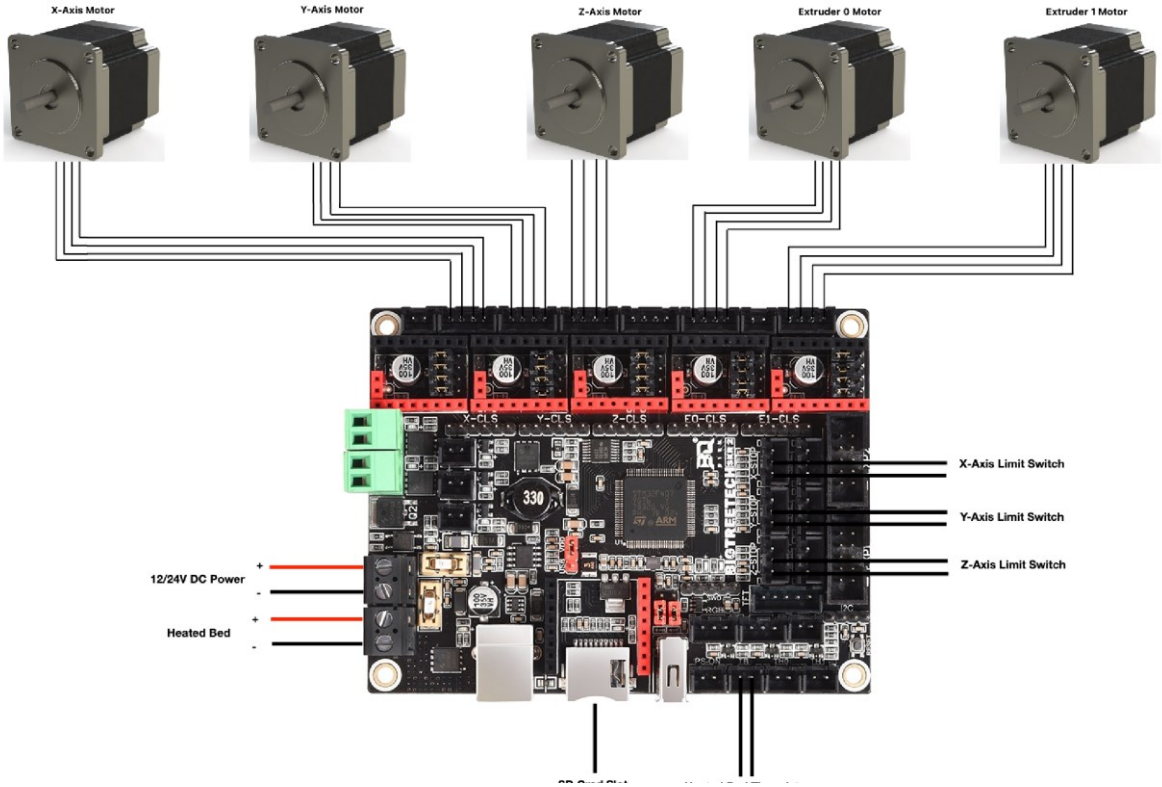

Fig. 49. Circuit Diagram of the Connections

4 Experimental Work

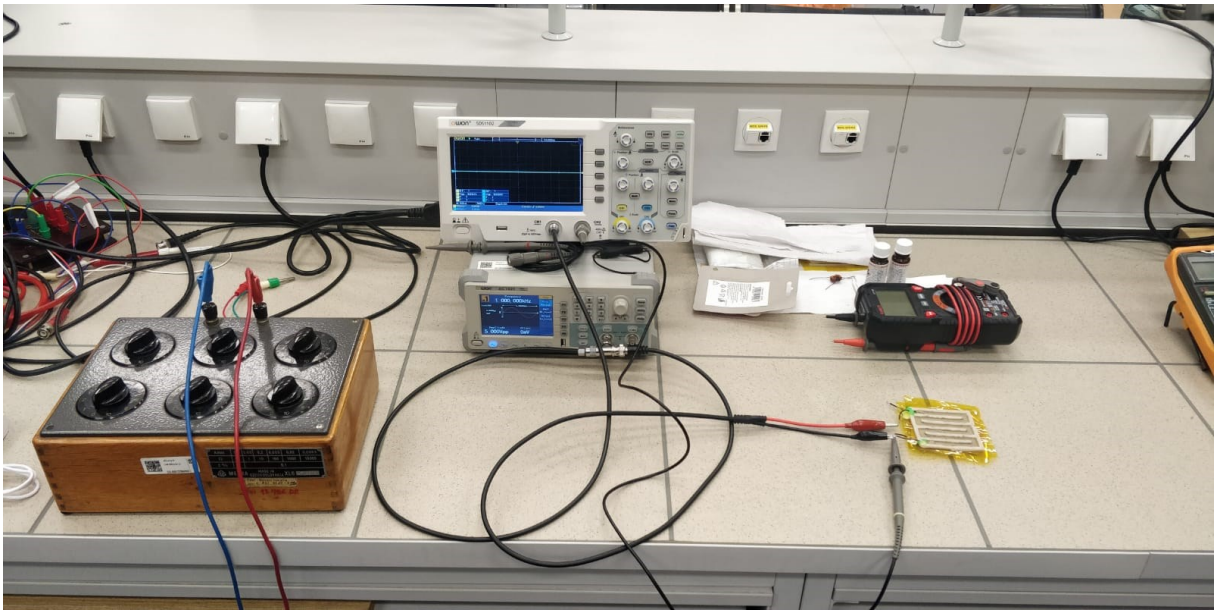

5 Results and Discussion

5.1 Experiment One

- Voltage Source = 10 [V]

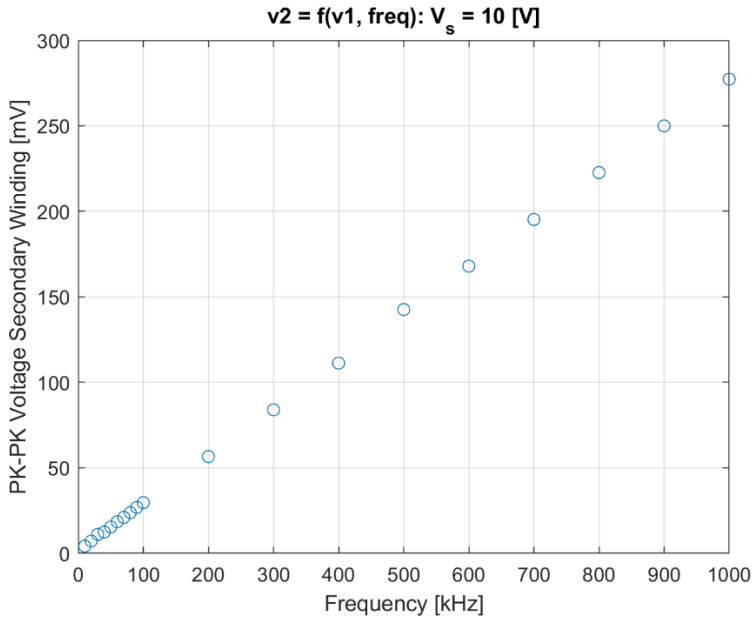

- Voltage Source = 5 [V]

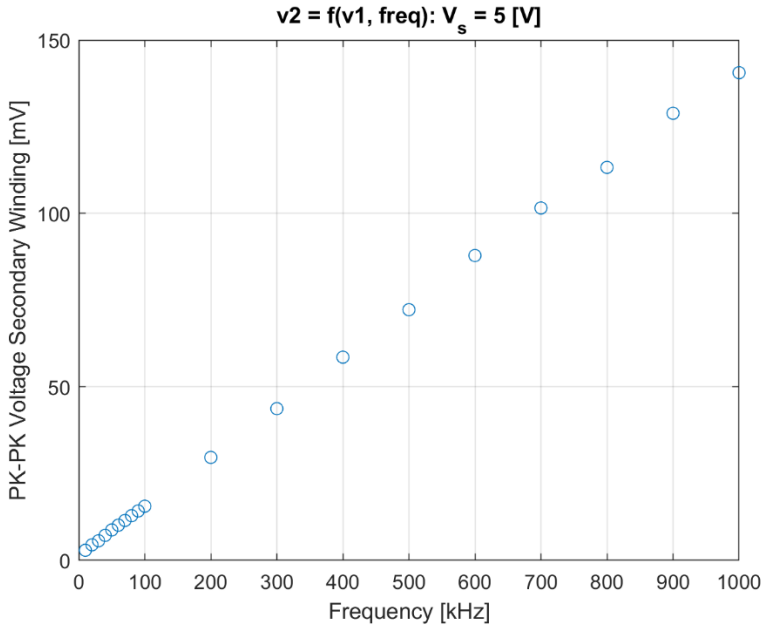

5.2 Experiment Two

5.2.1. Misalignment X-Axis

- (x, y) = (15 , 0) >> Misalignment measured in [mm]

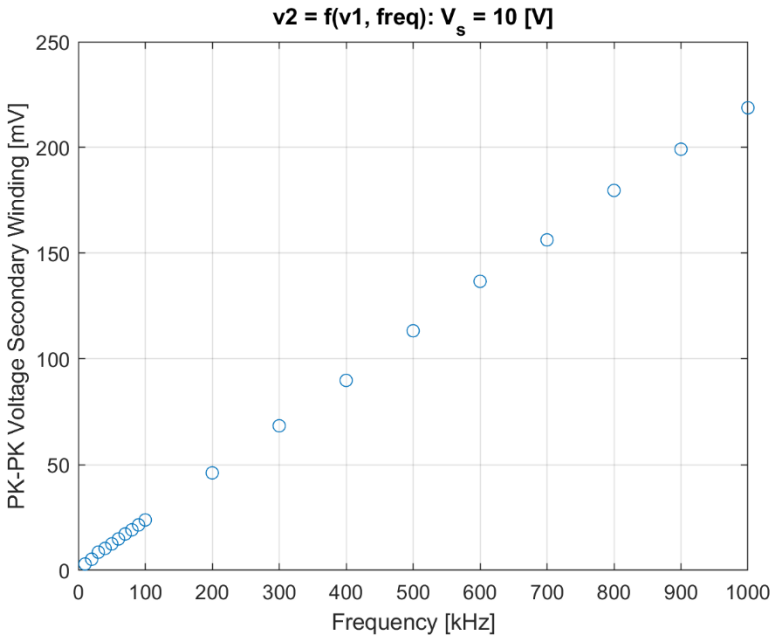

- (x, y) = (30 , 0) >> Misalignment measured in [mm]

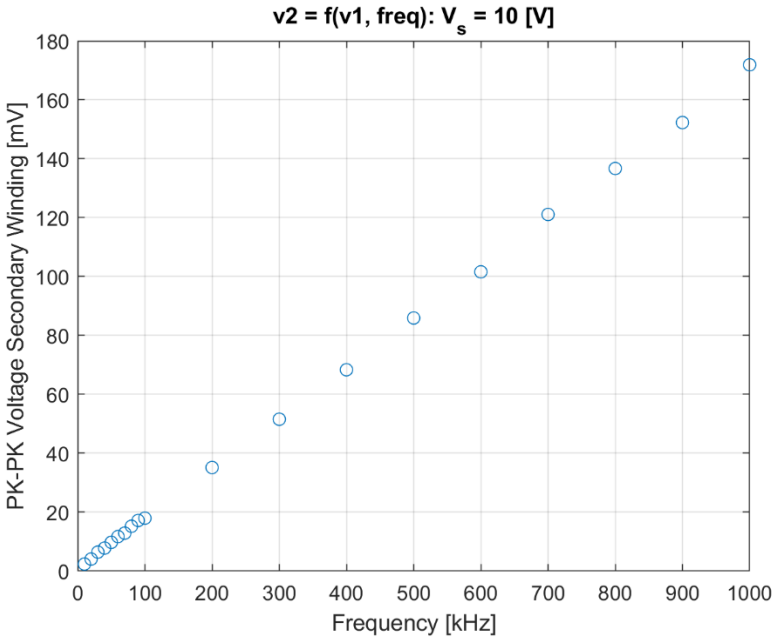

- (x, y) = (45 , 0) >> Misalignment measured in [mm]

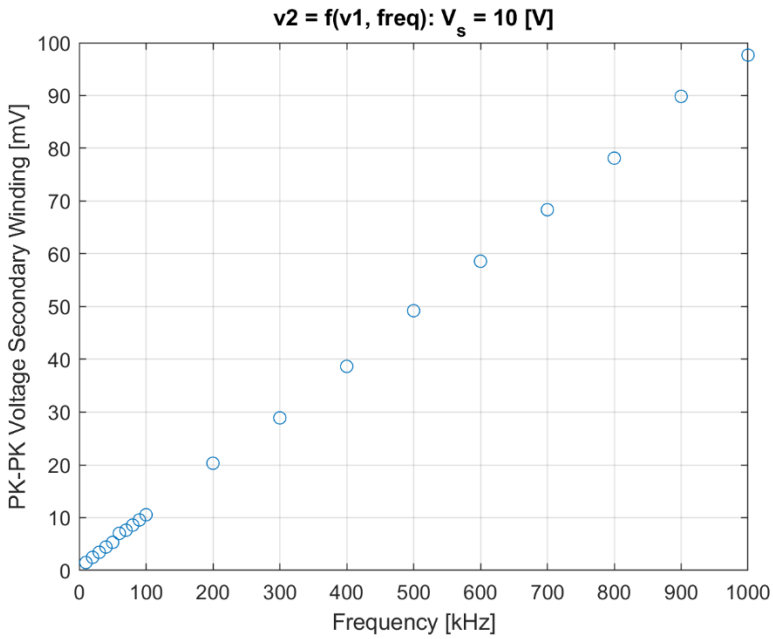

5.2.2. Misalignment Y-Axis

- (x, y) = (0 , 15) >> Misalignment measured in [mm]

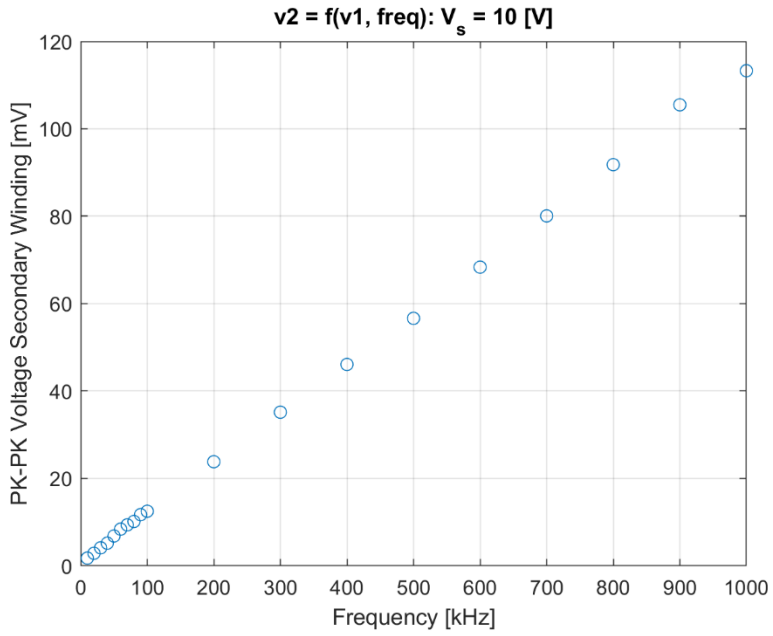

- (x, y) = (0 , 30) >> Misalignment measured in [mm]

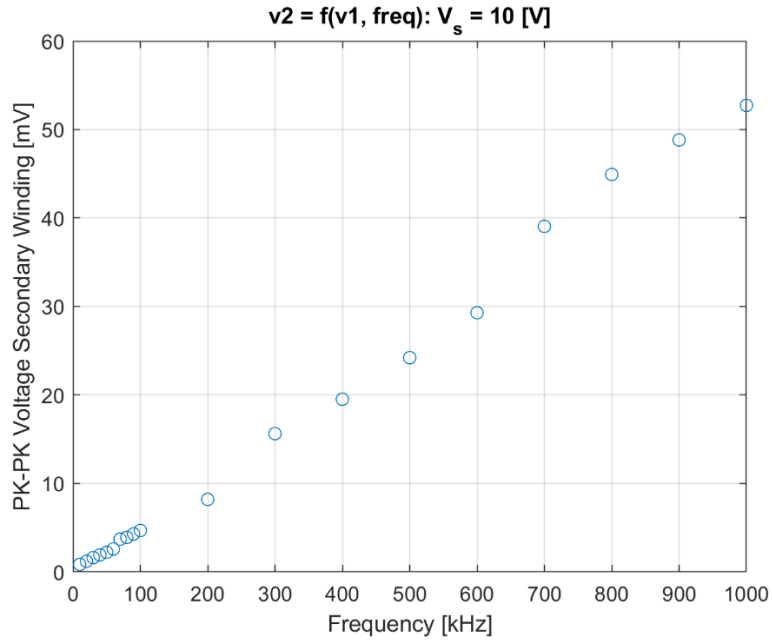

- (x, y) = (0 , 45) >> Misalignment measured in [mm]

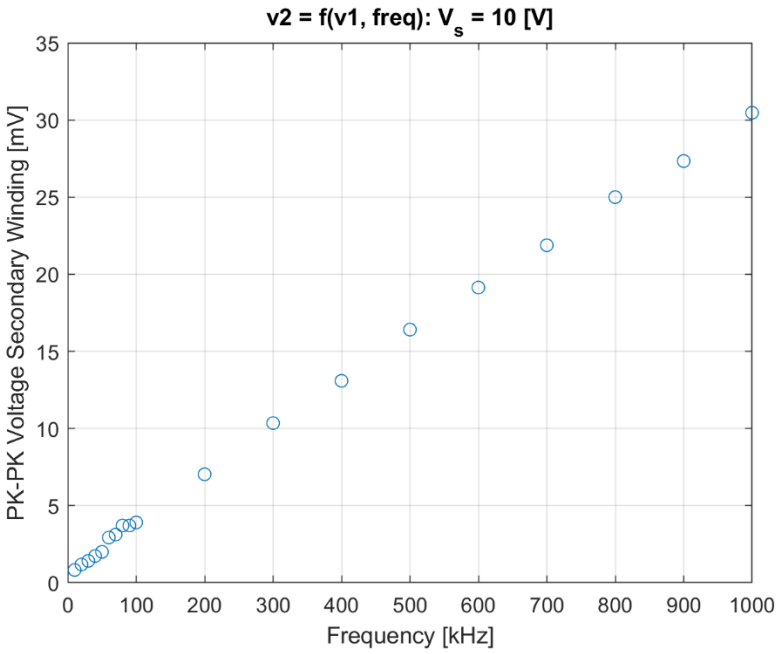

5.2.3. Misalignment X- & Y-Axes

- (x, y) = (30, 22.5) >> Misalignment measured in [mm]

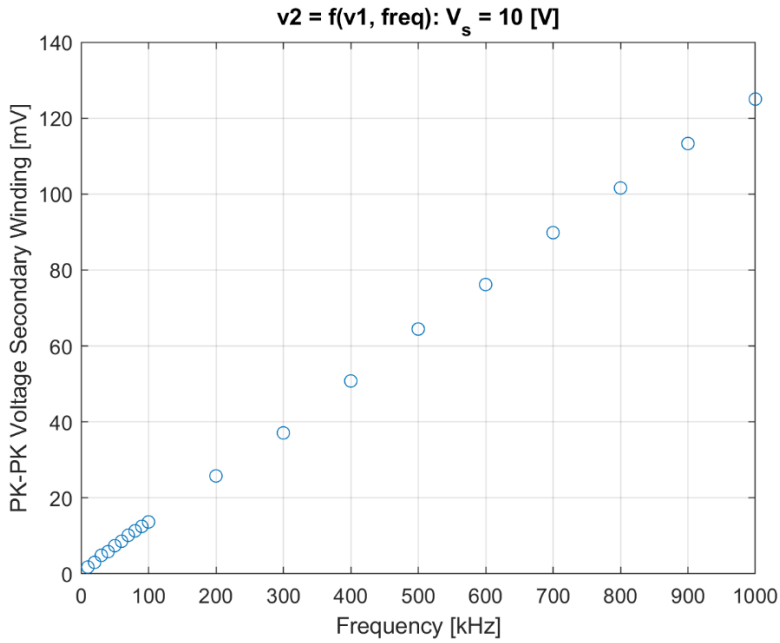

5.3 Experiment Three

- Distance gap between primary and secondary winding: 10 [mm]

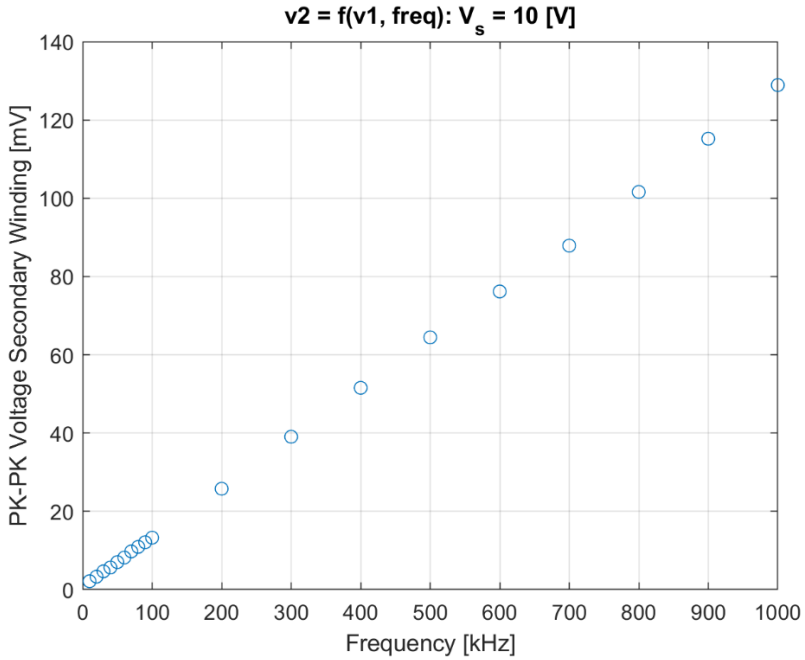

- Distance gap between primary and secondary winding: 20 [mm]

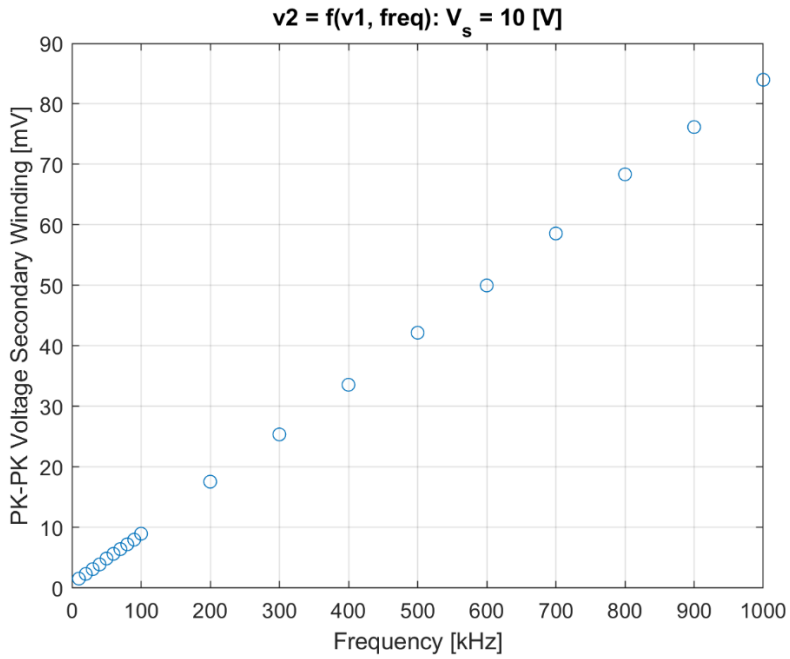

- Distance gap between primary and secondary winding: 30 [mm]

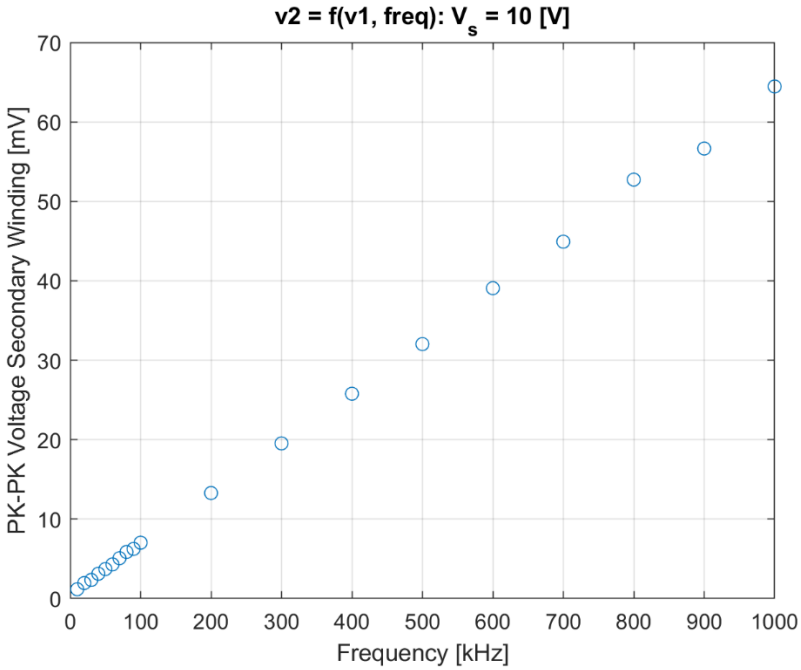

5.4 Experiment Four

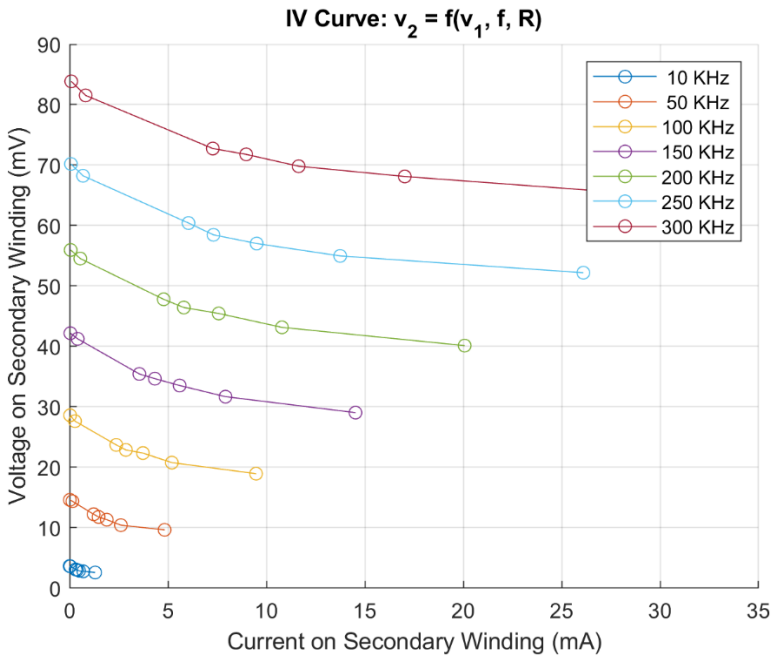

6 Conclusion

In conclusion, this thesis has examined the possibility of 3d printing of electrical machines. By analyzing the research in this field, it has become more apparent that additive manufacturing for fabricating devices such as transformers and motors is more beneficial than conventional methods for prototyping and testing new design methods and approaches that increase the performance of the total machine, such as magnetic cores, conductive wiring/windings, and insulation. The thesis analyzed the potential of using multi-material paste extrusion for fabricating high-frequency coreless transformers by designing and building a dual extruder for an existing 3d printer. Conductive and non-conductive materials were able to be printed from the built machine. However, limited funding sources forced this research to use a conductive material applied manually within the printed ceramic tracks. Overall, multiple high-frequency coreless transformers were printed and tested. The results showed linear dependency between the secondary winding voltage and frequency when higher frequency ranges were applied. Besides, a measurement with a load was applied to the transformer, the current on

the secondary winding was measured, and the IV curve was obtained. The curve indicated that the specific design of the transformer might have influenced the transformer's behavior.

Moving forward, it is recommended that future research in this field focus on understanding the specific factors that contribute to the performance of a 3D-printed transformer and explore the potential for research for fabricating electrical motors.

In summary, this thesis highlights the potential creating electrical machines using 3D-printing by exploring available technologies and apply new machine designs and study their potential in functional applications.

Works Cited

[1] G.N. Levy, R. Schindel, J.P. Kruth, Rapid manufacturing and rapid tooling with layer manufacturing (LM) technologies, state of the art and future perspectives, CIRP Ann. Manuf. Technol. 52 (2) (2003) 589–609, https://www.sciencedirect.com/science/article/pii/S0007850607602066

[2] K.V. Wong, A. Hernandez, A review of additive manufacturing, ISRN Mech.Eng. 2012 (2012) 1–10, http://dx.doi.org/10.5402/2012/208760.

[3] W.J. Sames, F.A. List, S. Pannala, R.R. Dehoff, S.S. Babu, The metallurgy and processing science of metal additive manufacturing, Int. Mater. Rev. 61 (5)(2016) 315–360. https://www.tandfonline.com/doi/full/10.1080/09506608.2015.1116649

[4] L. Gibson, D.W. Rosen, B. Stucker, Additive Manufacturing Technologies,2010th ed., Springer, Boston, 2010, http://dx.doi.org/10.1007/978-1-4419-1120-9

[5] Subramanian, K. P. Additive Manufacturing of Electric Machines: A Review. IEEE Trans. Ind. Appl. 2020, 56 (3), 1746–1754.

[6] Liu, J.; Wang, Z.; Zhang, Y.; Zhang, X. Additive manufacturing of electrical machines: A review. J. Manufacturing Syst. 2019, 55, 69–78.

[7] Hedden, A. K.; Denwood, T. A.; Blake, J. R. Additive manufacturing of electric machines: A review. J. Engineering Manufacture 2016, 230 (6), 887–898.

[8] L.E. Andersson, M. Larsson, Device and arrangement for producing a three-dimensional object, US Patent US 7537722 B2, 2000.

[9] C. McAlister, J. Wood, The potential of 3D printing to reduce the environmental impacts of production, in: Proceeding of the ECEEE, 2014, pp.213–221. https://www.scopus.com/record/display.uri?eid=2-s2.0-85028456273&origin=inward

[10] l.E. Hawary, E. Mohamed, Principles of electric machines with power electronic applications, United States, 1986. https://www.osti.gov/biblio/5901271

[11] T. Wohlers, Additive Manufacturing and 3D Printing, State of the Industry, Annu. World. Prog. Rep. Wohlers Assoc., USA, 2012. http://refhub.elsevier.com/S2352-9407(18)30443-8/sbref0095

[12] L. Gibson, D.W. Rosen, B. Stucker, Additive Manufacturing Technologies,2010th ed., Springer, Boston, 2010, http://dx.doi.org/10.1007/978-1-4419-1120-9.

[13] M.C. Guo, Leu, Additive manufacturing: technology, applications and research needs, Front. Mech. Eng. 8 (3) (2013) 215–243. https://link.springer.com/article/10.1007/s11465-013-0248-8

[14] C.W. Hull, 1986. Apparatus for production of three-dimensional objects by stereolithography. US Patent 4,575,330.

[15] F.P. Jeantette, D.M. Keicher, J.A. Romero, L.P. Schanwald, Method and system for producing complex-shape objects, US Patent US 6046426 A, 1996.

[16] Nammari, A., Caskey, L., Negrete, J., & Bardaweel, H. (2018). Fabrication and characterization of non-resonant magneto-mechanical low-frequency vibration energy harvester. *Mechanical Systems and Signal Processing*, *102*, 298–311. https://doi.org/10.1016/j.ymssp.2017.09.036

[17] Hayes, A., Sethuraman, L., Dykes, K., & Fingersh, L. J. (2018). Structural Optimization of a Direct-Drive Wind Turbine Generator Inspired by Additive Manufacturing. *Procedia Manufacturing*, *26*, 740–752. https://doi.org/10.1016/j.promfg.2018.07.084

[18] GE Nine Sigma, Names 10 Finalists in GE Global 3D Printing Production Quest, Cleveland, https://www.ninesigma.com/press-release/ninesigma-ge-announce-selection-of-10-finalists-in-ge-global-3d-printing-production-quest,2013.

[19] Hirt, L., Reiser, A., Spolenak, R., & Zambelli, T. (2017). Additive Manufacturing of Metal Structures at the Micrometer Scale. *Advanced Materials*, *29*(17), 1604211. https://doi.org/10.1002/adma.201604211

[20] Urban, N., Huber, F., & Franke, J. (2017). *Influences of process parameters on Rare Earth Magnets produced by Laser Beam Melting*. In: Electric Drives Production Conference (EDPC), 2017 7th International, 2017, pp. 1–5.

[21] Li, L., Jones, K., Sales, B., Pries, J. L., Nlebedim, I. C., Jin, K., Bei, H., Post, B. K., Kesler, M. S., Rios, O., Kunc, V., Fredette, R., Ormerod, J., Williams, A., Lograsso, T. A., & Paranthaman, M. P. (2018). Fabrication of highly dense isotropic Nd-Fe-B nylon bonded magnets via extrusion-based additive manufacturing. *Additive Manufacturing*, *21*, 495–500. https://doi.org/10.1016/j.addma.2018.04.001

[22] H. Martin, J. Krishnasamy, S. Sah, T. Bashaw, Spray-Formed Hybrid-Field Electric Motor, in: ASME 2016 International Design Engineering Technical Conferences and Computers and Information in Engineering Conference, American Society of Mechanical Engineers, 2016, V003T01A034. https://refhub.elsevier.com/S2352-9407(18)30443-8/sbref0415

[23] K. Jayaraman, M. Hosek, Spray-Formed Hybrid-Field Traction Motor, No.2017-01-1225. SAE Technical Paper, 2017. https://refhub.elsevier.com/S2352-9407(18)30443-8/sbref0420

[24] Zhang, Z.-Y., Tsai, M.-C., Huang, P.-W., Cheng, C.-W., & Huang, J.-M. (2015, October). Characteristic comparison of transversally laminated anisotropic synchronous reluctance

motor fabrication based on 2D lamination and 3D printing. *2015 18th International Conference on Electrical Machines and Systems (ICEMS)*. 2015 18th International Conference on Electrical Machines and Systems (ICEMS). https://doi.org/10.1109/icems.2015.7385161

[25] Zhang, Z.-Y., Jhong, K. J., Cheng, C.-W., Huang, P.-W., Tsai, M.-C., & Lee, W.-H. (2016, March). Metal 3D printing of synchronous reluctance motor. *2016 IEEE International Conference on Industrial Technology (ICIT)*. 2016 IEEE International Conference on Industrial Technology (ICIT). https://doi.org/10.1109/icit.2016.7474912

[26] Jagdale, V., & Tangudu, J. (2016, September 20). Topology Optimized End Winding for Additively Manufactured Induction Motor with Distributed Winding. *SAE Technical Paper Series*. SAE 2016 Aerospace Systems and Technology Conference. https://doi.org/10.4271/2016-01-2060

[27] Tseng, G.-M. (2016). Application of additive manufacturing for low torque ripple of 6/4 switched reluctance motor. In *International Conference on Electrical Machines and Systems*. https://refhub.elsevier.com/S2352-9407(18)30443-8/sbref0440

[28] M.G. Urdaneta, R. Probst, P.Y. Stepanov, I.N. Weinberg, S.T. Fricke, Goodbye wires and formers: 3-D additive manufacturing and fractal cooling applied to construction of MRI gradient coils, in: Nuclear Science Symposium and Medical Imaging Conference (NSS/MIC), 2011, pp. 2479–2482. https://refhub.elsevier.com/S2352-9407(18)30443-8/sbref0450

[29] M. Saari, B. Cox, E. Richer, P.S. Krueger, A.L. Cohen, Fiber encapsulation additive manufacturing: An enabling technology for 3D printing of electromechanical devices and robotic components, 3D Printing AdditiveManuf. 2 (1) (2015) 32–39. https://refhub.elsevier.com/S2352-9407(18)30443-8/sbref0455

[30] Simpson, N., & Mellor, P. H. (2017, May). Additive manufacturing of shaped profile windings for minimal AC loss in gapped inductors. *2017 IEEE International Electric Machines and Drives Conference (IEMDC)*. 2017 IEEE International Electric Machines and Drives Conference (IEMDC). https://doi.org/10.1109/iemdc.2017.8002337

[31] Y. Daniel, S. Gross, N. Meyer, Energy Vision 2013-Energy Transitions: Past and Future, World Economic Forum, 2013, https://www3.weforum.org/docs/WEF_EN_EnergyVision_Report_Contributors_2013.pdf

[32] W. Paul, C.U. Brunner, Energy-efficiency policy opportunities for electric motor-driven systems, Int. Energy (2011) 1–127, https://www.oecd-ilibrary.org/energy/energy-efficiency-policy-opportunities-for-electric-motor-driven-systems_5kgg52gb9gjd-en

[33] Jacob, D., & Nithiyananthan, K. (2008). Effective methods for power systems grounding, WSEAS TRANSACTIONS on BUSINESS and ECONOMICS. In *Volume* (Vol. 5) (1) (2008) 151–160. http://wseas.us/e-library/transactions/economics/2008/30-642.pdf

[34] Waterman, J., Clucas, A., Costa, T. B., Zhang, Y., & Zhang, J. (2015, May). Numerical modeling of 3D printed electric machines. *2015 IEEE International Electric Machines & Drives Conference (IEMDC)*. 2015 IEEE International Electric Machines & Drives Conference (IEMDC). https://doi.org/10.1109/iemdc.2015.7409227

[35] (1), M. G., (1), C. G., (1), I. A., (1), R. H., of Engineering, H. M. (1) 1: F., of Nottingham, T. U., Park, U., NG, N., 2RD, & UK. (2014). *The Impact of Additive Manufacturing on the Development of Electrical Machines for MEA Applications: A Feasibility Study*. https://hal.science/hal-01178353

[36] Wawrzyniak, B. I., & Tangudu, J. (2016, September 20). Design Analysis of High Power Density Additively Manufactured Induction Motor. *SAE Technical Paper Series*. SAE 2016 Aerospace Systems and Technology Conference. https://doi.org/10.4271/2016-01-2063

[37] Urata, S., Enokizono, M., Todaka, T., & Shimoji, H. (2006). Magnetic characteristic analysis of the motor considering 2-D vector magnetic property. *IEEE Transactions on Magnetics*, *42*(4), 615–618. https://doi.org/10.1109/tmag.2006.871468

[38] Gracia, M. H., & Hameyer, Influence of the magnetic anisotropy on electrical machines, Adv. Comput. Techniq. Appl. Electromagnet. 30 (2008)39–47, K. (2007). ISEF 2007 - XIII International Symposium on Electromagnetic Fields in Mechatronics, Electrical and Electronic Engineering. In *ISEF* (Vol. 29). http://bib.iem.rwth-aachen.de/IEMpublications/AltesBib/2008MHGInfluence.pdf

[39] C. Garrett, H. Song, J. Nielsen, J. Stasiak, M. Khavari, A. Jander, P. Dhagat, 3D printing magnetic material with arbitrary anisotropy, in: NIP & Digital Fabrication Conference 2015, 2015, pp. 307–310. https://www.researchgate.net/profile/Han-Song-4/publication/282403986_3D_Printing_Magnetic_Material_with_Arbitrary_Anisotropy/links/56e77c9108ae4cbe4d42f885/3D-Printing-Magnetic-Material-with-Arbitrary-Anisotropy.pdf

[40] O. Andersen, T. Studnitzky, J. Bauer, PM Lightweight and Porous Materials: Direct Typing-a New Method for the Production of Cellular P/M Parts, in: European Congress and Exhibition on Powder Metallurgy. European PM Conference Proceedings 4, 2004, pp. 189–194. https://www.scopus.com/record/display.uri?eid=2-s2.0-33750292624&origin=inward

[41] B. Patrick, M. Lindner, T. Studnitzky, B. Kieback, J. Rudolph, R. Werner, G.Krause, 3D Screen Printing technology—Opportunities to use revolutionary materials and machine designs, in: Electric Drives Production Conference(EDPC), 2012, pp. 1–5, http://dx.doi.org/10.1109/EDPC.2012.6425124.

[42] P. Matshediso, Power transformer noise: sources, factors and remedies, Powertech Transformers, Powertech Transformer Ltd., energize, 2013, pp.33–37, https://refhub.elsevier.com/S2352-9407(18)30443-8/sbref0265

[43] G.C. Stone, E.A. Boulter, I. Culbert, H. Dhirani, Electrical insulation for rotating machines: design, evaluation, aging, testing, and repair, John Wiley& Sons, USA, 2004, ISBN 0-471-4450 6-1. https://refhub.elsevier.com/S2352-9407(18)30443-8/sbref0380

[44] Staton, D., Boglietti, A., & Cavagnino, A. (2005). Solving the More Difficult Aspects of Electric Motor Thermal Analysis in Small and Medium Size Industrial Induction Motors. *IEEE Transactions on Energy Conversion*, *20*(3), 620–628. https://doi.org/10.1109/tec.2005.847979

[45] Xu, Y. (2016). Kilowatt Three-phase Rotary Transformer Design for a Permanent Magnet DC Motor with On-rotor Drive System. In *Examiner*. http://www.diva-portal.org/smash/get/diva2:932733/FULLTEXT01.pdf

[46] Yamazaki, K., & Fukushima, N. (2010). Iron-Loss Modeling for Rotating Machines: Comparison Between Bertotti's Three-Term Expression and 3-D Eddy-Current Analysis. *IEEE Transactions on Magnetics*, *46*(8), 3121–3124. https://doi.org/10.1109/tmag.2010.2044384

[47] W.R. Mischler, Laminated motor stator structure with molded composite pole pieces. U.S. Patent 4,255,684, 1981. https://patentimages.storage.googleapis.com/14/cb/9d/bb24f4f034afaf/US4255684.pdf

[48] Ranjan, R., & Tangudu, J. (2014, September). Thermal design of high power-density additively-manufactured induction motors. *2014 IEEE Energy Conversion Congress and Exposition (ECCE)*. 2014 IEEE Energy Conversion Congress and Exposition (ECCE). https://doi.org/10.1109/ecce.2014.6953554

[49] C. Galitsky, E. Worrell, C. Galitsky, E. Masanet, W. Graus, Energy Efficiency Improvement and Cost Saving Opportunities for the Glass Industry, An ENERGY STAR Guide for Energy and Plant Managers (No.LBNL-57335-Revision), Lawrence Berkeley National Lab. (LBNL), Berkeley,CA (United States), 2008. https://www.osti.gov/servlets/purl/927883-Pndaxj/

[50] Zhao, X., Chen, J., Lin, X., & Huang, W. (2008). Study on microstructure and mechanical properties of laser rapid forming Inconel 718. *Materials Science and Engineering: A*, *478*(1–2), 119–124. https://doi.org/10.1016/j.msea.2007.05.079

[51] Tiismus, H., Kallaste, A., Vaimann, T., Rassolkin, A., & Belahcen, A. (2021, January 27). Additive Manufacturing of Prototype Axial Flux Switched Reluctance Electrical Machine. 2021 28th International Workshop on Electric Drives: Improving Reliability of Electric Drives (IWED). 2021 28th International Workshop on Electric Drives: Improving Reliability of Electric Drives (IWED). https://doi.org/10.1109/iwed52055.2021.9376337

[52] Yap, C. Y., Chua, C. K., Dong, Z. L., Liu, Z. H., Zhang, D. Q., Loh, L. E., & Sing, S. L. (2015). Review of selective laser melting: Materials and applications. Applied Physics Reviews, 2(4), 041101. https://doi.org/10.1063/1.4935926

[53] Clare, A. T., Chalker, P. R., Davies, S., Sutcliffe, C. J., & Tsopanos, S. (2007). Selective laser melting of high aspect ratio 3D nickel–titanium structures two way trained for MEMS

applications. International Journal of Mechanics and Materials in Design, 4(2), 181–187. https://doi.org/10.1007/s10999-007-9032-4

[54] Kempen, K., † L. T., Yasa, E., Badrossamay, M., Verheecke°, W., & Kruth, J.-P. (2011). PROCESS OPTIMIZATION AND MICROSTRUCTURAL ANALYSIS FOR SELECTIVE LASER MELTING OF AlSi10Mg. In REVIEWED. https://repositories.lib.utexas.edu/bitstream/handle/2152/88371/2011-37-Kempen.pdf?sequence=2

[55] Tran, T. Q., Chinnappan, A., Lee, J. K. Y., Loc, N. H., Tran, L. T., Wang, G., Kumar, V. V., Jayathilaka, W. A. D. M., Ji, D., Doddamani, M., & Ramakrishna, S. (2019). 3D Printing of Highly Pure Copper. Metals, 9. https://doi.org/10.3390/met9070756

[56] Tiismus, H., Kallaste, A., Belahcen, A., Vaimann, T., Rassõlkin, A., & Lukichev, D. (2020). Hysteresis Measurements and Numerical Losses Segregation of Additively Manufactured Silicon Steel for 3D Printing Electrical Machines. Applied Sciences, 10(18), 6515. https://doi.org/10.3390/app10186515

[57] Jafari, D., & Wits, W. W. (2018). The utilization of selective laser melting technology on heat transfer devices for thermal energy conversion applications: A review. *Renewable and Sustainable Energy Reviews*, *91*, 420–442. https://doi.org/10.1016/j.rser.2018.03.109

[58] Martin, J.D. Exploring Additive Manufacturing Processes for Direct 3D Printing of Copper Induction Coils. In Proceedings of the ASME 2017 International Mechanical Engineering Congress and Exposition, Tampa, FL, USA, 3–9 November 2017. http://dx.doi.org/10.1115/IMECE2017-71685

[59] Dizon, J. R. C., Espera, A. H., Jr., Chen, Q., & Advincula, R. C. (2018). Mechanical characterization of 3D-printed polymers. *Additive Manufacturing*, *20*, 44–67. https://doi.org/10.1016/j.addma.2017.12.002

[60] Popescu, D., Zapciu, A., Amza, C., Baciu, F., & Marinescu, R. (2018). FDM process parameters influence over the mechanical properties of polymer specimens: A review. *Polymer Testing*, *69*, 157–166. https://doi.org/10.1016/j.polymertesting.2018.05.020

[61] Rochus, P., Plesseria, J.-Y., Van Elsen, M., Kruth, J.-P., Carrus, R., & Dormal, T. (2007). New applications of rapid prototyping and rapid manufacturing (RP/RM) technologies for space instrumentation. *Acta Astronautica*, *61*(1–6), 352–359. https://doi.org/10.1016/j.actaastro.2007.01.004

[62] Blok, L. G., Longana, M. L., Yu, H., & Woods, B. K. S. (2018). An investigation into 3D printing of fibre reinforced thermoplastic composites. *Additive Manufacturing*, *22*, 176–186. https://doi.org/10.1016/j.addma.2018.04.039

[63] Lalehpour, A., & Barari, A. (2016). Post processing for Fused Deposition Modeling Parts with Acetone Vapour Bath. *IFAC-PapersOnLine*, *49*(31), 42–48. https://doi.org/10.1016/j.ifacol.2016.12.159

[64] Chen, Y.-F., Wang, Y.-H., & Tsai, J. (2019). Enhancement of surface reflectivity of fused deposition modeling parts by post-processing. *Optics Communications*, *430*, 479–485. https://doi.org/10.1016/j.optcom.2018.07.011

[65] Kumbhar, N. N., & Mulay, A. V. (2016). Post Processing Methods used to Improve Surface Finish of Products which are Manufactured by Additive Manufacturing Technologies: A Review. *Journal of The Institution of Engineers (India): Series C*, *99*(4), 481–487. https://doi.org/10.1007/s40032-016-0340-z

[66] McCullough, E. J., & Yadavalli, V. K. (2013). Surface modification of fused deposition modeling ABS to enable rapid prototyping of biomedical microdevices. *Journal of Materials Processing Technology*, *213*(6), 947–954. https://doi.org/10.1016/j.jmatprotec.2012.12.015

[67] Department of Mechanical Engineering. (2000). Prashant Kulkarni Debasish Dutta. In *Õ Vol* (Vol. 122). Investigations for improving the surface finish of FDM based ABS replicas by chemical vapor smoothing process: a case study. Assem Autom 37(1):13–21. https://doi.org/10.1108/AA-12-2015-127

[68] Boschetto, A., Bottini, L., & Veniali, F. (2016). Finishing of Fused Deposition Modeling parts by CNC machining. *Robotics and Computer-Integrated Manufacturing*, *41*. https://doi.org/10.1016/j.rcim.2016.03.004

[69] Daminabo, S. C., Goel, S., Grammatikos, S. A., Nezhad, H. Y., & Thakur, V. K. (2020). Fused deposition modeling-based additive manufacturing (3D printing): techniques for polymer material systems. *Materials Today Chemistry*, *16*, 100248. https://doi.org/10.1016/j.mtchem.2020.100248

[70] Bryll, K., Piesowicz, E., Szymański, P., Ślączka, W., & Pijanowski, M. (2018). Polymer Composite Manufacturing by FDM 3D Printing Technology. *MATEC Web of Conferences*, *237*, 02006. https://doi.org/10.1051/matecconf/201823702006

[71] Alizadeh-Osgouei, M., Li, Y., & Wen, C. (2019). A comprehensive review of biodegradable synthetic polymer-ceramic composites and their manufacture for biomedical applications. *Bioactive Materials*, *4*, 22–36. https://doi.org/10.1016/j.bioactmat.2018.11.003

[72] Postiglione, G., Natale, G., Griffini, G., Levi, M., & Turri, S. (2015). Conductive 3D microstructures by direct 3D printing of polymer/carbon nanotube nanocomposites via liquid deposition modeling. *Composites Part A: Applied Science and Manufacturing*, *76*, 110–114. https://doi.org/10.1016/j.compositesa.2015.05.014

[73] Fafenrot, S., Grimmelsmann, N., Wortmann, M., & Ehrmann, A. (2017). Three-Dimensional (3D) Printing of Polymer-Metal Hybrid Materials by Fused Deposition Modeling. *Materials*, *10*(10), 1199. https://doi.org/10.3390/ma10101199

[74] Farahani, R. D., Dubé, M., & Therriault, D. (2016). Three-Dimensional Printing of Multifunctional Nanocomposites: Manufacturing Techniques and Applications. *Advanced Materials*, *28*(28), 5794–5821. https://doi.org/10.1002/adma.201506215

[75] Leigh, S. J., Bradley, R. J., Purssell, C. P., Billson, D. R., & Hutchins, D. A. (2012). A Simple, Low-Cost Conductive Composite Material for 3D Printing of Electronic Sensors. *PLoS ONE*, *7*(11), e49365. https://doi.org/10.1371/journal.pone.0049365

[76] Manzanares Palenzuela CL, Novotný F, Krupička P, Sofer Z, Pumera M (2018) 3D-printed graphene/polylactic acid electrodes promise high sensitivity in electroanalysis. Anal Chem 90(9): 5753–5757. https://doi.org/10.1021/acs.analchem.8b000 83

[77] Junpha, J., Wisitsoraat, A., Prathumwan, R., Chaengsawang, W., Khomungkhun, K., & Subannajui, K. (2020). Electronic tongue and cyclic voltammetric sensors based on carbon nanotube/polylactic composites fabricated by fused deposition modelling 3D printing. *Materials Science and Engineering: C*, *117*, 111319. https://doi.org/10.1016/j.msec.2020.111319

[78] Dawoud, M., Taha, I., & Ebeid, S. J. (2018). Strain sensing behaviour of 3D printed carbon black filled ABS. *Journal of Manufacturing Processes*, *35*, 337–342. https://doi.org/10.1016/j.jmapro.2018.08.012

[79] Podsiadły B, Skalski A, Słoma M (2020) Conductive ABS/Ni composite filaments for fused deposition modeling of structural electronics. Adv Intell Syst Comput 1044:62–70. https://doi.org/10.1007/978-3- 030-29993-4_8

[80] Metsä-Kortelainen, S.; Lindroos, T.; Savolainen, M.; Jokinen, A.; Revuelta, A.; Pasanen, A.; Ruusuvuori, K.; Pippuri, J. Manufacturing of topology optimized soft magnetic core through 3D printing. In Proceedings of the NAFEMS Exploring the Design Freedom of Additive Manufacturing through Simulation, Helsinki, Finland, 22–23 November 2016. http://www.vttresearch.com/Documents/Factory%20of%20the%20future/3D%20printing/2 NAFEMS_2016_Finland_Fe-Co_rotors_Pippuri.pdf

[81] Freeman, F. S. H. B., Lincoln, A., Sharp, J., Lambourne, A., & Todd, I. (2018). Exploiting thermal strain to achieve an in-situ magnetically graded material. *Materials & Design*, *161*. https://doi.org/10.1016/j.matdes.2018.11.011

[82] Urbanek, S., Frey, P., Magerkohl, S., Zimmer, D., Tasche, L., Schaper, M., & Ponick, B. (2021, May 17). Design and Experimental Investigation of an Additively Manufactured PMSM Rotor. *2021 IEEE International Electric Machines & Drives Conference (IEMDC)*. 2021 IEEE International Electric Machines & Drives Conference (IEMDC). https://doi.org/10.1109/iemdc47953.2021.9449566

[83] Ayat, S., Simpson, N., Daguse, B., Rudolph, J., Lorenz, F., & Drury, D. (2020, August 23). Design of Shaped-Profile Electrical Machine Windings for Multi-Material Additive Manufacture. *2020 International Conference on Electrical Machines (ICEM)*. 2020 International Conference on Electrical Machines (ICEM). https://doi.org/10.1109/icem49940.2020.9270945

[84] Simpson, N., North, D. J., Collins, S. M., & Mellor, P. H. (2020). Additive Manufacturing of Shaped Profile Windings for Minimal AC Loss in Electrical Machines. *IEEE Transactions on Industry Applications*, *56*(3), 2510–2519. https://doi.org/10.1109/tia.2020.2975763

[85] Wu, F., EL-Refaie, A. M., & Al-Qarni, A. (2021, October 10). Additively Manufactured Hollow Conductors for High Specific Power Electrical Machines: Aluminum vs Copper. *2021 IEEE Energy Conversion Congress and Exposition (ECCE)*. 2021 IEEE Energy Conversion Congress and Exposition (ECCE). https://doi.org/10.1109/ecce47101.2021.9595470

[86] Bollig, L. M., Hilpisch, P. J., Mowry, G. S., & Nelson-Cheeseman, B. B. (2017). 3D printed magnetic polymer composite transformers. *Journal of Magnetism and Magnetic Materials*, *442*. https://doi.org/10.1016/j.jmmm.2017.06.070

[87] Amza, C., Zapciu, A., & Popescu, D. (2017). Paste Extruder—Hardware Add-On for Desktop 3D Printers. *Technologies*, *5*(3), 50. https://doi.org/10.3390/technologies5030050

[88] Horne, R. RepRap Development and Further Adventures in DIY 3D Printing: Universal Paste Extruder. 6 April 2012. Available online: http://richrap.blogspot.com/2012/04/universal-paste-extruder-ceramic-food.html (Accessed on 10th of February 2023).

[89] World's Advanced Saving Project (WASP). WASP Launches the New Professional Clay Extruder. 22 May 2016. Available online: http://www.wasproject.it/w/en/wasp-launches-the-new-professional-clay-extruder/ (Accessed on 10th of February 2023).

[90] Algahtani, M. S., Mohammed, A. A., & Ahmad, J. (2019). Extrusion-Based 3D Printing for Pharmaceuticals: Contemporary Research and Applications. *Current Pharmaceutical Design*, *24*(42), 4991–5008. https://doi.org/10.2174/1381612825666190110155931

[91] Y. Yan, Chao Ding, K. D. T. Ngo, Y. Mei and G. -Q. Lu, "Additive manufacturing of planar inductor for Power Electronics applications," *2016 International Symposium on 3D Power Electronics Integration and Manufacturing (3D-PEIM)*, Raleigh, NC, USA, 2016, pp. 1-16, doi: 10.1109/3DPEIM.2016.7570536

[92]Johnson, F.; Osama, M.; Jassal, A.K.; Adharapurapu, R.R. Method of Heat-Treating Additively Manufactured Ferromagnetic Components. U.S. Patent 10,946,444, 16 March 2021.

[93] Garibaldi, M. Laser Additive Manufacturing of Soft Magnetic Cores for Rotating Electrical Machinery: Materials Development and Part Design. Ph.D. Thesis, University of Nottingham, Nottingham, UK, 2018.

[94] Zhang, B., Fenineche, N.-E., Liao, H., & Coddet, C. (2013). Magnetic properties of in-situ synthesized FeNi3 by selective laser melting Fe-80%Ni powders. *Journal of Magnetism and Magnetic Materials*, *336*. https://doi.org/10.1016/j.jmmm.2013.02.014

[95] Zhang, B., Fenineche, N.-E., Liao, H., & Coddet, C. (2013). Microstructure and Magnetic Properties of Fe–Ni Alloy Fabricated by Selective Laser Melting Fe/Ni Mixed Powders. *Journal of Materials Science & Technology*, *29*(8), 757–760. https://doi.org/10.1016/j.jmst.2013.05.001

[96] Pullanchiyodan, A., & Surendran, K. P. (2016). Formulation of Sol–Gel Derived Bismuth Silicate Dielectric Ink for Flexible Electronics Applications. *Industrial & Engineering Chemistry Research*, *55*(26), 7108–7115. https://doi.org/10.1021/acs.iecr.6b00871

[97] H. Xiaoya, X.C. Yijie, Ng. Siu, Z. Jie, S.C. Joseph, Formulation of novel screen-printable dielectric ink for fully-printed TIPs pentacene OFETs, RSC Adv.4 (2014) 37687–37690. https://doi.org/10.1039/c0xx00000x

List of Appendices